High-Affinity Protein Binder Design via Flow Matching and In Silico Maturation

Qilin Yu[a,†], Liangyue Guo[a,†], Xiayan Qin[a,†], Xikun Huang[a,†], Baihui Tian[a], Hongzhun Wang[a], Yu Liu[a], Yunzhi Lang[a], Di Wang[a], Zhouhanyu Shen[a], Jie Lin[a], and Mingchen Chen[a,*]

[a]Changping Laboratory

Abstract

The de novo design of high-affinity protein binders remains a central challenge in protein engineering and therapeutic discovery. While deep generative models have advanced backbone generation and interface design, achieving picomolar or nanomolar binding affinities typically demands extensive experimental screening or iterative in vitro maturation. A general computational approach for the direct production of high-affinity binders has remained elusive. Here, we introduce an integrated framework that synergizes PPIFlow, a flow-matching-based generative model, with a novel in silico maturation strategy. PPIFlow employs a pairformer architecture to explicitly reason over pairwise geometric and chemical interactions, modeling protein backbone rigid-body transformations as continuous flows. To bridge the affinity gap, we implement a dedicated in silico affinity maturation stage that combines interface rotamer enrichment with partial flow refinement to optimize energetic packing. This pipeline is further accelerated by AF3Score, a score-only adaptation of AlphaFold3 that enables high-fidelity and computationally efficient candidate prioritization. Across a diverse set of therapeutic targets, this synergistic approach consistently produces picomolar and nanomolar affinity binders without experimental affinity maturation. Notably, the framework proves highly effective for the de novo design of single-domain antibodies (VHHs), producing sub-nanomolar binders across multiple targets. These results establish that coupling robust backbone generation with focused in silico maturation renders the purely computational design of high-affinity binders feasible.

[†]These authors contributed equally to this work.
[*]Corresponding author: mingchenchen@cpl.ac.cn

1 Introduction

Protein–protein interactions (PPIs) underpin nearly all cellular processes and represent a primary class of therapeutic targets. The ability to design proteins that bind specific epitopes with high affinity and precision would revolutionize applications in pathway modulation, diagnostics, and biologic drug development [1]. Traditional binder discovery, relying on immunization [2], library screening [3, 4], and directed evolution [5, 6], remains resource-intensive and often offers limited control over the targeted epitope or the resulting molecular geometry.

Deep learning has recently catalyzed a paradigm shift in *de novo* protein design. Generative approaches utilizing structure hallucination [7, 8], inverse folding [1, 9], and diffusion models [10, 11] have enabled the creation of novel folds and functional binders. Notable frameworks such as RFdiffusion and BindCraft have significantly improved backbone sampling and diversity, and design of binders [10, 12, 13, 14]. However, a critical bottleneck remains: most computationally designed binders exhibit only modest affinities, typically requiring extensive experimental screening or iterative *in vitro* maturation to achieve therapeutic relevance.

Achieving high-affinity binding is fundamentally more challenging than generating plausible interfaces. High-affinity PPIs require exacting geometric complementarity, optimized side-chain packing, and cooperative interactions that are difficult for backbone-centric generative models to capture [14]. Antibodies, which naturally achieve strong and specific protein–protein interactions, therefore represent a particularly stringent benchmark for *de novo* design. While recent advances in *de novo* antibody design, such as RFantibody and Germinal, have expanded the accessible space for complementarity-determining regions (CDRs) [11, 15], generation of high-affinity binders and single-domain antibodies (VHHs) with high success rate and without the need for library-based directed evolution remains an elusive goal.

Flow matching has recently emerged as a powerful alternative to diffusion, offering superior training stability and efficient sampling by learning continuous mappings between simple distributions and com-

plex structures [16, 17, 18, 19]. Here, we introduce **PPIFlow**, a flow-matching–based framework and integrated design workflow for the *de novo* generation of high-affinity binders targeting precise epitopes (Fig. 1a). PPIFlow integrates a pairformer module to explicitly model interface contacts and utilizes a multi-stage training scheme for robust generalization across diverse protein scaffolds. To achieve *in silico* affinity maturation, we introduce three key innovations: (i) **interface rotamer enrichment** to identify energetically optimal residues; (ii) **partial flow refinement** to optimize interface packing by perturbing and regenerating existing designs; and (iii) **AF3Score**, an efficient score-only adaption of AlphaFold3 (Fig. 1c) for high-confidence complex prioritization[20].

Using this integrated platform, we demonstrate unprecedented performance, successfully generating pM-affinity binders for six out of seven diverse therapeutic targets and pM to nM-affinity VHHs for seven out of eight targets. These results establish PPIFlow as a reliable platform for the *de novo* design of protein and antibody therapeutics with epitope precision.

2 Results

2.1 A flow matching based protein generation model

PPIFlow models protein binder design as a continuous rigid-body flow. We represent protein backbones as collections of rigid residue frames in SE(3) [21] (Fig. 1a). Unlike diffusion-based approaches [10], PPIFlow employs flow matching to directly learn the translational and rotational velocity fields that transport random distributions to physically realistic structures [16, 18]. This formulation provides a geometrically consistent parameterization of rigid-body dynamics, enabling stable training and precise conditioning on interface constraints.

The pairformer module jointly updates residue-level and pairwise embeddings to explicitly capture structured geometric relationships across binding interfaces [22]. These representations are decoded into frame updates via Invariant Point Attention (IPA) [21], balancing generation accuracy with parameter efficiency (Fig. 2c).

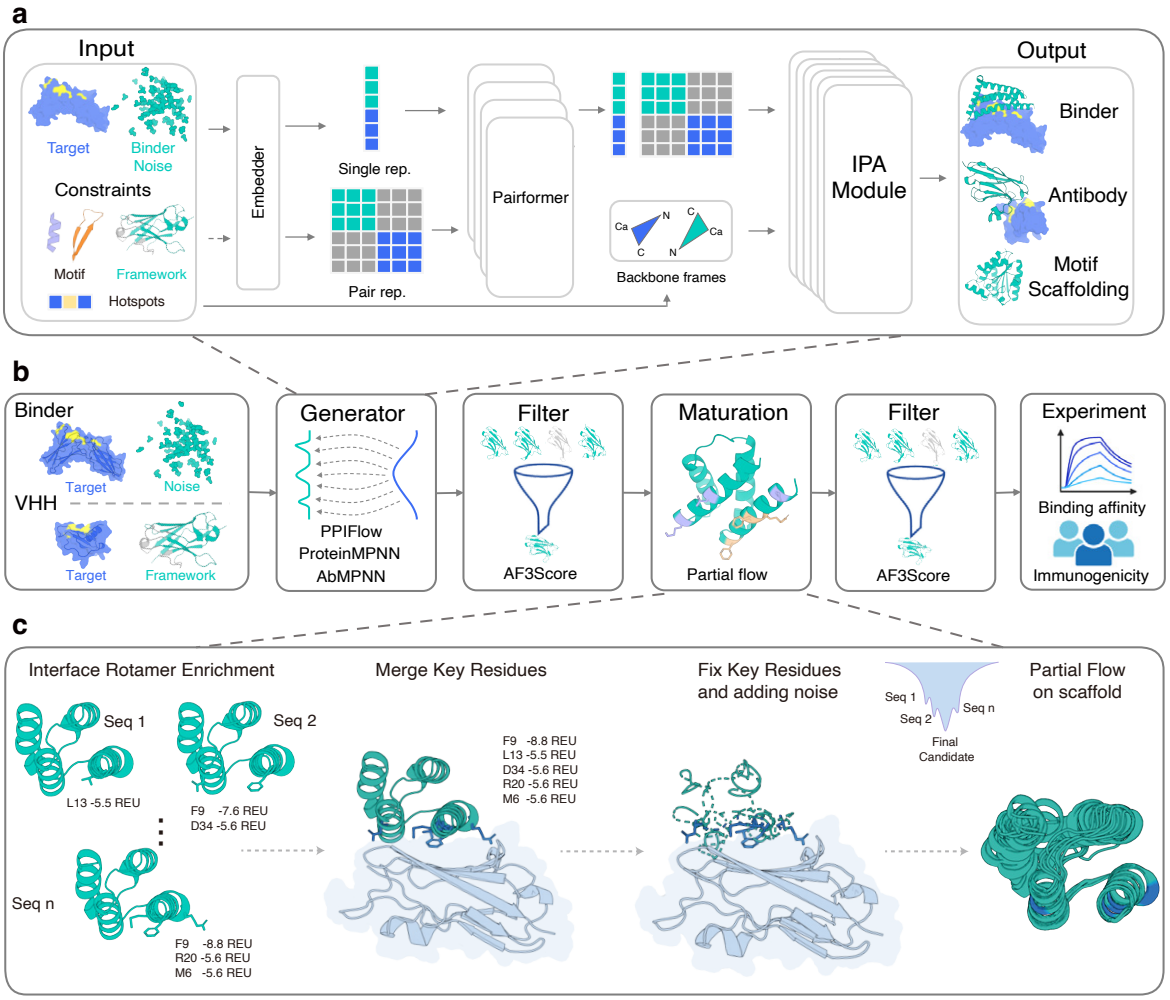

Figure 1: PPIFlow model architecture and high-affinity design workflow. a, Overview of the PPIFlow model framework. b, End-to-end design pipeline. PPIFlow-generated backbones undergo sequence design via ProteinMPNN (monomers, motifs, binders) or AbMPNN (VHHs, scFvs). High-confidence candidates are identified via AF3Score filtering and prioritized for *in silico* maturation and template-free AlphaFold3 validation. c, *In silico* maturation strategy: (1) interface rotamer enrichment to identify energetically favorable residues; (2) selection and merging of key interface residues; (3) fixation of critical residues with concomitant noise addition to neighboring backbone regions; and (4) partial flow-based refinement of unconstrained regions to optimize interfacial packing.

Training follows a staged curriculum that adapts the model from general backbone generation to constrained PPI design (Fig. 2a). Optimization relies on a flow-matching objective [17] supplemented by auxiliary geometric loss terms to promote interface stability. We validated these design choices through ablation studies, and demonstrated that both staged curriculum and geometric constraints are critical for achieving robust binder generation (Fig. 2b).

2.2 PPIFlow generates high-designability proteins

PPIFlow performs robustly across five generative tasks. For monomers (up to 700 residues), the model achieved >90% design success (scRMSD $<$ 2 Å vs. ESMFold) while maintaining structural novelty and diversity (Fig. 2d; Fig. S1) [23, 24, 10, 18, 13]. In motif scaffolding, PPIFlow outperformed state-of-the-art methods on MotifBench (score 42.38 vs. 28.6 for RFdiffusion) [25], solving challenging multi-segment cases (e.g., 4JHW, 4XOJ) where prior approaches failed (Fig. S2) [10, 26].

We further validated PPIFlow on minibinder design (75/120/160/200 residues) against 15 diverse targets. The model surpassed recent open-source methods like RFdiffusion, BindCraft and BoltzGen in design success, novelty, and diversity (Fig. 2e and Fig. S3) [12, 27]. Notably, PPIFlow shows a pronounced advantage for larger binders, as reflected by both AF3Score-based designability and Rosetta-derived interface energetics. This length-dependent improvement likely stems from the multi-stage training strategy combined with PPIFlow's outstanding monomer designability (Fig. S3).

In VHH and antibody design, PPIFlow generated diverse CDRs while preserving input frameworks (median RMSD 0.18 Å) (Fig. S4, S5). The model targeted epitopes precisely (median hotspot coverage > 0.9) (Fig. 2f), yielding complexes with well-packed, high-quality interactions (Fig. 2g).

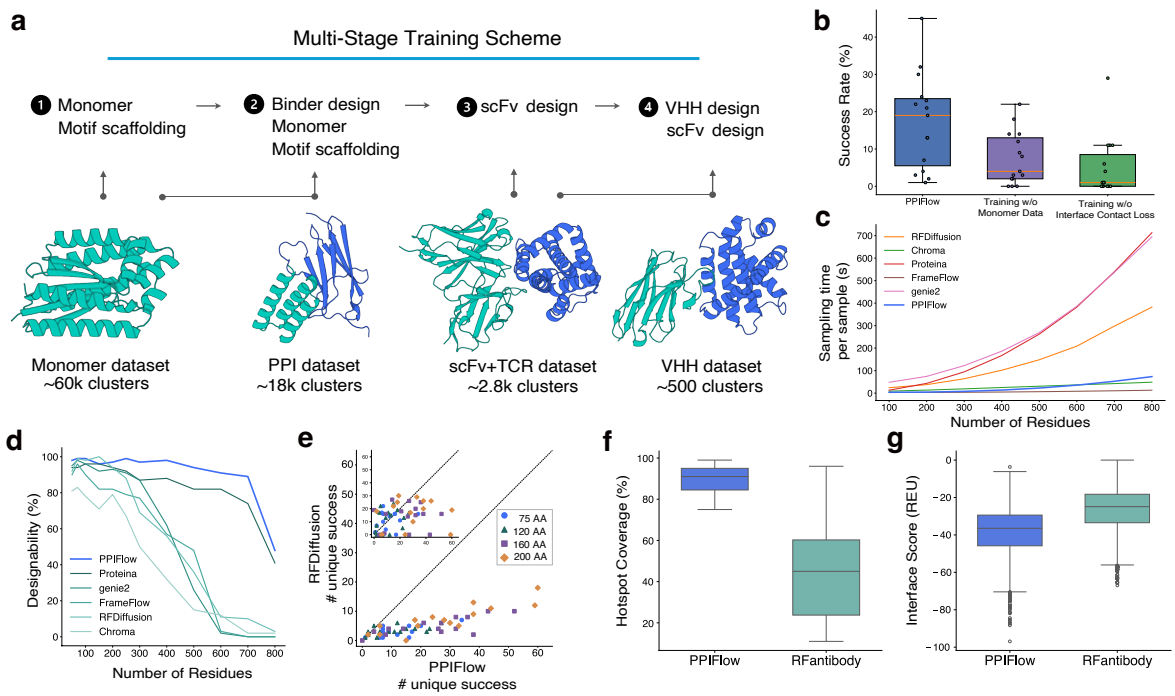

Figure 2: Training curriculum and *in silico* performance benchmarks. a, Multi-stage training scheme of PPIFlow. The foundation model is first trained on a monomeric protein dataset for structure recovery and scaffolding. Subsequent fine-tuning stages progressively adapt the model to protein–protein interactions (PPI), scFv generation, and VHH design, leveraging both general and antibody-specific datasets to preserve framework integrity. b, Ablation analysis of the training objective, highlighting the necessity of monomer dataset integration and interface contact loss for optimal binder design. c, Inference efficiency comparison of PPIFlow against representative generative architectures. d, Designability benchmarks for monomers. e, Designability benchmarks for binders, inset: comparison between PPIFlow (x-axis) & BindCraft (y-axis). f–g, VHH design quality metrics, including predicted hotspot coverage (**f**) and Rosetta interface scores (**g**) for generated antibody–antigen complexes.

2.3 High-affinity design via interface rotamer enrichment and partial flow

While generative models have streamlined binder design [28], achieving picomolar affinity typically requires experimental optimization. To bridge this gap, we developed a pipeline integrating interface rotamer enrichment with partial flow refinement (Fig. 1c). In the **initial generation stage**, PPIFlow generates backbones targeting a predefined epitope (Fig. 1b). We design sequences using ProteinMPNN [29] or AbMPNN [30] and filter candidates via AF3Score to retain structurally plausible designs.

During maturation, we identify energetic "anchor" residues (< -5 Rosetta Energy Units) on the interface [31]. We fix these rotamers while perturbing the backbone to an intermediate flow state ($t = 0.6$). Crucially, this plasticity allows the backbone to escape local minima and resolve steric clashes

imposed by the anchors, reshaping the binding interface rather than merely repacking side chains [32]. We then regenerate perturbed regions and redesign unconstrained sequences ($T = 0.1$). This active remodeling accommodates enriched residues and significantly improves binding compatibility (Fig. S3).

Matured designs are re-evaluated via AF3Score, Rosetta Interface Analyzer, and template-free AlphaFold3. We prioritize the top 30 candidates, selected by a composite score (AF3 ipTM $\times$ 100 $-$ Rosetta interface score), for experimental validation.

2.4 *De novo* design of high-affinity mini-binders

To experimentally validate the pipeline, we designed *de novo* binders against seven therapeutically relevant targets: IL7RA, IFNAR2, IL17A, PD-L1, TRKA, PDGFR, and VEGFA (Fig. 3a). Spanning diverse structural classes and functional roles in oncology and autoimmune disease, these targets provide a stringent benchmark. We characterized 30 candidates per target; all 210 expressed successfully, with 76 (36.2%) binders showing affinities better than 1 μM by Bio-Layer Interferometry (BLI) (Fig. 3b,c; Fig. S6; Table S7), spanning diverse structures and sequences (Table S6,S7). Notably, we identified picomolar-affinity binders for six of the seven targets without post-design experimental optimization.

Success stems largely from the *in silico* maturation stage. Structural comparisons reveal that interface rotamer enrichment followed by partial flow creates compact, highly connected interfaces featuring specific hydrogen bonds, salt bridges, and hydrophobic interactions formed during refinement (Fig. 3d,e; Fig. S9). Across all targets, this maturation systematically improved folding confidence and interface quality, significantly increasing AF3Score pTM and ipTM values (Fig. 3f). In the case of IFNAR2, interface rotamer enrichment markedly outperformed baseline pipelines, yielding superior interface metrics (Fig. 3g,h).

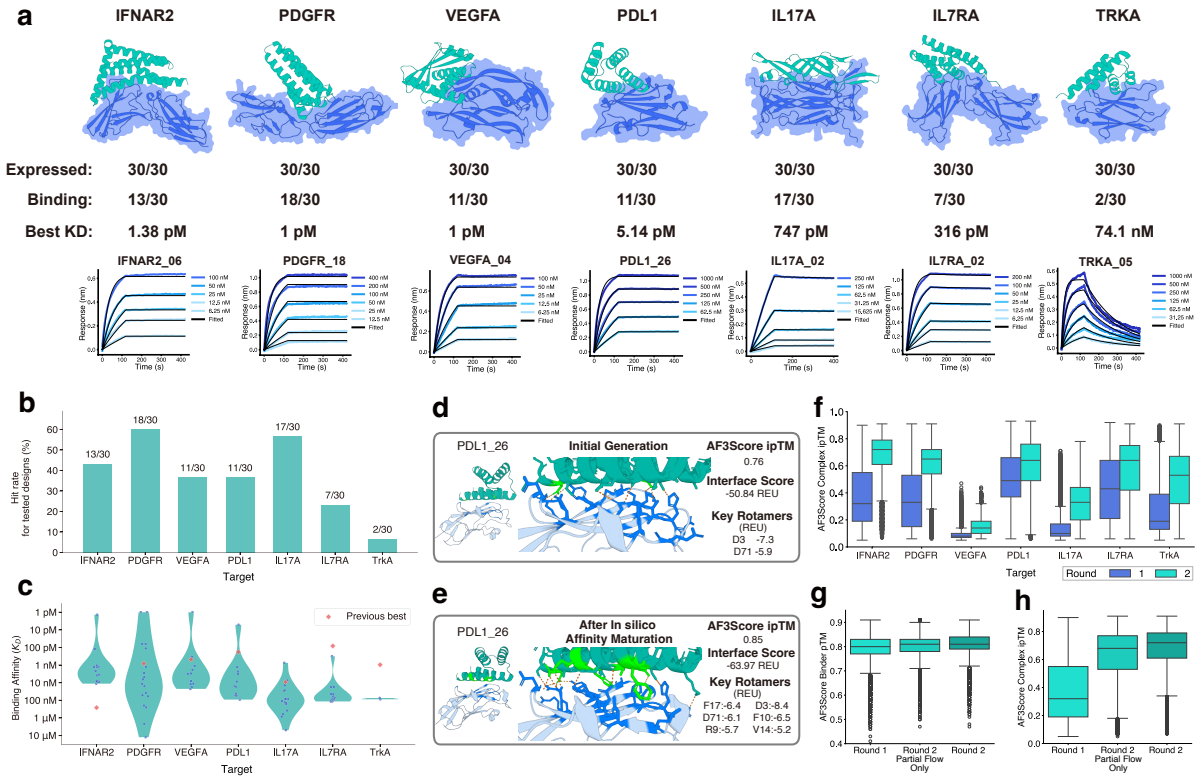

Figure 3: Experimental validation and high-affinity binder generation. a, Structural models of the highest-affinity *de novo* binders for each target. Accompanying data include expression success, binding hit rates, peak affinities, and representative BLI sensorgrams. b–c, Experimental performance across seven therapeutic targets, showing (**b**) hit rates and (**c**) the distribution of binding affinities (violin plots), demonstrating consistent picomolar-to-nanomolar potency. d–e, Illustration of interface side-chain packing after (**d**) initial generation and after (**e**) *in silico* affinity maturation for PDL1_26. f, Comparison of AF3Score profiles between initial Round 1 designs and matured Round 2 designs, illustrating the systematic quality improvement achieved through *in silico* maturation. g–h, Performance comparison of design strategies for IFNAR2. Metrics for AF3Score pTM (**g**) and ipTM (**h**) demonstrate that interface rotamer enrichment combined with partial flow refinement markedly outperforms both Round 1 baselines and partial flow alone.

2.5 *De novo* design of high-affinity VHHs

We extended PPIFlow to the *de novo* generation of single-domain antibodies (VHHs) against eight therapeutic targets: CCL2, HNMT, PDGFR, 1433E, BHRF1, S100A4, EFNA1, and IL13. To prioritize developability, we sampled frameworks from five therapeutically validated scaffolds, generating and maturing CDRs via the PPIFlow-VHH pipeline (see Supplementary Information).

BLI characterization of 240 candidates (30 per target) confirmed 100% expression success. We identified binders for seven of the eight targets, with several achieving exceptional potency without optimization. Notably, VHH CCL2_21 reached 250 pM affinity, while binders for HNMT, PDGFR, and 1433E achieved single-digit nM affinities (Fig. 4a). The overall hit rate was 33.8% (81/240), with 27.9% (67/240) showing affinities better than 1 μM, and these successful designs span diverse structures and sequences (Fig. 4b,c; Fig. S7; Table S6,S8).

As with general protein binders, AF3Score analysis confirms that *in silico* maturation, combining interface rotamer enrichment with partial flow, was critical. This stage systematically improved structural confidence and interface quality (Fig. 4f), evidenced by compact side-chain packing and energetically favorable interactions (Fig. 4d,e; Fig. S10). Benchmarks on CCL2 show that interface rotamer enrichment significantly outperforms baselines, yielding higher AF3Score ipTM values and superior experimental outcomes (Fig. 4g,h).

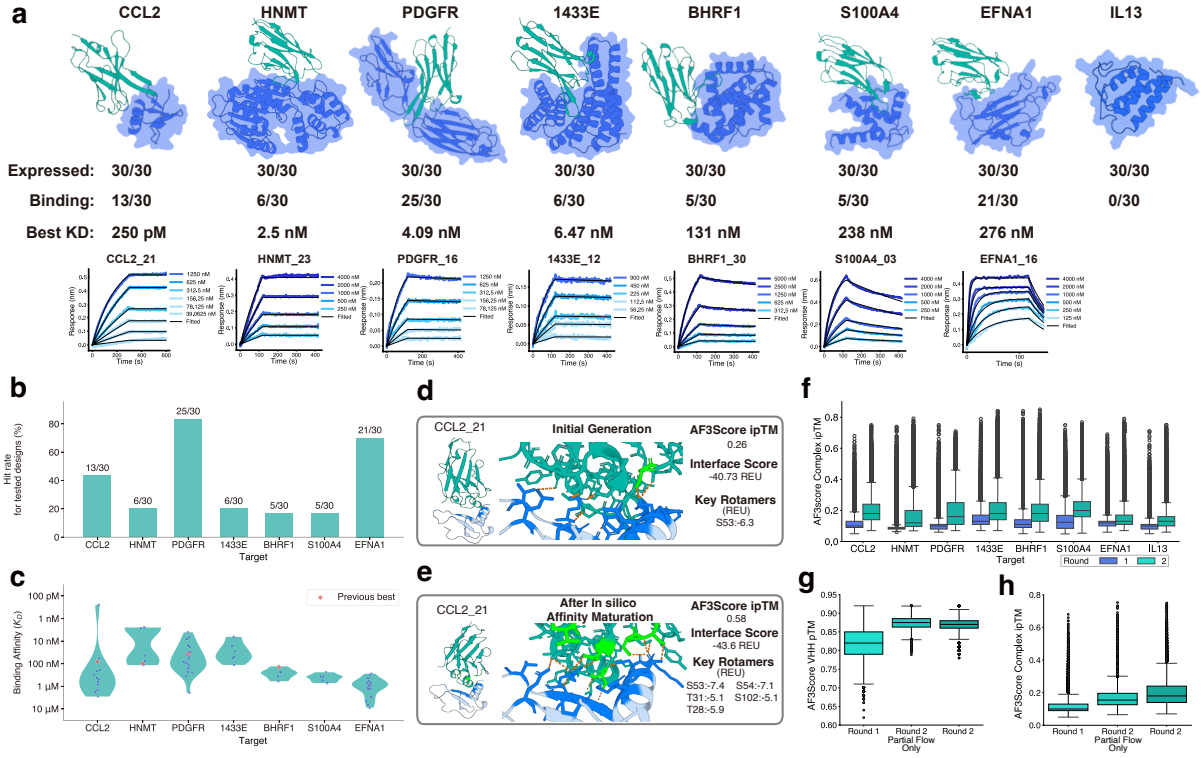

Figure 4: Computational design and experimental validation of high-affinity VHHs. a, Structural models of the highest-affinity *de novo* VHHs for each target, paired with expression data, binding hit rates, peak affinities (K_D), and representative BLI sensorgrams. b–c, Experimental performance across VHH targets, showing (**b**) hit rates and (**c**) affinity distributions (violin plots), highlighting the discovery of sub-nanomolar binders for CCL2, PDGFR, and 1433E. d–e, Illustration of interface side-chain packing after (**d**) initial generation and after (**e**) *in silico* affinity maturation for CCL2_21. f, Comparison of AF3Score profiles between initial (Round 1) and matured (Round 2) VHH designs, demonstrating consistent improvement in predicted interface quality across all targets. g–h, Evaluation of design strategies for the CCL2 target. AF3Score pTM (**g**) and ipTM (**h**) metrics confirm that the full maturation protocol, integrating interface rotamer enrichment with partial flow, significantly outperforms baseline generative and refinement-only pipelines.

3 Discussion

The ability of PPIFlow to generate picomolar affinity binders and VHHs purely *in silico* marks a shift from "design-then-screen and optimize" toward de novo binder generation. Traditionally, bridging the "affinity gap" required massive experimental libraries or directed evolution. Recent retrospective analyses have shown that AlphaFold3 interface confidence scores are strongly predictive of experimental binding success and can therefore serve as an effective structural consistency filter [11]. By incorporating AF3Score, a score-only adaptation of AlphaFold3, PPIFlow bypasses MSA construction and iterative recycling, accelerating evaluation by approximately two orders of magnitude compared to standard inference [20]. This enables rapid, high-fidelity candidate prioritization without the computational burden of traditional protocols.

A central conceptual advance of this work is the integration of global backbone topology sampling with local interface optimization. While flow matching explores diverse architectures, interface rotamer enrichment acts as a computational analogue of affinity maturation. This hybrid approach resolves the tension between broad fold exploration and the stringent geometric requirements of high-affinity binding, addressing the observation that high in silico designability alone does not guarantee experimental success [28, 27].

Although PPIFlow outperforms existing methods such as BindCraft on backbone feasibility metrics, its superior experimental hit rates also stem from the pipeline's synergy. Furthermore, PPIFlow significantly reduces the computational burden associated with binder design. Unlike protocols such as BindCraft that typically necessitate computationally expensive full AlphaFold predictions for filtering, our workflow leverages AF3Score to rank complexes directly, accelerating candidate prioritization by approximately 100-fold. Unlike standard generation methods, PPIFlow robustly accommodates the constraints imposed during "Interface Rotamer Enrichment", allowing the subsequent "Partial Flow" stage to refine packing without breaking the fold. Thus, it is not the generator in isolation, but the holistic integration of pairformer, energy-guided anchoring, and flow-based refinement that bridges the gap between

computational plausibility and picomolar potency.

Limitations remain. PPIFlow currently operates as a backbone-only generator, meaning side-chain packing is handled post-generation [33]. While our maturation pipeline mitigates this, a fully atomistic generative framework could more natively capture the highly specific hydrogen-bonding networks and hydrophobic packing required for certain complex interfaces. We also observed target-dependent variation in success rates. For example, IL13 remained challenging. In such cases, the interface rotamer enrichment stage may fail to identify stable energetic anchors ($<$ -5 REU), preventing effective partial flow refinement. Consistent with this, VHHs generated against IL13 showed systematically lower confidence scores (Fig. 4f).

Finally, the current model is limited to protein–protein complexes; extending the framework to nucleic acids, glycans, and small molecules is essential. Nevertheless, PPIFlow establishes a generalizable platform for rapid, purely computational binder design, significantly reducing reliance on experimental iteration.

4 Data and materials availability

The code and relevant data for PPIFlow will be available at https://github.com/Mingchenchen/PPIFlow. AF3Score is available at https://github.com/Mingchenchen/AF3Score: A Score-Only Adaptation of AlphaFold3 for Biomolecular Structure Evaluation. All relevant data will be available at Zenodo.

References

[1] Longxing Cao et al. “Design of protein-binding proteins from the target structure alone”. In: *Nature* 605.7910 (2022), pp. 551–560.

[2] Georges Köhler and Cesar Milstein. “Continuous cultures of fused cells secreting antibody of predefined specificity”. In: *Nature* 256.5517 (1975), pp. 495–497.

[3] George P Smith. “Filamentous fusion phage: novel expression vectors that display cloned antigens on the virion surface”. In: *Science* 228.4705 (1985), pp. 1315–1317.

[4] Greg Winter et al. “Making antibodies by phage display technology”. In: *Annual review of immunology* 12.1 (1994), pp. 433–455.

[5] Frances H Arnold. “Directed evolution: bringing new chemistry to life”. In: *Angewandte Chemie (International Ed. in English)* 57.16 (2017), p. 4143.

[6] Frances H Arnold. “Design by directed evolution”. In: *Accounts of chemical research* 31.3 (1998), pp. 125–131.

[7] Ivan Anishchenko et al. “De novo protein design by deep network hallucination”. In: *Nature* 600.7889 (2021), pp. 547–552.

[8] Jue Wang et al. “Scaffolding protein functional sites using deep learning”. In: *Science* 377.6604 (2022), pp. 387–394.

[9] Milong Ren et al. “Accurate and robust protein sequence design with CarbonDesign”. In: *Nature Machine Intelligence* 6.5 (2024), pp. 536–547.

[10] Joseph L Watson et al. “De novo design of protein structure and function with RFdiffusion”. In: *Nature* (2023), pp. 1–3.

[11] Nathaniel R Bennett et al. “Atomically accurate de novo design of antibodies with RFdiffusion”. In: *Nature* (2025), pp. 1–11.

[12] Martin Pacesa et al. “One-shot design of functional protein binders with BindCraft”. In: *Nature* 646.8084 (2025), pp. 483–492.

[13] John B Ingraham et al. “Illuminating protein space with a programmable generative model”. In: *Nature* 623.7989 (2023), pp. 1070–1078.

[14] Pablo Gainza et al. “De novo design of protein interactions with learned surface fingerprints”. In: *Nature* 617.7959 (2023), pp. 176–184.

[15] Luis S Mille-Fragoso et al. “Efficient generation of epitope-targeted de novo antibodies with Germinal”. In: *bioRxiv* (2025).

[16] Yaron Lipman et al. “Flow matching for generative modeling”. In: *International Conference on Learning Representations* (2023).

[17] Ricky T. Q. Chen and Yaron Lipman. “Flow Matching on General Geometries”. In: *International Conference on Learning Representations* (2024).

[18] Jason Yim et al. “Fast protein backbone generation with SE(3) flow matching”. In: *arXiv preprint arXiv:2310.05297* (2023).

[19] Avishek Joey Bose et al. “Se (3)-stochastic flow matching for protein backbone generation”. In: *arXiv preprint arXiv:2310.02391* (2023).

[20] Yu Liu et al. “Af3score: A score-only adaptation of alphafold3 for biomolecular structure evaluation”. In: *Journal of Chemical Information and Modeling* 65.15 (2025), pp. 8207–8214.

[21] John Jumper et al. “Highly accurate protein structure prediction with AlphaFold”. In: *Nature* 596.7873 (2021), pp. 583–589.

[22] Josh Abramson et al. “Accurate structure prediction of biomolecular interactions with AlphaFold 3”. In: *Nature* 630.8016 (2024), pp. 493–500.

[23] Yeqing Lin et al. “Out of many, one: Designing and scaffolding proteins at the scale of the structural universe with genie 2”. In: *arXiv preprint arXiv:2405.15489* (2024).

[24] Tomas Geffner et al. “Proteina: Scaling flow-based protein structure generative models”. In: *arXiv preprint arXiv:2503.00710* (2025).

[25] Zhuoqi Zheng et al. “MotifBench: A standardized protein design benchmark for motif-scaffolding problems”. In: *arXiv preprint arXiv:2502.12479* (2025).

[26] Tianyu Lu et al. “Conditional protein structure generation with protpardelle-1c”. In: *bioRxiv* (2025).

[27] Hannes Stark et al. “Boltzgen: Toward universal binder design”. In: *bioRxiv* (2025), pp. 2025–11.

[28] Nathaniel R Bennett et al. “Improving de novo protein binder design with deep learning”. In: *Nature Communications* 14.1 (2023), p. 2625.

[29] Justas Dauparas et al. “Robust deep learning–based protein sequence design using ProteinMPNN”. In: *Science* 378.6615 (2022), pp. 49–56.

[30] Frédéric A Dreyer et al. “Inverse folding for antibody sequence design using deep learning”. In: *arXiv preprint arXiv:2310.19513* (2023).

[31] Rebecca F Alford et al. “The Rosetta all-atom energy function for macromolecular modeling and design”. In: *Journal of chemical theory and computation* 13.6 (2017), pp. 3031–3048.

[32] Matthias Glögl et al. “Target-conditioned diffusion generates potent TNFR superfamily antagonists and agonists”. In: *Science* 386.6726 (2024), pp. 1154–1161.

[33] Jin Sub Lee and Philip M Kim. “FlowPacker: protein side-chain packing with torsional flow matching”. In: *Bioinformatics* 41.3 (2025), btaf010.

[34] Ian Sillitoe et al. “CATH: increased structural coverage of functional space”. In: *Nucleic acids research* 49.D1 (2021), pp. D266–D273.

[35] Helen M Berman et al. “The protein data bank”. In: *Nucleic acids research* 28.1 (2000), pp. 235–242.

[36] Martin Steinegger and Johannes Söding. “MMseqs2 enables sensitive protein sequence searching for the analysis of massive data sets”. In: *Nature biotechnology* 35.11 (2017), pp. 1026–1028.

[37] James Dunbar et al. “SAbDab: the structural antibody database”. In: *Nucleic acids research* 42.D1 (2014), pp. D1140–D1146.

Supplementary Information

Contents

1 Introduction **2**

2 Results **3**

2.1 A flow matching based protein generation model 3

2.2 PPIFlow generates high-designability proteins 5

2.3 High-affinity design via interface rotamer enrichment and partial flow 6

2.4 *De novo* design of high-affinity mini-binders 7

2.5 *De novo* design of high-affinity VHHs 9

3 Discussion **11**

4 Data and materials availability **12**

A Supplementary Methods **18**

A.1 Notation 18

A.2 Datasets 18

A.2.1 Data Curation 18

A.2.2 Input Features 20

A.3 Input Embeddings 20

A.4 Model Architecture 23

A.5 Loss Functions 24

A.6 Training and Inference Details 26

A.7 Ablation Studies 29

B Design Workflow **30**

B.1 Binder design workflow 30

B.2 VHH design workflow 31

C Experimental Materials & Methods **32**

C.1 Binder experimental methods 32

C.1.1 Gene Synthesis and Subcloning 32

C.1.2 Cell-Free Protein Expression 32

C.1.3 Cell-Free Protein Purification and Analysis 33

C.1.4 Target protein preparation 33

C.1.5 Binding characterization of binders 33

C.2 VHH experimental methods 35

C.2.1 Framework selection 35

C.2.2 Gene Synthesis and Subcloning 35

C.2.3 VHHs Expression in CHO Cells 36

C.2.4 Protein Purification and Analysis 36

C.2.5 Target protein preparation 36

C.2.6 Binding characterization of VHHs 36

D Supplementary Figures **39**

E Supplementary Tables **58**

Appendix A Supplementary Methods

A.1 Notation

We denote the number of residues in a protein structure by N, and each residue is represented by a *frame* $T = (x, r) \in \mathrm{SE}(3)$, where $x \in \mathbb{R}^3$ denotes a translation vector and $r \in \mathrm{SO}(3)$ a rotation matrix. Our model generates backbone atoms, i.e. $\Omega = \{N, C, C_\alpha, O\}$, and we denote by $z \in \mathbb{R}^3$ the global coordinates of a single atom. For binder design tasks, we denote the target backbone atoms and the binder backbone atoms by $\mathcal{B}$ and $\mathcal{T}$ respectively. The set of atom pairs between the target and the binder whose backbone atoms are separated by a distance less than 10 Å is denoted by $\mathcal{P}$ which is used in loss computation.

We establish the following notation for operators employed in the subsequent algorithms. Capitalized operator names are exclusively reserved for modules containing learnable parameters. For instance, LINEAR signifies a parameterized linear transformation, defined by a weight matrix W and a bias vector b. The term LAYERNORM specifically denotes layer normalization applied across the channel dimensions. Conversely, lowercase names are utilized for functions that operate without learnable parameters (e.g., `sigmoid`, `softmax`) and standard non-parameterized mathematical operations (e.g., `sin`, `cos`, and `exp`).

A.2 Datasets

A.2.1 Data Curation

We curated a unified structural dataset comprising three complementary data sources: monomeric protein structures, protein–protein interaction (PPI) complexes, and antibody-like binders, including VHH and scFv.

Monomeric protein structures were obtained from two sources: protein domains curated in the CATH database [34] and single-chain structures from the RCSB Protein Data Bank (PDB) [35]. We filtered the data based on the following criteria:

- non canonical amino acid ratio less than 20%.
- Sequence length is between 25 and 512.
- Coil percent is less than 0.8
- Radius of gyration is within the lowest 96% of the distribution.

Sequence redundancy was reduced by clustering all sequences using MMseqs2 [36]. After filtering and deduplication, the monomer dataset comprised approximately 60k clusters, spanning a broad range of lengths and folds. This dataset was used primarily for unconditional structure learning, enabling the model to learn general protein structures.

We curated a protein–protein interaction (PPI) dataset consisting of both chain–chain interactions (CCI) and domain–domain interactions (DDI). We filter the data based on the following criteria:

- number of contact pairs larger than 80 where contact pair is defined as interchain residues within the distance of 10 Å.
- non canonical amino acid ratio less than 20%.
- structure similarity between target and binder is less than 0.6.
- binder radius of gyration divided by length less than k, where $k = 0.15$ if binder size is larger than 100, $k = 0.16$ if binder size is between 70 and 100, $k = 0.18$ if binder size is less than 70.
- binder main chain SASA ration is less than 17.
- Sequence length is less than 570.
- Binder sequence length is less than 256 and target sequence length is larger than 30.

After filtering and redundancy removal, the combined CCI + DDI dataset contained approximately 18k interaction pairs. This dataset was used to train the model to capture general interface geometry and inter-chain spatial organization, which are essential for downstream binder generation.

Table S1: Input features to the model. N is the number of residues.

Feature & Shape	Description
`aatype` [N]	The input amino acid sequence.
`residue_index` [N]	The index into the original amino acid sequence.
`chain_index` [N]	0 for the target chain and 1 for the binder chain.
`diffuse_mask` [N]	0 for the diffused regions to be generated and 1 for the conditioned regions (e.g., target or motifs).
`hotspot_mask` [N]	Indicating whether a residue is a hotspot.
`noise_level` [N]	Representing the amount of noise injected at the current timestep, ranging from 0 to 1.
`noised_trans` [$N, 3$]	Noised CA coordinates.

To specialize the model for antibody-like binder design, we curated a dataset of antibody, VHH and TCR structures from SAbDab [37]. The dataset comprised approximately 6.9k antibody structures, 1.2k VHH structures, and 350 TCR structures, clustered into 2.6k, 500 and 200 clusters, respectively.

A.2.2 Input Features

In Table S1, we list the input features to the model. These features will be embedded into the single embedding network and pair embedding network.

A.3 Input Embeddings

Initial embedding details are presented in Algorithm 1 and Algorithm 2.

Algorithm 1: Embeddings for initial single representations

def `SingleEmbedder(`$\{\mathbf{f}_i^{aatype}\}, \{\mathbf{f}_i^{residue_index}\}, \{\mathbf{f}_i^{chain_index}\}, \{\mathbf{f}_i^{diffuse_mask}\}, \{\mathbf{f}_i^{hotspot_mask}\}, \{\mathbf{f}_i^{noise_level}\}$`)`**:**

$\mathbf{r}_i = \text{ResidueIndexEmbedder}(\mathbf{f}_i^{\text{residue_index}})$

$\mathbf{n}_i = \text{NoiseLevelEmbedder}(\mathbf{f}_i^{\text{noise_level}})$

$\mathbf{a}_i = \text{Linear}(\text{one_hot}(\mathbf{f}_i^{\text{aatype}}))$

$\mathbf{o}_i = \text{concat}(\mathbf{r}_i, \mathbf{n}_i, \mathbf{a}_i, \mathbf{f}_i^{\text{chain_index}}, \mathbf{f}_i^{\text{diffuse_mask}}, \mathbf{f}_i^{\text{hotspot_mask}})$

$\mathbf{s}_i = \text{Linear}(\mathbf{o}_i)$ $\qquad \mathbf{s}_i \in \mathbb{R}^{c_s},\ c_s = 256$

return $\{\mathbf{s_i}\}$

Algorithm 2: Embeddings for initial pair representations

def `PairEmbedder(`$\{\mathbf{s}_i\}, \{\mathbf{f}_i^{residue_index}\}, \{\mathbf{f}_i^{chain_index}\}, \{\mathbf{f}_i^{diffuse_mask}\}, \{\mathbf{f}_i^{noised_trans}\}$`)`**:**

$\mathbf{a}_i = \text{Linear}(\mathbf{s}_i)$

$\mathbf{n}_{ij} = \text{concat}(\mathbf{a}_i, \mathbf{a}_j)$

$\mathbf{r}_{ij} = \text{relpos}\left(\{\mathbf{f}_i^{\text{residue_index}}\}\right)$

$\{\mathbf{D}_{ij}\} = \text{distogram}\left(\{\mathbf{f}_i^{\text{noised_trans}}\}\right)$

$\mathbf{m}_{ij} = \text{concat}(\mathbf{f}_i^{\text{diffuse_mask}}, \mathbf{f}_j^{\text{diffuse_mask}})$

$\mathbf{e}_{ij} = \text{concat}(\mathbf{n}_{ij}, \mathbf{r}_{ij}, \mathbf{D}_{ij}, \mathbf{m}_{ij})$

$\mathbf{z}_{ij} = \text{Linear}(\mathbf{e}_{ij})$ $\qquad \mathbf{z}_{ij} \in \mathbb{R}^{c_z \times c_z},\ c_z = 128$

return $\{\mathbf{z}_{ij}\}$

Algorithm 3: Embeddings for residue index

def `ResidueIndexEmbedder` $(\{\mathbf{f}_i^{residue_index}\}, embed_size = 128, max_len = 2056)$ **:**

$k = \text{arange}\left(\frac{\text{embed_size}}{2}\right)$

$\mathbf{p}_i = \sin(\mathbf{f}_i^{\text{residue_index}} \times \frac{\pi}{(\text{max_len})^{(2k/\text{embed_size})}})$

$\mathbf{q}_i = \cos(\mathbf{f}_i^{\text{residue_index}} \times \frac{\pi}{(\text{max_len})^{(2k/\text{embed_size})}})$

$\mathbf{r}_i = \text{concat}(\mathbf{p}_i, \mathbf{q}_i)$

return $\{\mathbf{r}_i\}$

Algorithm 4: Embeddings for noise level

def `NoiseLevelEmbedder` $(\{\mathbf{f}_i^{noise_level}\}, embed_size = 128, max_positions = 2056)$ **:**

$t_i = \mathbf{f}_i^{\text{noise_level}} \times \text{max_positions}$

$\text{half_dim} = \left\lfloor \frac{\text{embed_size}}{2} \right\rfloor$

$\text{scale} = \frac{\log(\text{max_positions})}{\text{half_dim}-1}$

$\text{freq} = \exp(-\text{arange}(\text{half_dim}) \times \text{scale})$

$\mathbf{p}_i = t_i \times \text{freq}$

$\mathbf{n}_i = \text{concat}(\sin(\mathbf{p}_i), \cos(\mathbf{p}_i))$

return $\{\mathbf{n}_i\}$

Algorithm 5: Relative position encoding

def `relpos` $(\{\mathbf{f}_i^{residue_index}\})$ **:**

$\mathbf{d}_{ij} = \mathbf{f}_i^{\text{residue_index}} - \mathbf{f}_j^{\text{residue_index}}$

$\mathbf{r}_{ij} = \text{ResidueIndexEmbedder}(\mathbf{d}_{ij})$

$\mathbf{r}_{ij} = \text{Linear}(\mathbf{r}_{ij})$

return $\{\mathbf{r}_{ij}\}$

Algorithm 6: Compute distogram from atomic coordinates

def `distogram`$(\{\mathbf{p}_i\}, \mathbf{d}_{\min}, \mathbf{d}_{\max}, K)$**:**

  $\mathbf{d}_{ij} \leftarrow \|\mathbf{p}_i - \mathbf{p}_j\|_2$

  $\mathbf{b}_k = \mathbf{d}_{\min} + (k-1)\frac{\mathbf{d}_{\max} - \mathbf{d}_{\min}}{K-1}$ for $k = 1 \ldots K$

  for $i, j = 1 \ldots N$ **do**

    for $k = 1 \ldots K$ **do**

      $\mathbf{D}_{ij,k} \leftarrow 1[\,\mathbf{b}_k < \mathbf{d}_{ij} \leq \mathbf{b}_{k+1}\,]$

  return $\{\mathbf{D}_{ij}\}$

A.4 Model Architecture

Our model follows a hierarchical architecture that integrates both sequence-level and structure-level reasoning. Specifically, we employ two key components that have become standard in protein structure modeling: the **Pairformer** and the **Invariant Point Attention (IPA)** module.

The Pairformer module is used to jointly model residue-wise and pairwise representations through interleaved attention and transition layers. It allows effective information exchange between the one-dimensional sequence features and the two-dimensional pairwise geometric features, enabling the network to reason about both local and long-range residue interactions. We adopt the standard Pairformer design as introduced in AlphaFold-style architectures, without modification. We use 4 Pairformer blocks in our model.

Following AlphaFold [21], we use the Invariant Point Attention module to transform pairwise relational information into 3D coordinate updates. The IPA performs attention over residue embeddings in SE(3)-invariant space, ensuring that the resulting structural representations are equivariant to rotations and translations. This design allows the model to learn spatial relationships in a physically meaningful and symmetry-preserving manner. Our model includes 6 IPA layers.

Our model consists of 23.2M parameters. Together, these modules enable our model to integrate sequence context, pairwise geometry, and spatial reasoning in a unified framework for protein structure

generation and refinement.

A.5 Loss Functions

Flow matching loss in $\mathrm{SE}(3)$**.** Following the flow-matching framework, the model learns to predict the continuous velocity field that transforms a noisy structure toward its clean counterpart. Each residue is represented in $\mathrm{SE}(3)$ space by a translation vector $x \in \mathbb{R}^3$ and a rotation matrix $r \in \mathrm{SO}(3)$.

Given a clean structure $\mathbf{T}_1$ and a noisy structure $\mathbf{T}_t$ sampled along the flow trajectory, the target velocity is defined as the time derivative of the flow:

$$\mathbf{v}_t = \frac{d\mathbf{T}_t}{dt}. \tag{1}$$

The $\mathrm{SE}(3)$ flow-matching loss minimizes the discrepancy between predicted and ground-truth velocities on both translational and rotational components:

$$\mathcal{L}_{\text{flow}} = \mathbb{E}_{t,\, p_0,\, p_1}\left[\sum_{i=1}^{N}\left(\left\|\hat{\mathbf{v}}_{t,x}^{(i)}(\mathbf{T}_t, t) - \mathbf{v}_{t,x}^{(i)}\right\|_{\mathbb{R}^3}^2 + \left\|\hat{\mathbf{v}}_{t,r}^{(i)}(\mathbf{T}_t, t) - \mathbf{v}_{t,r}^{(i)}\right\|_{\mathrm{SO}(3)}^2\right)\right],$$

where p_0 and p_1 denote noise distribution and data distribution respectively, $p_0 = \mathcal{N}(0, I_3) \otimes \mathcal{U}(\mathrm{SO}(3))$, $t \sim \mathcal{U}([0, 1])$.

Following FrameFlow [18], the model predicts the clean frames $\mathbf{T}_1$ given the corrupted frames $\mathbf{T}_t$ at time t, and the velocity can be approximated as

$$\hat{\mathbf{v}}_{t,x}^{(i)} = \frac{\hat{\mathbf{x}}_1^{(i)} - \mathbf{x}_t^{(i)}}{1 - t} \tag{2}$$

$$\hat{\mathbf{v}}_{t,r}^{(i)} = \frac{\log_{\mathbf{r}_t^{(i)}}(\hat{\mathbf{r}}_1^{(i)})}{1 - t}, \tag{3}$$

where $\log_{\mathbf{r}_t^{(i)}}$ is the logarithmic map on $\mathrm{SO}(3)$. As a result, the objective can be reparameterized as

$$\mathcal{L}_{\text{flow}} = \mathbb{E}_{t,\,p_0,\,p_1}\Bigg[\frac{1}{(1-t)^2}\sum_{i=1}^{N}\Big(\big\|\hat{\mathbf{x}}_1^{(i)}(\mathbf{T}_t,t)-\mathbf{x}_1^{(i)}\big\|_{\mathbb{R}^3}^2 + \big\|\log_{\mathbf{r}_t^{(i)}}\big(\hat{\mathbf{r}}_1^{(i)}(\mathbf{T}_t,t)\big)-\log_{\mathbf{r}_t^{(i)}}\big(\mathbf{r}_1^{(i)}\big)\big\|_{\mathrm{SO}(3)}^2\Big)\Bigg]. \tag{4}$$

Interface contact loss. We introduce interface contact loss to improve the learning of target to binder interaction. Since we observed that some sampled results positioned binders too far from the target, leading to weak contacts, we designed this interface contact loss to improve the quality of interfaces. This loss is defined on residue pairs across binder and target. We examine on interchain residue pairs within 10 Å in native structures, and compare the predicted pairwise distances of these pairs against true pairwise distances. Let $\mathcal{P} = \big\{(i,j) \mid z_i \in \mathcal{B}, z_j \in \mathcal{T}, \|z_i - z_j\|_2 \leq 10\,\text{Å}\big\}$, where z_i and $\hat{z}_i$ are the ground-truth and predicted coordinates of backbone atoms respectively. Then the interface contact loss can be written as

$$\mathcal{L}_{\text{interface}} = \frac{1}{|\mathcal{P}|}\sum_{(i,j)\in\mathcal{P}} \big\|\|\hat{z}_i - \hat{z}_j\|_2 - \|z_i - z_j\|_2\big\|_2^2. \tag{5}$$

Backbone atom loss. The backbone atom coordinates are reconstructed from the predicted translation and rotation vectors, and we compute the mean squared error (MSE) between the predicted and ground-truth coordinates of the backbone atoms. The backbone atom loss is defined as

$$\mathcal{L}_{\text{bb}} = \frac{1}{|\mathcal{B}|}\sum_{i\in\mathcal{B}} \|\hat{z}_i - z_i\|_2^2. \tag{6}$$

Binder pairwise distance loss. By minimizing binder pairwise distance loss, the model is trained to accurately predict the spatial relationship (the pairwise distances) between residues in the binder, which is crucial for generating physically realistic proteins. This loss is defined as

Algorithm 7: SE(3) flow matching interpolation

```
def Interpolant(T_0, T_1, t):
    for i = 1, ..., N do
        // Translations
        x_t^(i) ← (1 − t) x_0^(i) + t x_1^(i)
        // Rotations
        r_t^(i) ← exp_{r_0^(i)}((1 − e^{−ct}) log_{r_0^(i)}(r_1^(i)))
        T_t^(i) ← (x_t^(i), r_t^(i))
    return T_t
```

Algorithm 8: PPIFlow training

```
def Train:
    while not converged do
        T_1 ~ p_1
        T^(0) ← SampleInit(N)
        t ~ U([0, 1])
        T_t ← Interpolant(T_0, T_1, t)
        if Uniform(0, 1) < 0.5 then
            // Train step without self-conditioning
            T̂_1^sc ← 0
        else
            // Train step with self-conditioning
            T̂_1^sc ← PPIFlow(T_t, t, 0)
            T̂_1^sc ← StopGradient(T̂_1^sc)
        T̂_1 ← PPIFlow(T_t, t, T̂_1^sc)
        θ = optimizer(θ, L, T_1, T̂_1)
```

$$\mathcal{L}_{\text{dist}} = \frac{1}{|\mathcal{B}|^2} \sum_{i,j \in \mathcal{B}} \| \|\hat{z}_i - \hat{z}_j\|_2 - \|z_i - z_j\|_2 \|_2^2. \tag{7}$$

A.6 Training and Inference Details

To enable our model to support diverse protein generation tasks—including monomer generation, motif scaffolding, binder design, scFv generation, and VHH generation—we adopt a multi-stage training strategy. The model is trained progressively in four stages, with each stage initializing from the checkpoint of the previous one. This staged training allows the model to first acquire general protein structural priors and then gradually specialize toward increasingly complex multi-chain and antibody-specific generation tasks. Algorithm 8 summarizes the training procedure. Below we introduce each training stage in detail.

The first stage: monomer pretraining with motif scaffolding. In the first stage, the model is trained on a large-scale monomeric protein dataset to learn general protein structures. During this stage, we jointly train the model on two tasks:

- Monomer generation, where the model learns to generate full-length single-chain protein structures.
- Motif scaffolding, where a subset of residues corresponding to functional or structural motifs is provided as conditioning input, and the model generates a complete protein scaffold consistent with the motif geometry.

During this stage, 20% of the samples are generated unconditionally, while for the remaining 80%, 10%–90% of residues are randomly selected as motifs, and the corruption is applied only to the non-motif residues. By mixing motif scaffolding with unconditional monomer generation, the model learns to preserve local structural constraints while maintaining global fold coherence. This stage establishes a strong structural prior and serves as the foundation for all subsequent finetuning stages.

The second stage: binder design finetuning. In the second stage, the model is finetuned for binder design where the model generates a binder protein conditioned on a target protein. Training data consist of a mixture of monomer structures and protein–protein complex (PPI) structures. The training objective is formulated as a multi-task mixture of: monomer generation, motif scaffolding, and binder design. Specifically, we downsample monomer data to 25% since the total amount of monomers is much larger than that of complexes. If a sample is monomer, then we follow the motif sample strategy used in the first stage. If a sample is a complex, then we generate the binder unconditional for 50% of the time and with motifs otherwise. For binder design task, we define target interface as residues whose CA position is within 10 Å to the binder. During training, we randomly select 0–20% percent of the interface residues as hotspots, and at least 3 hotspots are selected.

Including monomer and motif scaffolding tasks alongside binder design helps prevent catastrophic forgetting and stabilizes training (refer to ablation study). This stage equips the model with the ability

to reason about inter-chain geometric constraints and protein–protein interfaces, which are essential for downstream antibody-related tasks.

The third stage: scFv finetuning with framework conditioning. In the third stage, we finetune the model for single-chain variable fragment (scFv) generation, conditioned on a given antigen. Training data are collected from SAbDab and TCR. In this stage, the model is trained to generate an scFv structure given an antigen structure as input.

To support antibody–antigen systems and framework-aware generation, we introduce two key architectural modifications: chain group encoding and framework-aware pair embedding. Antibody–antigen complexes often contain multiple chains. Instead of using raw chain IDs, we replace them with chain group IDs, where all antigen chains belong to one group and all antibody chains belong to another. This modification enables the model to better distinguish inter-group (antigen–antibody) interactions from intra-group interactions while remaining invariant to arbitrary chain labeling. To explicitly control framework generation, we provide a reference framework structure as part of the input. We augment the pair embedding module with an additional layer that extracts pairwise distance features within the reference framework. These features are injected into the model's pair representations, allowing the model to condition on the reference framework geometry.

As a result, the model is trained to generate both the framework and CDR regions simultaneously, while ensuring that the generated framework remains highly consistent with the provided reference. This design allows controlled antibody generation without freezing or hard-constraining the framework coordinates.

The fourth stage: VHH finetuning. In the final stage, the model is finetuned for VHH (single-domain antibody) generation. Training data are drawn from SAbDab and TCR datasets, including both scFV and VHH. This stage reuses the architectural modifications introduced in the third stage, including chain group encoding and framework-aware pair embeddings. Because VHHs consist of a single variable domain, this stage further refines the model's ability to generate compact, stable antibody structures

Algorithm 9: PPIFlow inference

```
def SampleInit(N):
    // Random initial structure for N residues
    for i = 1, ..., N do
        x_0^(i) ~ N(0, I_3)^N
        r_0^(i) ~ U(SO(3))^N
        T_0^(i) ← (x_0^(i), r_0^(i))
    return T_0

def ReverseStep(T_t, T̂_1, c = 10):
    // One step of reverse flow
    for i = 1, ..., N do
        (x_t^(i), r_t^(i)) ← T_t^(i)
        (x̂_1^(i), r̂_1^(i)) ← T̂_1^(i)
        // Update translations
        x_{t+1/k}^(i) ← (x̂_1^(i) − x_t^(i)) / (1 − t) × 1/k
        // Update rotations
        r_{t+1/k}^(i) ← exp_{r_t^(i)}(c × log_{r_t^(i)}(r̂_1^(i)))
        T_{t+1/k}^(i) ← (x_{t+1/k}^(i), r_{t+1/k}^(i))
    return T_{t+1/k}

def Sample(N, k = 100):
    // Generation of N-residue backbone structure
    T_0 ← SampleInit(N)
    T̂_1^sc ← 0                          // Initialize self-conditioning
    for t = 0, 1/k, ..., (k − 1)/k do
        T̂_1 ← PPIFlow(T_t, t, T̂_1^sc)
        T_{t+1/k} ← ReverseStep(T_t, T̂_1)
        T̂_1^sc ← T̂_1
    return T_1
```

while preserving antigen-binding specificity.

A.7 Ablation Studies

To rigorously assess the contribution of key components in our binder design methodology, we conducted an ablation study focusing on two critical aspects: the training data strategy and the objective function.

Training data strategy ablation Our primary training strategy involves jointly utilizing data from both binder design tasks and monomer structures. To evaluate the necessity of this data mixture, we performed an ablation where the model was trained exclusively on data relevant to the binder design task, omitting the monomer structure data. We denote this variant as w/o Monomer Data.

Loss function ablation The full objective function incorporates an interface contact loss designed to explicitly guide the generation of favorable binding interfaces. We tested a variant, labeled w/o Interface Contact Loss, where this interface contact term was removed from the total loss during the training process.

The results demonstrate that both ablations lead to a degradation in the performance of the binder design task (Fig. 2b). Specifically, the w/o Monomer Data model exhibited a significant drop in pTM, indicating that the inclusion of monomer data is crucial for robust structural stability. Similarly, the w/o Interface Contact Loss variant showed diminished ability to generate high-quality interfaces, confirming that the explicit supervision provided by the interface contact loss is essential for optimizing inter-chain interactions.

These findings validate the necessity of both the mixed data training strategy and the interface contact loss term for achieving state-of-the-art results in protein binder design.

Appendix B Design Workflow

B.1 Binder design workflow

In the first design round, binder backbones were generated using PPIFlow and subsequently sequenced with ProteinMPNN. To balance sequence diversity and structural fidelity, ProteinMPNN was applied with a low sampling temperature (T = 0.2). As ProteinMPNN tends to under-sample bulky hydrophobic residues, such as phenylalanine, methionine, and tryptophan, which are often critical for stabilizing protein–protein interfaces, we adopted a dual-sequence design strategy. For each backbone, 8 sequences were generated using the vanilla ProteinMPNN checkpoint, while an additional 8 sequences were gener-

ated with bias toward large side-chain residues to enhance hydrophobic interactions at the interface. All designs were evaluated using AF3Score and filtered based on binder pTM and complex ipTM metrics to retain only structurally and functionally plausible complexes.

Candidates passing the first filtering stage were further optimized through an maturation process. Interface residues were analyzed using Rosetta residue-wise interaction energy calculations, and for each backbone, residues exhibiting strong energetic contributions (total interaction energy $<$ -5 Rosetta Energy Units) across the 16 designed sequences were merged to form an interface rotamer enriched design. To further refine the structural context of these enriched interfaces, we applied partial flow, a flow-matching analogue of partial diffusion. In this step, key interface residues were fixed, remaining backbone is perturbed to an intermediate flow state ($t = 0.6$). The perturbed regions were regenerated using PPIFlow. The unconstrained regions were then redesigned using the ProteinMPNN soluble checkpoint to improve folding stability (T = 0.1).

The matured designs were re-evaluated using AF3Score and filtered again based on binder pTM and complex ipTM. Surviving candidates were further assessed using AlphaFold3, and Rosetta interface analyzer. Top 30 candidates defined by a composite score (AF3_ipTM*100 - Interface Score) were selected for experimental validation.

B.2 VHH design workflow

For each target, 25,000 VHH backbone structures were sampled using PPIFlow-VHH. For each backbone, 8 CDR sequences were designed using ABMPNN with a sampling temperature of 0.5 to increase sequence diversity. All designs were evaluated using AF3Score, and candidates with ipTM $>$ 0.2 were retained for the second-round optimization. Interface residues were then analyzed using Rosetta residue-wise interaction energy calculations to identify key residues for binding.

In the second-round, for each backbone, interface residues with strong energetic contributions, total interaction energy < -5 Rosetta Energy Units, across the 8 first-round sequences were merged to construct a set of enriched interface rotamers. Partial flow was subsequently applied to the remaining

regions of the VHH backbone, while enriched key interface residues were held fixed, to regenerate 8 refined backbone conformations. For each refined structure, 4 sequences were redesigned using ABMPNN at a lower temperature (T = 0.1) to favor high-confidence sequence–structure compatibility.

All second-round designs were re-evaluated using AF3Score, and candidates with ipTM > 0.5 and pTM > 0.8 were subjected to further structural consistency validation with AlphaFold3. Designs were filtered based on agreement between AF3-predicted and designed structures (DockQ > 0.49), AF3 pTM > 0.8, and AF3 ipTM > 0.7. For each target, VHH candidates passing these filters were ranked by a composite score (AF3_ipTM*100 - Interface Score). Top 30 candidates were selected for experimental validation based on the composite score.

Appendix C Experimental Materials & Methods

C.1 Binder experimental methods

C.1.1 Gene Synthesis and Subcloning

The target DNA sequence was optimized for codons and synthesized by GenScript Biotechnology Co., Ltd. (Nanjing, China). The synthesized gene was subcloned into the pIVEX vector for protein expression in a cell-free system. Subcloning into the pIVEX vector yielded the following product: MSG-[protein]-GSGSHHWGSTHHHHHH, where the C-terminal SNAC cleavage tag and 6×His affinity tag are underlined, respectively.

C.1.2 Cell-Free Protein Expression

Cell-free protein synthesis reactions were assembled by combining S30 cell lysate, synthesis buffer, required enzymes, and plasmid DNA in a 24-deep-well plate. Each reaction had a final volume of 5 mL and was incubated at 25°C for 16 hours. Subsequently, the reaction mixture was then centrifuged at 4000 rpm for 5 minutes and the supernatant was collected for purification.

C.1.3 Cell-Free Protein Purification and Analysis

Target protein was obtained by Ni column purification using Hamilton instruments (Hamilton, MICRO LAB Starlet). The purified protein was then dialyzed in the desired buffer (either PBS, pH 7.4 or 50 mM Tris, 150 mM NaCl, 10% Glycerol, pH 8.0). Before subpackage and storage, the target protein was sterilized through a 0.22 μm filter. Protein concentration was determined by the A280 protein assay using bovine serum albumin (BSA) as the standard. Protein purity was verified by standard SDS-PAGE electrophoresis. For SDS-PAGE analysis: samples were mixed with 5× reducing loading buffer (300 mM Tris-HCl pH 6.8, 10% SDS, 30% glycerol, 0.5% bromophenol blue, and 250 mM DTT). Proteins were separated on a 12% homogeneous SDS-PAGE gel (GenScript, Cat. No. M00668) and visualized accordingly.

C.1.4 Target protein preparation

Since the binders designed in this study were expressed with His-tag, target proteins were preferentially selected without a His-tag to avoid potential interference during affinity assessment. Most of these target proteins were obtained with an Fc-tag or in untagged forms. For IL-17A, commercially available proteins lacking alternative tags were unavailable; therefore, biotin-labeled, His-tagged IL-17A variants were purchased. In such cases, affinity measurements were performed using immobilized antigens to evaluate binder binding. All purchased target proteins were commercially available reagents with validated biological activity.

C.1.5 Binding characterization of binders

Initial screening of binder designs for target protein binding was performed using Biolayer Interferometry (BLI, Gator Bio). For target proteins without the His-tag (TrkA, IFNAR2, IL-7RA, PD-L1, PDGFR, and VEGF-A), His-tagged binders were prepared at 5 μg/mL in PBSTA buffer (10 mM $Na_2HPO_4 \cdot 12H_2O$, 2 mM KH_2PO_4, 137 mM NaCl, 2.7 mM KCl, 0.05% Tween-20, 0.1% BSA, pH 7.4) for loading. Target proteins were diluted to different concentrations in PBSTA buffer (VEGF-A: 50 nM; IL-7R: 100 nM;

Table S2: Binder design target protein

Protein	Company	Description	Cat	Accession No.	Protein structure
TrkA	ACRO	Human TrkA/NTRK1 (33-417) Protein, Mouse IgG2a Fc Tag	TRA-H5259	P04629-2	TrkA(ALA33-Gly417)-mFc(glu98-lys330)
IFNAR2	ACRO	Human IFN-alpha/beta R2 Protein, Fc Tag	IF2-H5255	P48551-2	IFNAR2(Ile27-Lys243)-Fc(Pro100-Lys330)
IL17A	KACTUS	Biotinylated Human IL-17A/CTLA-8 Protein	ILA-HM418B	Q16552-1	IL-17A(Gly24-Ala155)-His-Avi
IL7RA	ACRO	Human IL-7 R alpha/CD127 Protein, Fc Tag	ILA-H525a	NP-054862.1	IL-7RA(Glu21-Asp239)-Fc(Pro100-Lys330)
PD-L1	ACRO	Human PD-L1/B7-H1 Protein (MALS verified)	PD1-H5258	NP-054862.1	PD-L1(Phe19-Arg238)-Fc(Pro100-Lys330)
PDGFR	ACRO	Human PDGF R beta/CD140b Protein, Fc Tag	PDB-H5259	P09619-1	PDGFRB(Leu33-Phe530)-Fc(Pro100-Lys330)
VEGF165	ACRO	Human VEGF165 Protein, premium grade	VE5-H4210	P15692-4	VEGF165(Ala27-Arg191)

IFNAR2: 200 nM; PDGFR: 400 nM; TrkA & PD-L1: 1000 nM each). Anti-His sensors (Gator Bio, Cat. No. 20-5066) were saturated with His-tagged binders. The BLI assay sequence was as follows: 60 s baseline, 120 s ligand loading, 60 s post-loading baseline, 120 s association phase, 300 s dissociation phase, and 30 s regeneration. Baseline-subtracted signals (in nanometers) were calculated to prioritize binders with specific binding to target proteins for further characterization. To determine the affinity of selected binder designs: His-tagged binders (5 μg/mL in PBSTA) were immobilized onto Anti-His sensors for 120 s. Serial dilutions of target proteins were prepared as follows: VEGF-A (50 nM to 3.125 nM), IL-7RA and IFNAR2 (400 nM to 6.25 nM), PDGFR (800 nM to 12.5 nM), and TrkA & PD-L1 (1000 nM to 15.625 nM). Diluted target proteins were allowed to associate with the immobilized ligand for 120 s, followed by dissociation in PBSTA buffer for 300 s. After background subtraction using buffer-only (PBSTA) control curves, dissociation constants (K_d) were determined using the 1:1 binding model in the Results & Analysis curve-fitting module. For His-tagged target protein IL-17A: Biotin-

labeled IL-17A was prepared at 5 μg/mL in PBSTA. The design binders were diluted to 1000 nM in PBSTA. Streptavidin (SA) sensors (Gator Bio, 20-5006) were saturated with Biotin-labeled IL-17A for 60 s. The design binders were then allowed to associate with the immobilized ligand for 120 s, followed by a dissociation step in PBSTA for 300 s. The baseline subtracted signals (in nanometers) were calculated and used to prioritize target proteins specific binders for further characterization. To determine the affinity of selected designs, 5 μg/mL Biotin-labeled IL-17A prepared in PBSTA was immobilized onto a Streptavidin (SA) sensor for 60 s. Serial dilutions of the design binders (1000 nM to 15.625 nM) were allowed to associate with the immobilized ligand for 120 s, followed by a dissociation step in PBSTA for 300 s. After background subtraction using buffer-only (PBSTA) control curves, K_d values were determined using the 1:1 binding model in the Results & Analysis curve-fitting module.

C.2 VHH experimental methods

C.2.1 Framework selection

VHH frameworks are randomly selected from 7EOW (caplacizumab), 8Z8V (ozoralizumab), 5JDS (envafolimab), 7XL0 (vobarilizumab), and 8COH (gefurulimab), highlighting their diverse structural architectures and clinical feasibility. For scFv design, frameworks are randomly selected from 6ZQK (trastuzumab), 6NOU (ixekizumab), 6TCS (omalizumab).

C.2.2 Gene Synthesis and Subcloning

VHH DNA sequences were codon-optimized and synthesized by GenScript Biotechnology Co., Ltd. (Nanjing, China). The synthesized genes were subcloned into the pCDNA3.4 vector for protein expression in CHO cell system. Subcloning into the pCDNA3.4 vector results in the following product: MGWSCIILFLVATATGVHS (signal peptide)-[Nanobody]-<u>GGGGSHHHHHH</u>, with the 6×His affinity tag underlined.

C.2.3 VHHs Expression in CHO Cells

Transfection-grade plasmids were prepared in large quantities using a GenScript self-developed plasmid extraction kit for CHO cell expression. Cells were maintained at 37°C with 5% CO_2 on an orbital shaker. One day before transfection, the cells were seeded at an appropriate density. On the day of transfection, DNA and Reagent (self-developed by GenScript) were mixed at an optimal ratio and then added into cells ready for transfection. Approximately 24 hours post transfection, Feed was added to each sample.

C.2.4 Protein Purification and Analysis

Cell culture broth was centrifuged and followed by filtration. Filtered cell culture supernatant was loaded onto an affinity purification column at an appropriate flowrate. After washing and elution with appropriate buffers, the eluted fractions were pooled and buffer exchanged to the final formulation buffer (PBS, pH 7.2). The purified protein was analyzed by SDS-PAGE and SEC-HPLC analysis to determine the molecular weight and purity. The concentration was determined by A280 method.

C.2.5 Target protein preparation

Since the VHHs designed in this study were expressed with a His-tag, target proteins were preferentially selected without a His-tag to avoid potential interference during affinity assessment. Most of these target proteins were obtained with an Fc-tag or in untagged forms. For CCL2 and BHRF1, commercially available proteins lacking alternative tags were unavailable. Therefore, BHRF1 was expressed with a His-SUMO tag in HEK293 cells, followed by tag cleavage. Biotin-labeled, His-tagged CCL2 was purchased. In such cases, affinity measurements were performed using immobilized antigens to evaluate binder binding.

C.2.6 Binding characterization of VHHs

Initial screening of VHH designs for target protein binding was performed using BLI (Gator Bio).

For target proteins without His-tag (PDGFR, 1433E, IL-13, BHRF1, S100A4 and HNMT), His-

Table S3: VHH design target protein

Protein	Company	Description	Cat No.	Accession	Protein structure
EFNA1	SinoBio	Recombinant Human Ephrin-A1 (hFc Tag)	10882-H02H	NP-004419.2	(Met1-Ser182)-hFc
PDGFR	SinoBio	Recombinant Human PDGFRB (ECD), HPLC-verified	10514-H02H1	NP-002600.1	(Met1-Phe530)-hFc
1433E	SinoBio	Recombinant Human 14-3-3 epsilon	10842-HNCE	NP-006752.1	Gly-Pro-(Met1-Gln255)
IL-13	SinoBio	Recombinant Human IL-13 (hFc Tag), HPLC-verified	10369-H01H	AAK53823.1	hFc-(Gly21-Asn132)
CCL2	KACTUS	Biotinylated Human MCP-1/CCL2	MCP-HM401B	P13500	(Gln24-Thr99)-His-Avi
BHRF1	Oritop	BHRF1	H202511 1402	P03182	His-SUMO-(Met1-Ser165)
S100A4	SinoBio	Recombinant Human S100A4 Protein (hFc Tag)	10185-H01H	NP-002952.1	hFc-(Met1-Lys101)
HNMT	SinoBio	Recombinant Human HNMT Protein (GST Tag)	13096-H09E	AAH20677.1	GST-(Met1-Ala292)

tagged VHHs were prepared at 5 μg/mL in PBSTA buffer. Target proteins were diluted to different concentrations in PBSTA buffer (PDGFR: 5000 nM; IL-13, 1433E, BHRF1, S100A4 and HNMT: 1000 nM each). Anti-His sensors (Gator Bio, Cat. No. 20-5066) were saturated with His-tagged VHHs. The BLI assay sequence was as follows: 60 s baseline, 120 s ligand loading, 60 s post-loading baseline, 120 s association phase, 300 s dissociation phase, and 30 s regeneration. Baseline-subtracted signals (in nanometers) were calculated to prioritize VHHs with specific binding to target proteins for further characterization. For EFNA1(1000 nM), the signal value detected by the HIS1K sensor was too low. Therefore, the ProA sensor was used for detection, and the detection conditions were the same as those of the HIS1K sensor.

To determine the affinity of selected designs, 5 μg/mL His tag design VHHs prepared in PBSTA were immobilized onto Anti-His sensor for 120 s. Serial dilutions of the target proteins (PDGFR, IL-13 and BHRF1: from 5000 nM diluted to 78 nM, 1433E: from 3600 nM diluted to 56.25 nM, S100A4 and HNMT from 4000 nM diluted to 125 nM,) were then allowed to associate with the immobilized ligand for 120 s, followed by a dissociation step in PBSTA for 300 s. After background subtraction

using buffer-only (PBSTA) control curves, K_d values were determined using the 1:1 binding model in the Results & Analysis curve-fitting module.For EFNA1(from 4000 nM diluted to 125 nM), the ProA sensor was used for detection, and the detection conditions were the same as those of the HIS1K sensor.

For His tag target protein CCL2: Biotin-labeled CCL2 was prepared at 5 μg/mL in PBSTA. VHHs were diluted to 5000 nM in PBSTA. Streptavidin (SA) sensors (Gator Bio, 20-5006) were saturated with biotin-labeled CCL2 for 60 s. VHHs were then allowed to associate with the immobilized ligand for 120 s, followed by a dissociation step in PBSTA for 300 s. Baseline-subtracted signals (in nanometers) were calculated to prioritize specific VHHs for further characterization.

To determine the affinity of selected VHHs for CCL2: Biotin-labeled CCL2 (5 μg/mL in PBSTA) was immobilized onto SA sensors for 60 s. Serial dilutions of VHHs (5000 nM to 78 nM) were allowed to associate with the immobilized ligand for 120 s, followed by dissociation in PBSTA buffer for 300 s. After background subtraction using buffer-only (PBSTA) control curves, K_d values were determined using the 1:1 binding model in the Results & Analysis curve-fitting module.

Appendix D Supplementary Figures

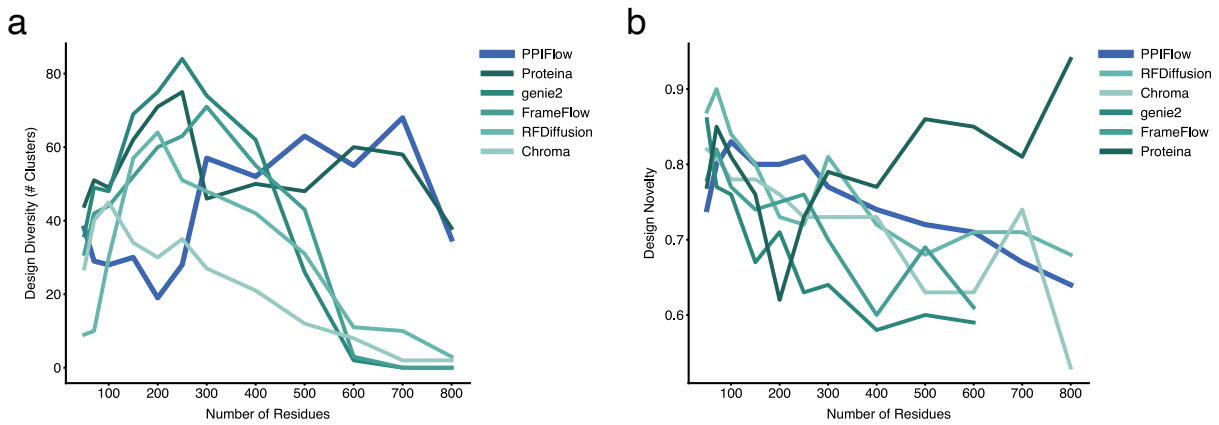

Figure S1: Benchmarking monomer generation performance across varying lengths.

(a) Evaluation of structural diversity in monomer generation tasks for sequences ranging from 50 to 800 amino acids (100 designs per length). PPIFlow is compared against Proteina, Genie2, FrameFlow, RFDiffusion, and Chroma. **(b)** Structural novelty analysis quantified by the maximum TM-score of successful designs against the PDB databases.

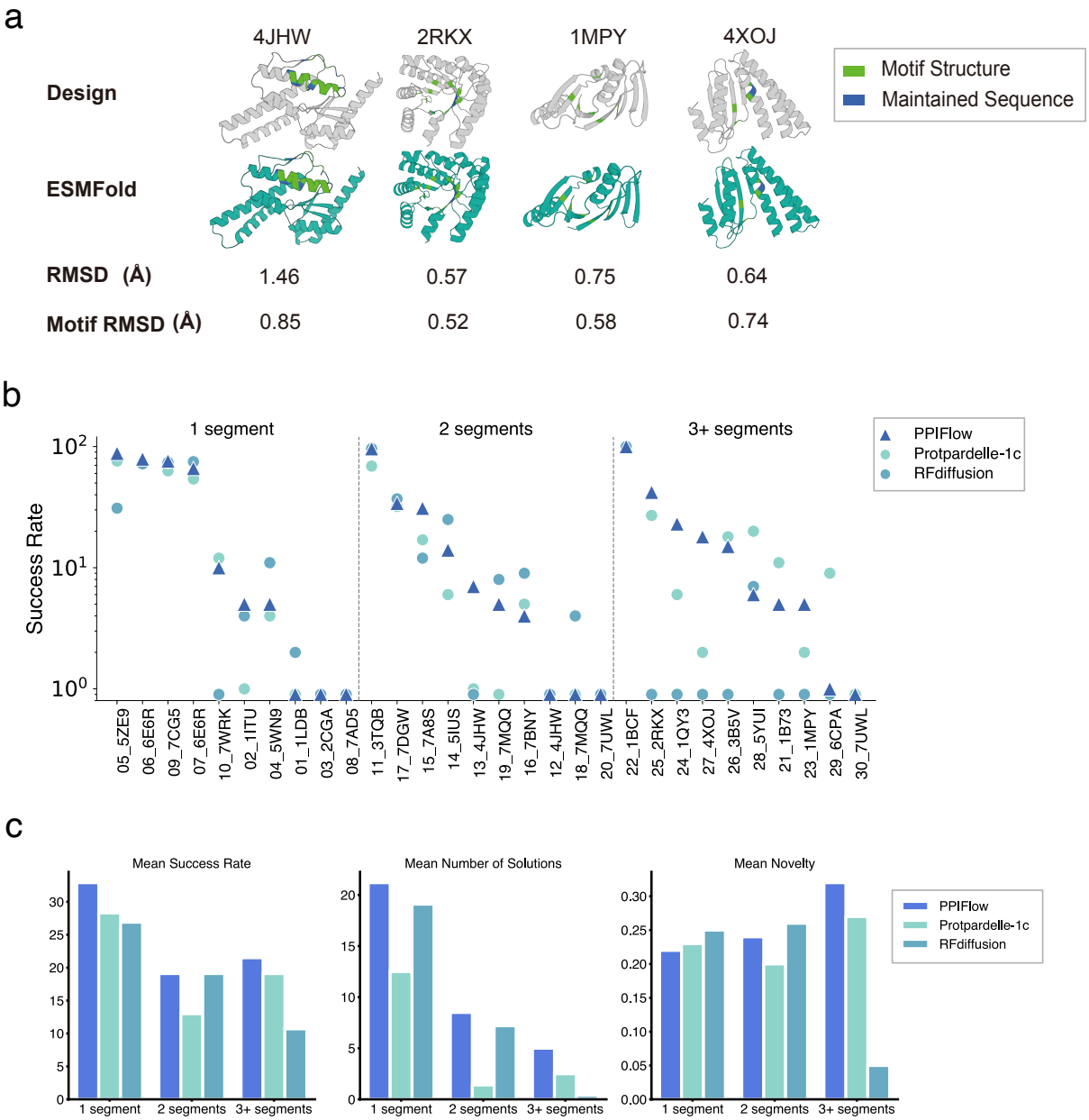

Figure S2: Assessment of motif scaffolding performance and structural fidelity.

(a) Performance of PPIFlow on four representative scaffolding tasks (PDB IDs: 4JHW, 2RKX, 1MPY, and 4XOJ). Panels show the alignment between PPIFlow-generated backbones and ESMFold-refolded structures, annotated with global Cα RMSD and motif-specific Cα RMSD values. **(b)** Comparison of design success rates on the MotifBench dataset between PPIFlow, Protpardelle-1c, and RFDiffusion. **(c)** Comprehensive comparison of the three models across mean success rate, solution diversity, and structural novelty.

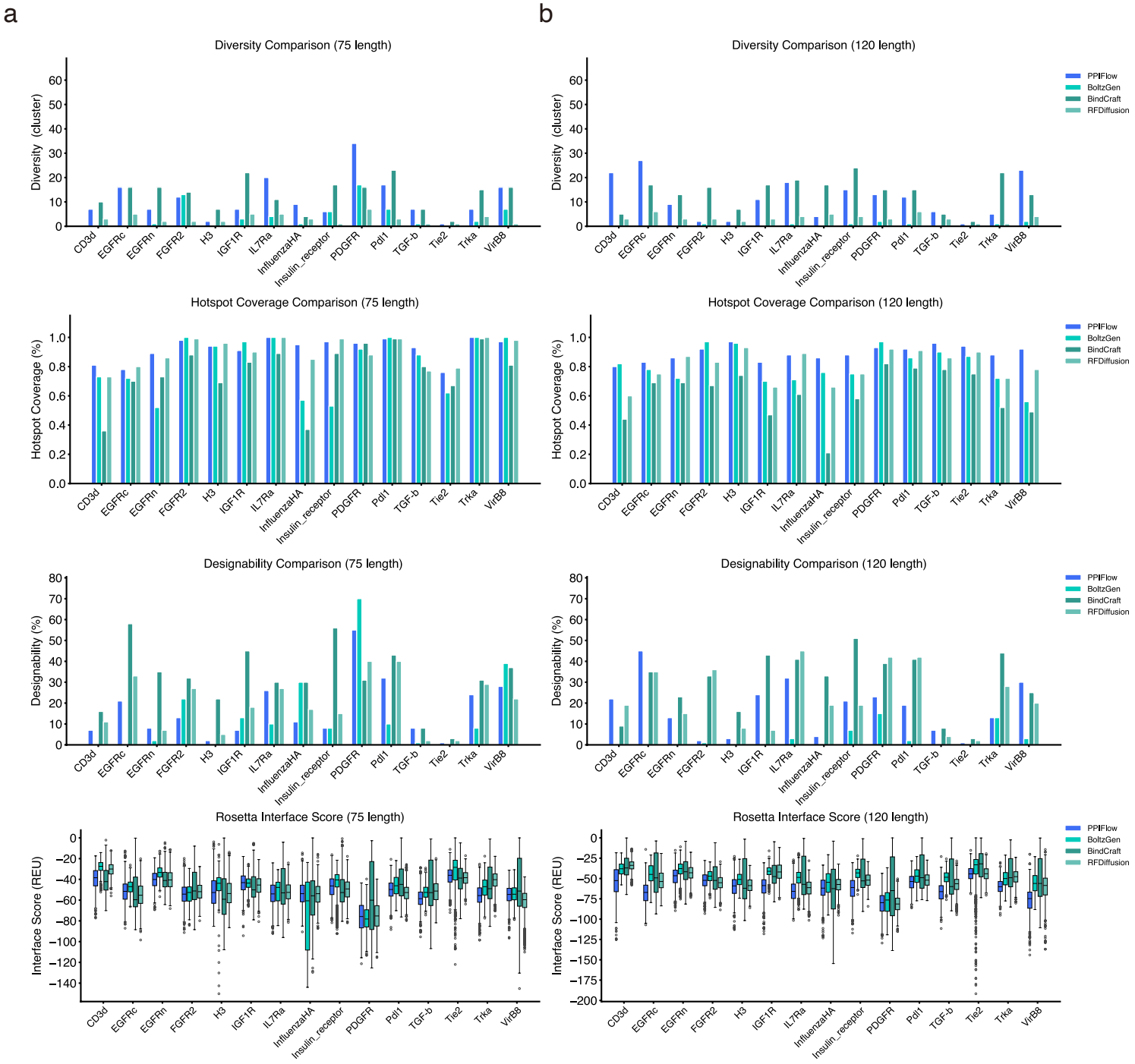
a
b
Diversity Comparison (75 length)
Diversity Comparison (120 length)
Diversity (cluster)
Hotspot Coverage Comparison (75 length)
Hotspot Coverage Comparison (120 length)
Hotspot Coverage (%)
Designability Comparison (75 length)
Designability Comparison (120 length)
Designability (%)
Rosetta Interface Score (75 length)
Rosetta Interface Score (120 length)
Interface Score (REU)
PPIFlow
BoltzGen
BindCraft
RFDiffusion
CD3d
EGFRc
EGFRn
FGFR2
H3
IGF1R
IL7Ra
InfluenzaHA
Insulin_receptor
PDGFR
Pdl1
TGF-b
Tie2
Trka
VirB8

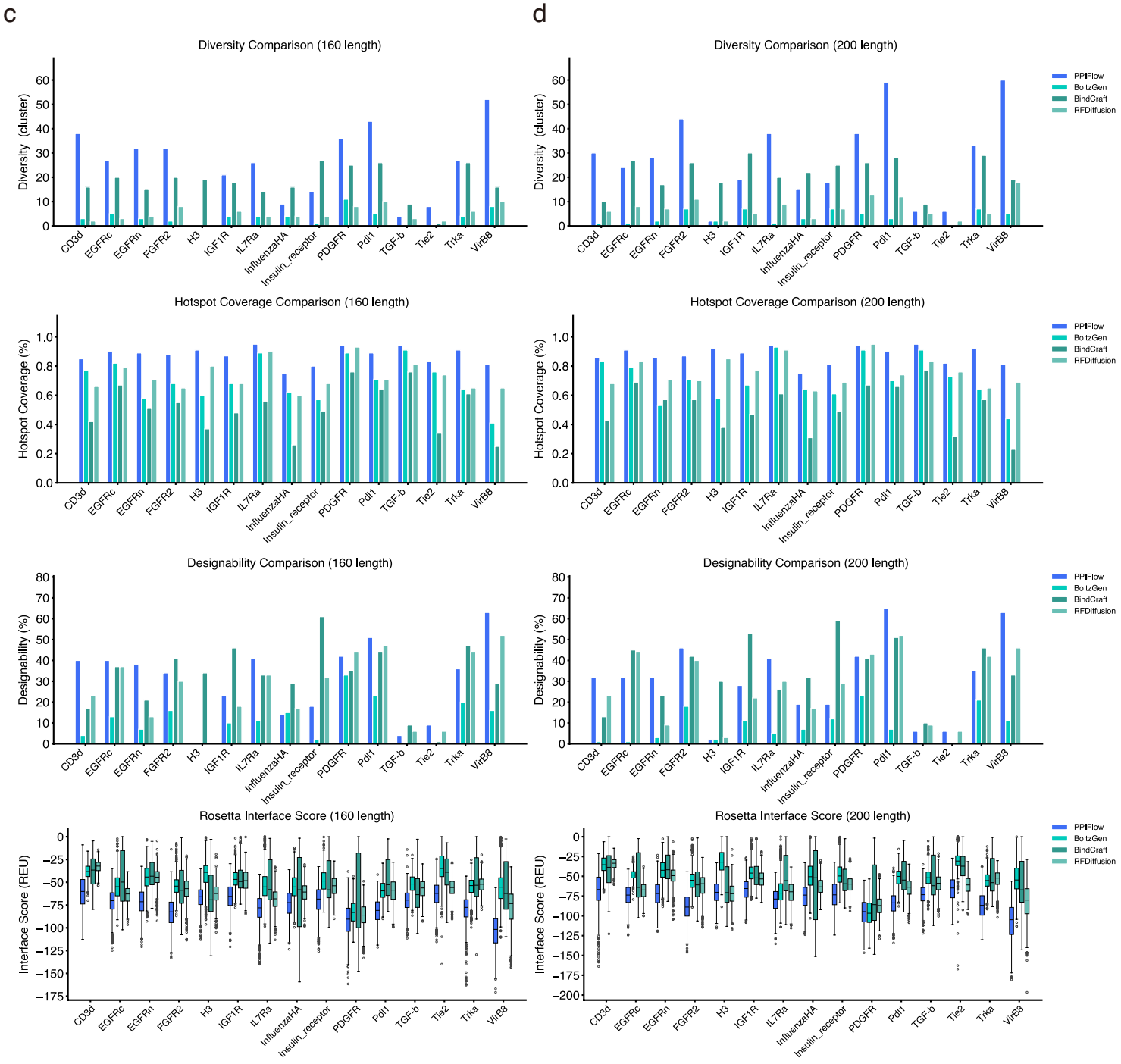
c
d
Diversity Comparison (160 length)
Diversity Comparison (200 length)
Diversity (cluster)
Hotspot Coverage Comparison (160 length)
Hotspot Coverage Comparison (200 length)
Hotspot Coverage (%)
Designability Comparison (160 length)
Designability Comparison (200 length)
Designability (%)
Rosetta Interface Score (160 length)
Rosetta Interface Score (200 length)
Interface Score (REU)
PPIFlow
BoltzGen
BindCraft
RFDiffusion
CD3d
EGFRc
EGFRn
FGFR2
H3
IGF1R
IL7Ra
InfluenzaHA
Insulin_receptor
PDGFR
Pdl1
TGF-b
Tie2
Trka
VirB8

Figure S3: Comparative analysis of de novo binder design efficiency.

Results are grouped by target sequence length: **(a)** 75 residues, **(b)** 120 residues, **(c)** 160 residues, and **(d)** 200 residues. For each group, four hierarchical performance metrics are evaluated (from top to bottom): *(i) Structural diversity*, quantifying the conformational breadth of the generated binder ensemble; *(ii) Hotspot coverage*, measuring the spatial conservation of critical target-interface residues; *(iii) Designability*, defined by the structural self-consistency (scRMSD) between generative backbones and forward-folded structures; *(iv) Binding energetics*, represented by Rosetta interface scores (REU). All subfigures share a common color scheme representing the four evaluated algorithms.

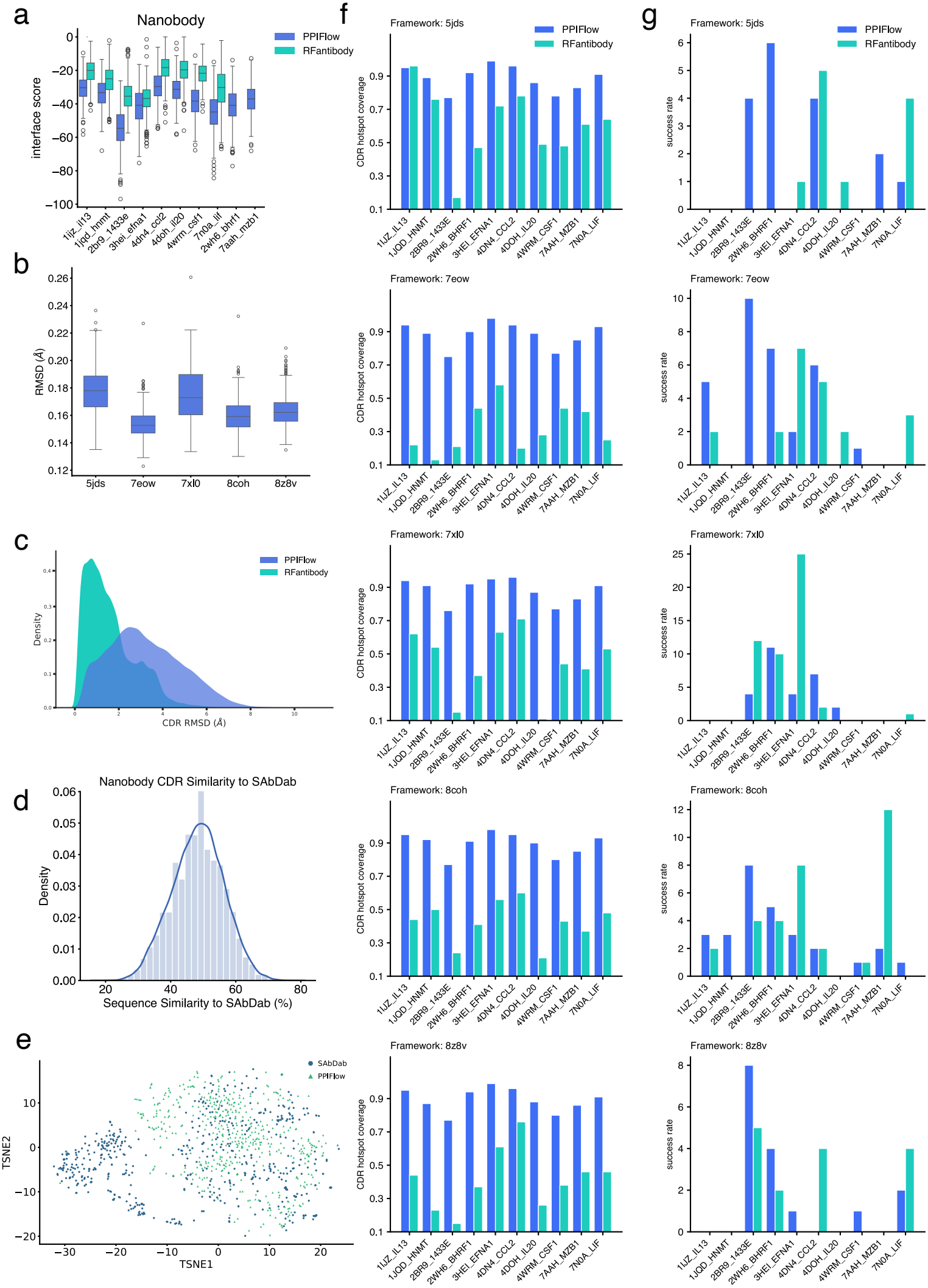
a
Nanobody
PPIFlow
RFantibody
interface score
1ijz_il13
1jqd_hmnt
2br9_1433e
3hei_efna1
4dn4_ccl2
4doh_il20
4wrm_csf1
7n0a_lif
2wh6_bhrf1
7aah_mzb1
b
RMSD (Å)
5jds
7eow
7xl0
8coh
8z8v
c
Density
CDR RMSD (Å)
d
Nanobody CDR Similarity to SAbDab
Density
Sequence Similarity to SAbDab (%)
e
SAbDab
PPIFlow
TSNE1
TSNE2
f
Framework: 5jds
Framework: 7eow
Framework: 7xl0
Framework: 8coh
Framework: 8z8v
CDR hotspot coverage
1UZ_IL13
1JQD_HNMT
2BR9_1433E
2WH6_BHRF1
3HEI_EFNA1
4DN4_CCL2
4DOH_IL20
4WRM_CSF1
7AAH_MZB1
7N0A_LIF
g
Framework: 5jds
Framework: 7eow
Framework: 7xl0
Framework: 8coh
Framework: 8z8v
success rate

Figure S4: Benchmarking nanobody (VHH) design precision and diversity.

(a) Distribution of Rosetta interface scores comparing PPIFlow and RFAntibody across nanobody design benchmarks. Notably, RFAntibody failed to generate valid binder candidates for the BHRF1 and MZB1 targets. **(b)** Structural recovery of framework regions (FRs), quantified by Cα RMSD (Å) across multiple nanobody template PDB IDs, highlighting the backbone stability of the designs. **(c)** Conformational fidelity of CDR3 loops, calculated using the PyMOL alignment algorithm. Structures were pre-aligned via framework regions, followed by CDR3 RMSD calculation without further rotation to assess loop positioning accuracy. **(d, e)** Sequence and structural landscape analysis. (d) Sequence diversity of designed CDR3 loops relative to the SAbDab database (training set); (e) Structural clustering of the generated ensembles, illustrating the breadth of the sampled conformational space compared to known antibody repertoires. **(f, g)** Comprehensive evaluation of design quality across framework templates, reporting (f) CDR hotspot coverage efficiency and (g) design success rates across the diverse target panel.

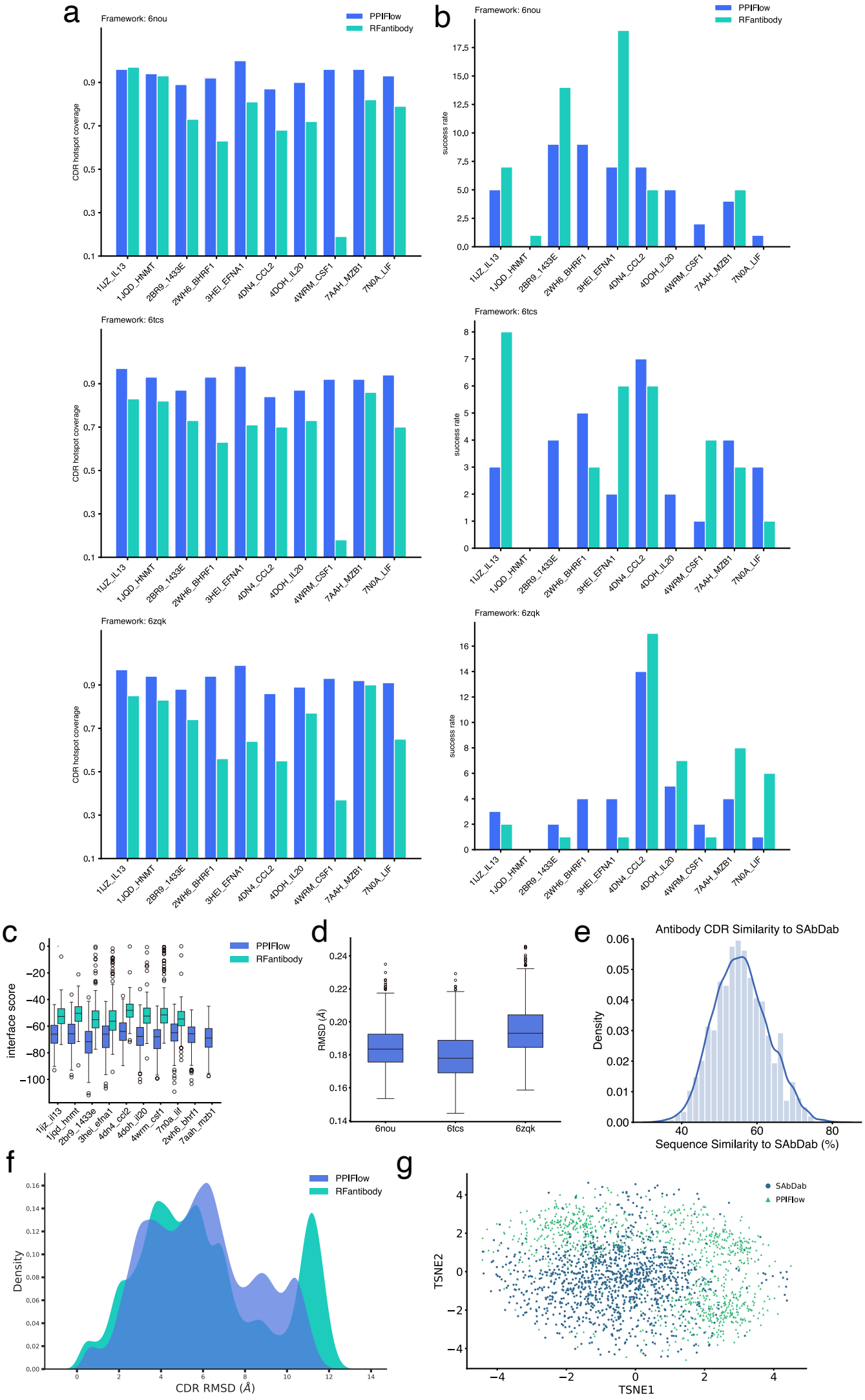
a
Framework: 6nou
PPIFlow
RFantibody
CDR hotspot coverage
b
success rate
Framework: 6tcs
Framework: 6zqk
1UZ_IL13
1JQD_HNMT
2BR9_1433E
2WH6_BHRF1
3HEI_EFNA1
4DN4_CCL2
4DOH_IL20
4WRM_CSF1
7AAH_MZB1
7N0A_LIF
c
interface score
d
RMSD (Å)
6nou
6tcs
6zqk
e
Antibody CDR Similarity to SAbDab
Density
Sequence Similarity to SAbDab (%)
f
CDR RMSD (Å)
g
SAbDab
TSNE1
TSNE2

Figure S5: Benchmarking scFv design precision.

(a, b) Detailed performance metrics for antibody design tasks across a library of diverse framework templates. Panels illustrate the efficiency of PPIFlow in maintaining CDR hotspot coverage and achieving high success rates for various antibody frameworks; **(c)** Distribution of Rosetta interface scores comparing PPIFlow and RFAntibody across scFv design benchmarks. Notably, RFAntibody failed to generate valid binder candidates for the BHRF1 and MZB1 targets. **(d)** Structural recovery of framework regions (FRs), quantified by Cα RMSD (Å) across multiple template PDB IDs, highlighting the backbone stability of the designs. **(e)** Sequence diversity of designed CDR3 loops relative to the SAbDab database (training set); **(f)** Conformational fidelity of CDR3 loops, calculated using the PyMOL alignment algorithm. Structures were pre-aligned via framework regions, followed by CDR3 RMSD calculation without further rotation to assess loop positioning accuracy. **(g)** Structural clustering of the generated ensembles, illustrating the breadth of the sampled conformational space compared to known antibody repertoires.

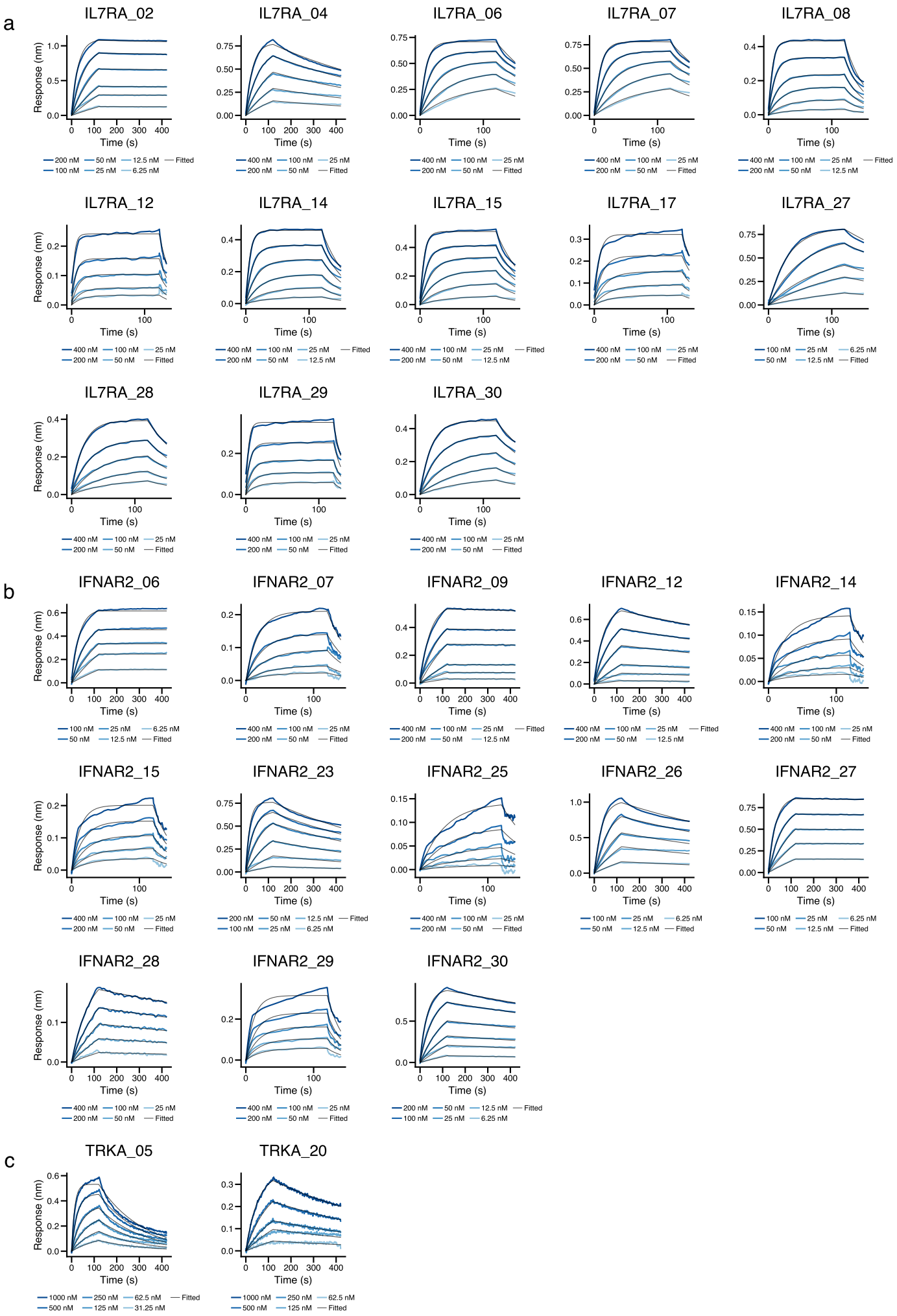
a
IL7RA_02
IL7RA_04
IL7RA_06
IL7RA_07
IL7RA_08
IL7RA_12
IL7RA_14
IL7RA_15
IL7RA_17
IL7RA_27
IL7RA_28
IL7RA_29
IL7RA_30
b
IFNAR2_06
IFNAR2_07
IFNAR2_09
IFNAR2_12
IFNAR2_14
IFNAR2_15
IFNAR2_23
IFNAR2_25
IFNAR2_26
IFNAR2_27
IFNAR2_28
IFNAR2_29
IFNAR2_30
c
TRKA_05
TRKA_20
Response (nm)
Time (s)
1000 nM
500 nM
250 nM
125 nM
62.5 nM
31.25 nM
200 nM
100 nM
50 nM
25 nM
12.5 nM
6.25 nM
Fitted

d

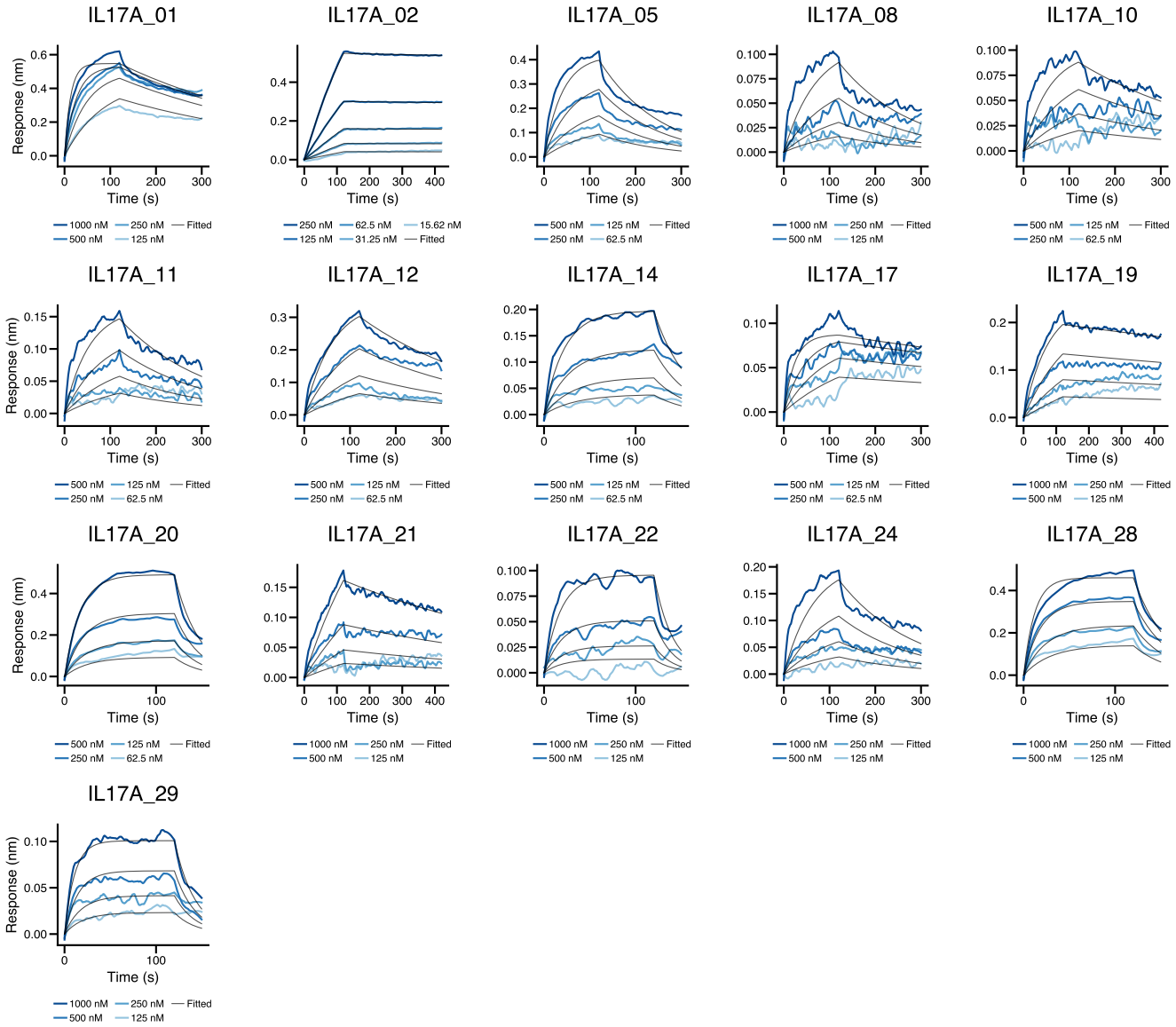
IL17A_01
IL17A_02
IL17A_05
IL17A_08
IL17A_10
IL17A_11
IL17A_12
IL17A_14
IL17A_17
IL17A_19
IL17A_20
IL17A_21
IL17A_22
IL17A_24
IL17A_28
IL17A_29
Response (nm)
Time (s)
1000 nM
500 nM
250 nM
125 nM
62.5 nM
31.25 nM
15.62 nM
Fitted

e

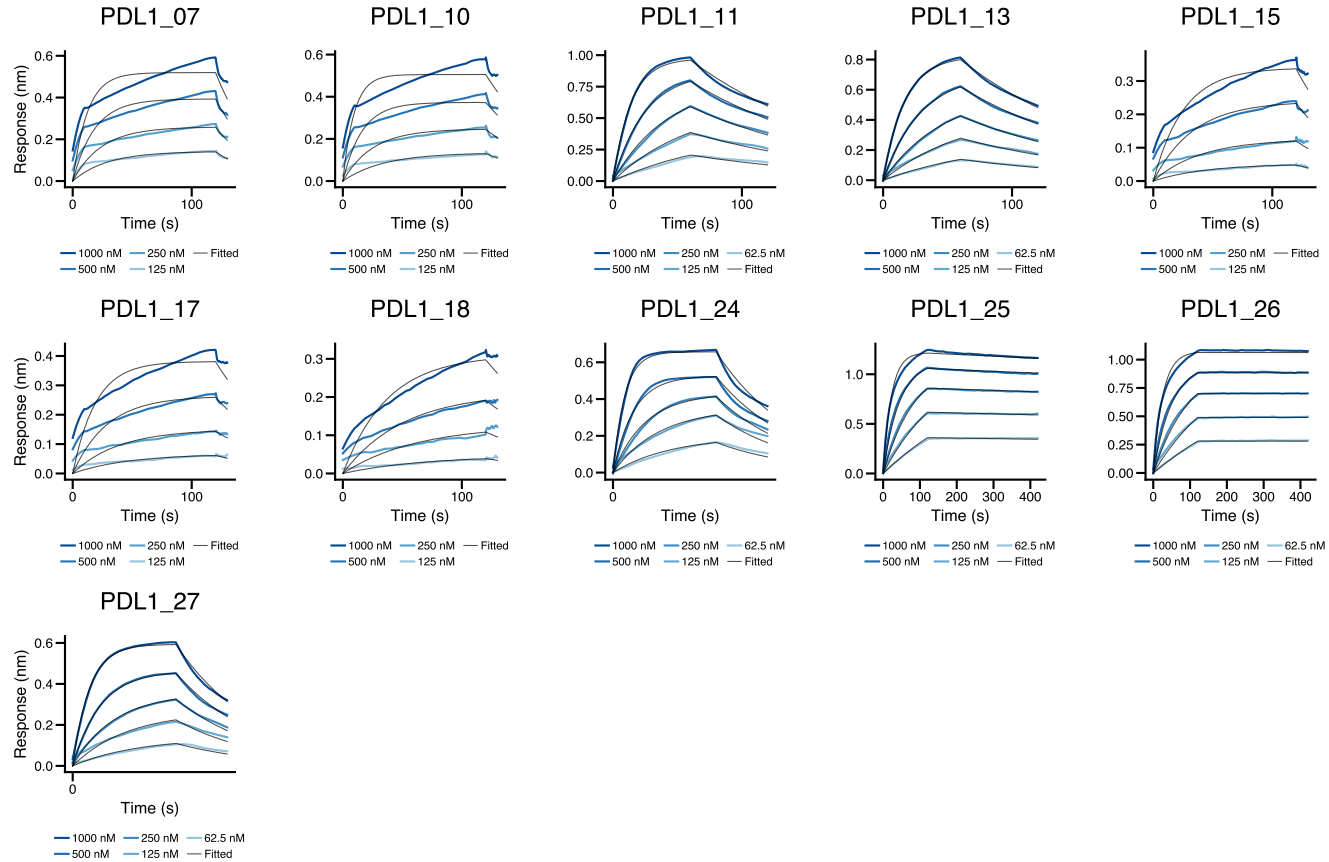
PDL1_07
PDL1_10
PDL1_11
PDL1_13
PDL1_15
PDL1_17
PDL1_18
PDL1_24
PDL1_25
PDL1_26
PDL1_27
Response (nm)
Time (s)
1000 nM
500 nM
250 nM
125 nM
62.5 nM
Fitted

f

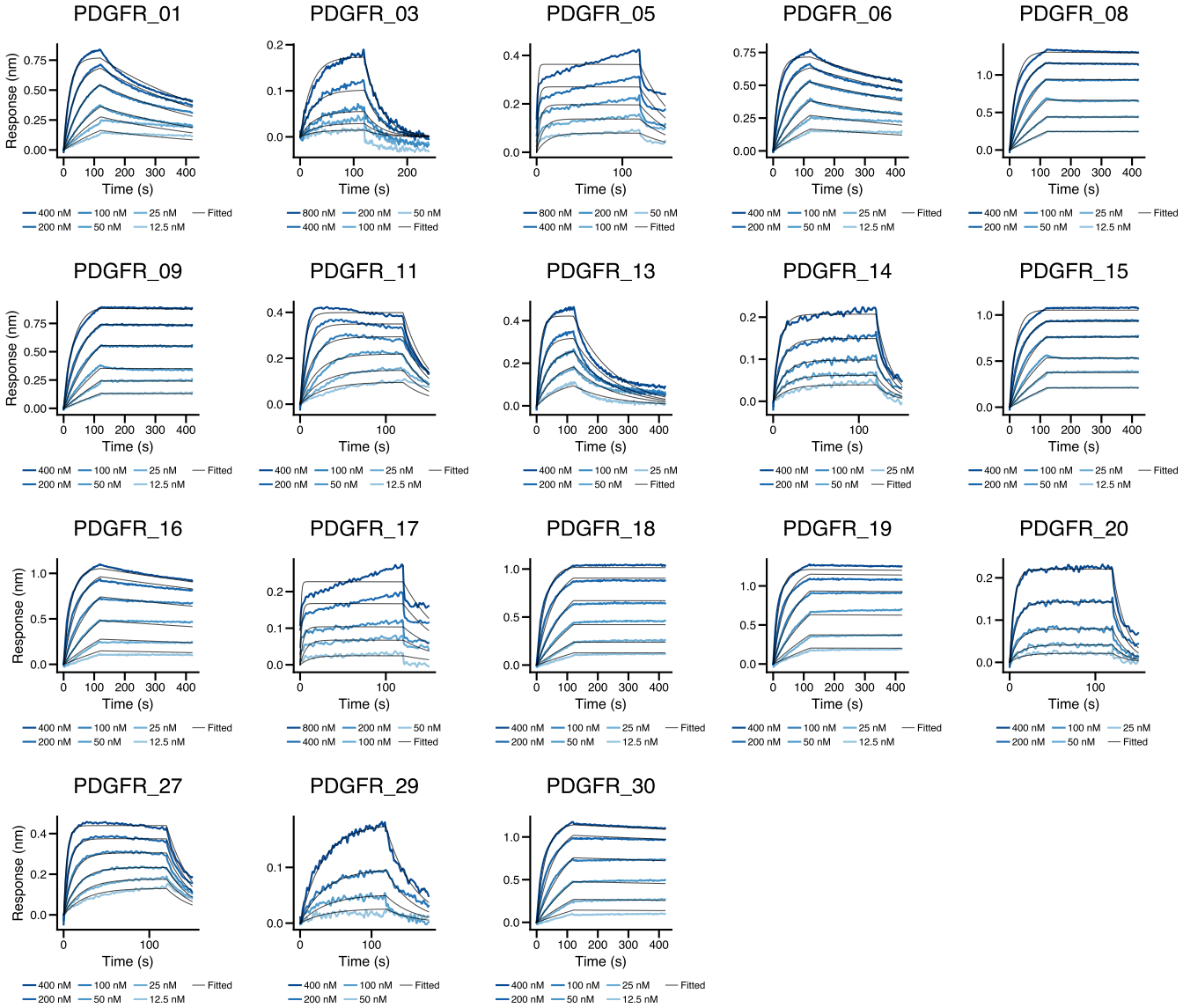
PDGFR_01
PDGFR_03
PDGFR_05
PDGFR_06
PDGFR_08
PDGFR_09
PDGFR_11
PDGFR_13
PDGFR_14
PDGFR_15
PDGFR_16
PDGFR_17
PDGFR_18
PDGFR_19
PDGFR_20
PDGFR_27
PDGFR_29
PDGFR_30
Response (nm)
Time (s)
800 nM
400 nM
200 nM
100 nM
50 nM
25 nM
12.5 nM
Fitted

g

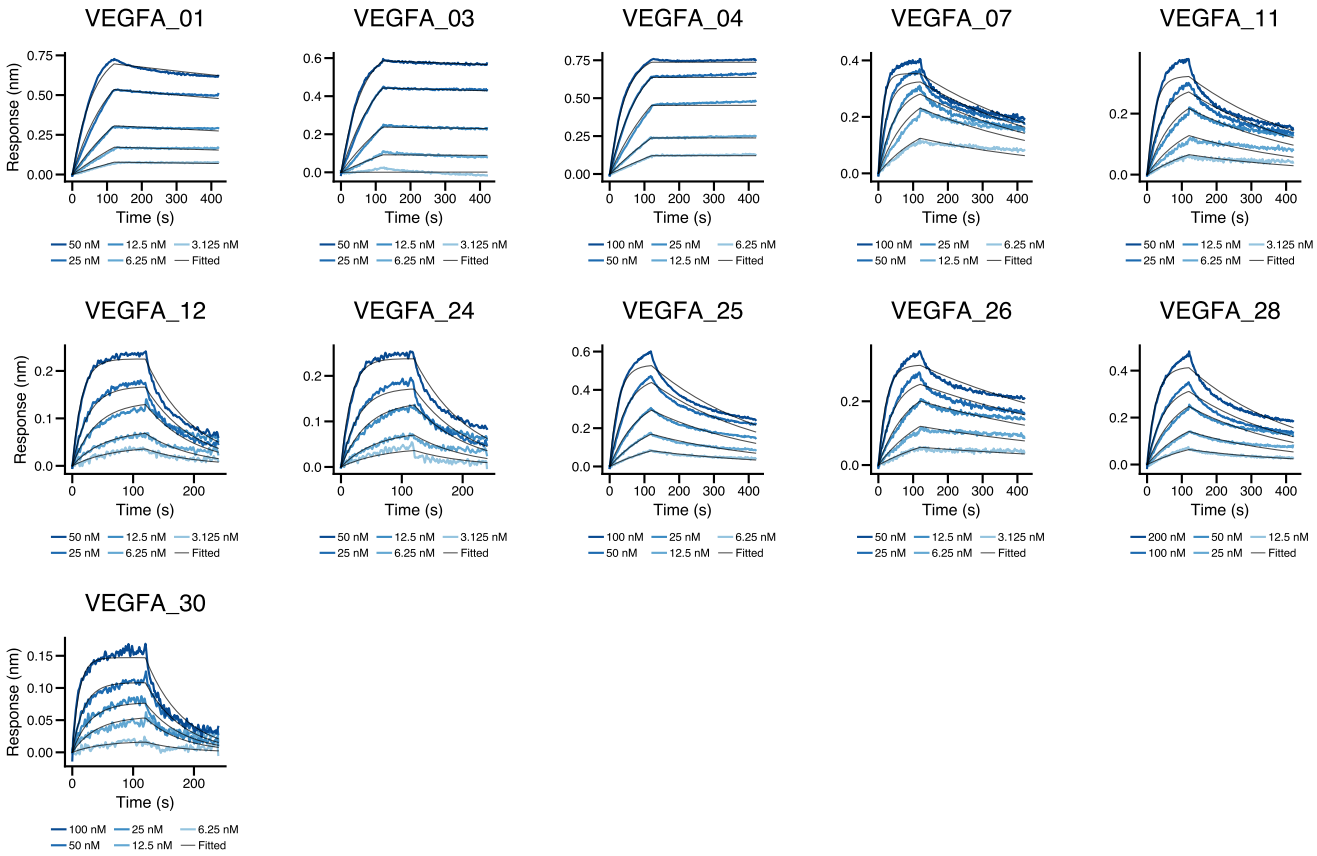
VEGFA_01
VEGFA_03
VEGFA_04
VEGFA_07
VEGFA_11
VEGFA_12
VEGFA_24
VEGFA_25
VEGFA_26
VEGFA_28
VEGFA_30
Response (nm)
Time (s)
100 nM
50 nM
25 nM
12.5 nM
6.25 nM
3.125 nM
200 nM
Fitted

Figure S6: Bio-layer interferometry (BLI) kinetic analysis of de novo designed binders.

Multi-cycle BLI sensorgrams illustrating the binding kinetics of synthetic binders against seven therapeutic targets: **(a)** IL7RA, **(b)** IFNAR2, **(c)** TrkA, **(d)** IL17A, **(e)** PDL1, **(f)** PDGFR, and **(g)** VEGFA. Raw data (colored lines) were globally fitted with a 1:1 binding model (black lines). Molar concentrations for each titration step are annotated below the respective sensorgrams.

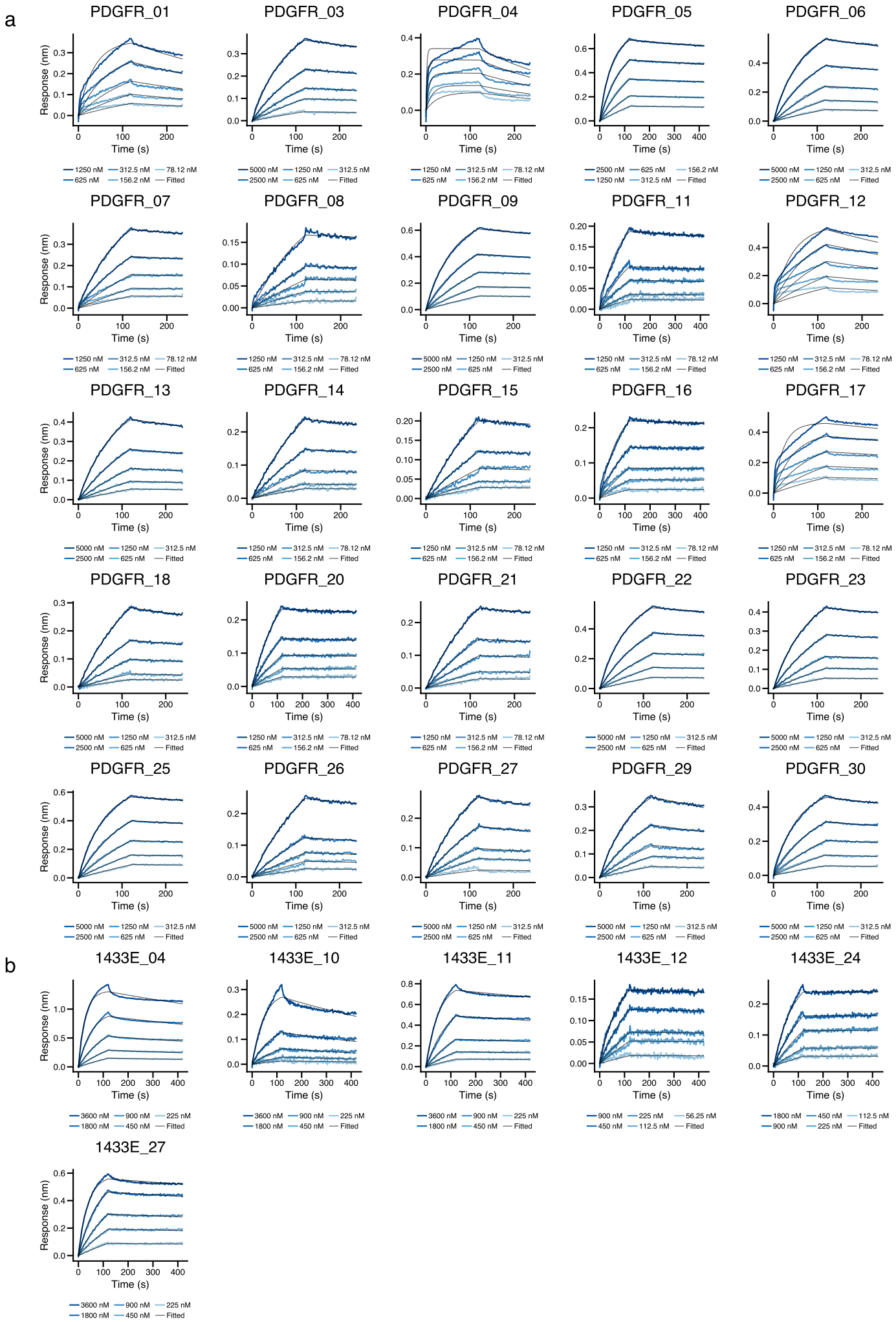
a
PDGFR_01
PDGFR_03
PDGFR_04
PDGFR_05
PDGFR_06
PDGFR_07
PDGFR_08
PDGFR_09
PDGFR_11
PDGFR_12
PDGFR_13
PDGFR_14
PDGFR_15
PDGFR_16
PDGFR_17
PDGFR_18
PDGFR_20
PDGFR_21
PDGFR_22
PDGFR_23
PDGFR_25
PDGFR_26
PDGFR_27
PDGFR_29
PDGFR_30
b
1433E_04
1433E_10
1433E_11
1433E_12
1433E_24
1433E_27
Response (nm)
Time (s)
5000 nM
2500 nM
1250 nM
625 nM
312.5 nM
156.2 nM
78.12 nM
Fitted
3600 nM
1800 nM
900 nM
450 nM
225 nM
112.5 nM
56.25 nM

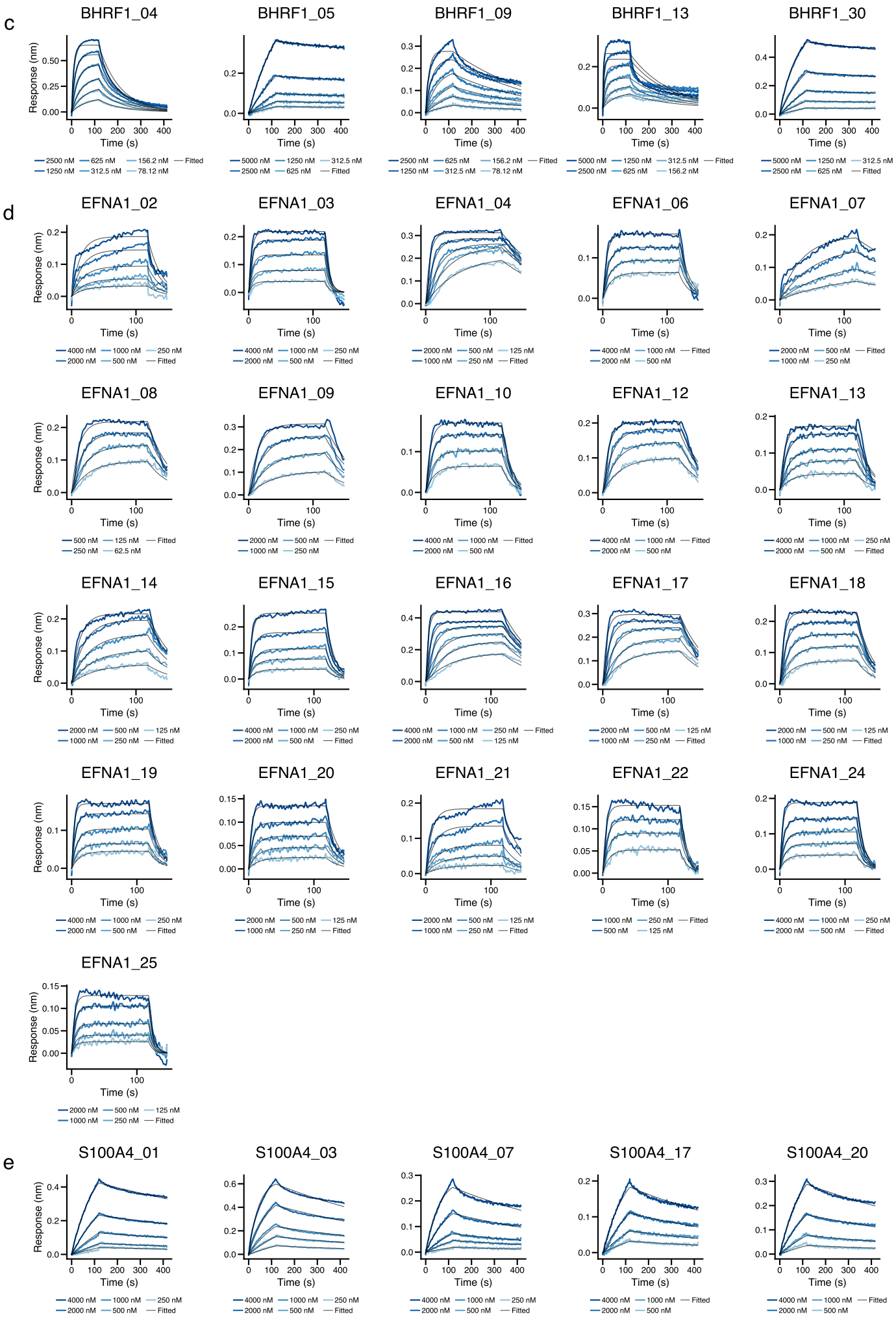
c
BHRF1_04
BHRF1_05
BHRF1_09
BHRF1_13
BHRF1_30
d
EFNA1_02
EFNA1_03
EFNA1_04
EFNA1_06
EFNA1_07
EFNA1_08
EFNA1_09
EFNA1_10
EFNA1_12
EFNA1_13
EFNA1_14
EFNA1_15
EFNA1_16
EFNA1_17
EFNA1_18
EFNA1_19
EFNA1_20
EFNA1_21
EFNA1_22
EFNA1_24
EFNA1_25
e
S100A4_01
S100A4_03
S100A4_07
S100A4_17
S100A4_20
Response (nm)
Time (s)

f

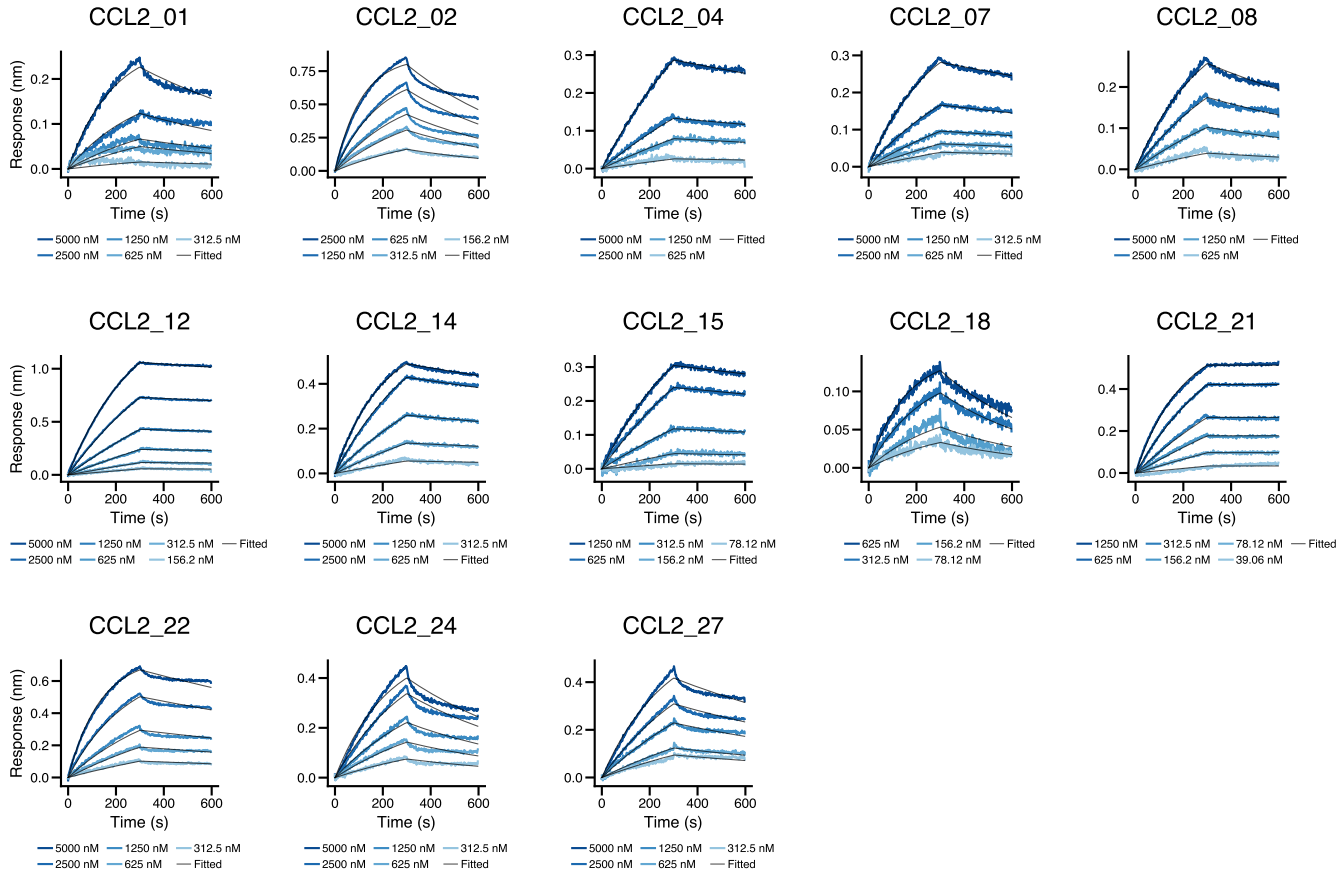
CCL2_01
Response (nm)
Time (s)
5000 nM 1250 nM 312.5 nM
2500 nM 625 nM Fitted
CCL2_02
Time (s)
2500 nM 625 nM 156.2 nM
1250 nM 312.5 nM Fitted
CCL2_04
Time (s)
5000 nM 1250 nM Fitted
2500 nM 625 nM
CCL2_07
Time (s)
5000 nM 1250 nM 312.5 nM
2500 nM 625 nM Fitted
CCL2_08
Time (s)
5000 nM 1250 nM Fitted
2500 nM 625 nM
CCL2_12
Response (nm)
Time (s)
5000 nM 1250 nM 312.5 nM Fitted
2500 nM 625 nM 156.2 nM
CCL2_14
Time (s)
5000 nM 1250 nM 312.5 nM
2500 nM 625 nM Fitted
CCL2_15
Time (s)
1250 nM 312.5 nM 78.12 nM
625 nM 156.2 nM Fitted
CCL2_18
Time (s)
625 nM 156.2 nM Fitted
312.5 nM 78.12 nM
CCL2_21
Time (s)
1250 nM 312.5 nM 78.12 nM Fitted
625 nM 156.2 nM 39.06 nM
CCL2_22
Response (nm)
Time (s)
5000 nM 1250 nM 312.5 nM
2500 nM 625 nM Fitted
CCL2_24
Time (s)
5000 nM 1250 nM 312.5 nM
2500 nM 625 nM Fitted
CCL2_27
Time (s)
5000 nM 1250 nM 312.5 nM
2500 nM 625 nM Fitted

g

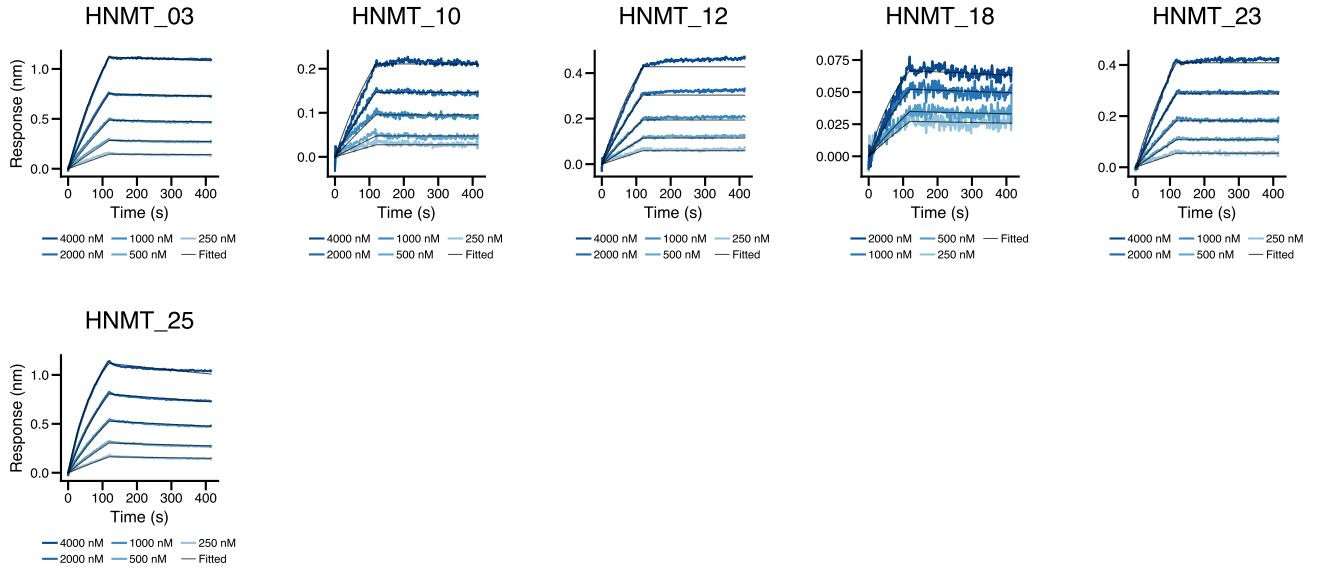
HNMT_03
Response (nm)
Time (s)
4000 nM 1000 nM 250 nM
2000 nM 500 nM Fitted
HNMT_10
Time (s)
4000 nM 1000 nM 250 nM
2000 nM 500 nM Fitted
HNMT_12
Time (s)
4000 nM 1000 nM 250 nM
2000 nM 500 nM Fitted
HNMT_18
Time (s)
2000 nM 500 nM Fitted
1000 nM 250 nM
HNMT_23
Time (s)
4000 nM 1000 nM 250 nM
2000 nM 500 nM Fitted
HNMT_25
Response (nm)
Time (s)
4000 nM 1000 nM 250 nM
2000 nM 500 nM Fitted

Figure S7: Kinetic characterization of designed VHH domains via BLI.

Representative BLI sensorgrams showing the binding affinity of designed VHH candidates against: **(a)** PDGFR, **(b)** 1433E, **(c)** BHRF1, **(d)** EFNA1, **(e)** S100A4, **(f)** CCL2 and **(g)** HNMT. Multi-point kinetic titrations were performed to evaluate binding specificity. The data confirm high-affinity interactions and diverse dissociation profiles across the tested VHH-target complexes.

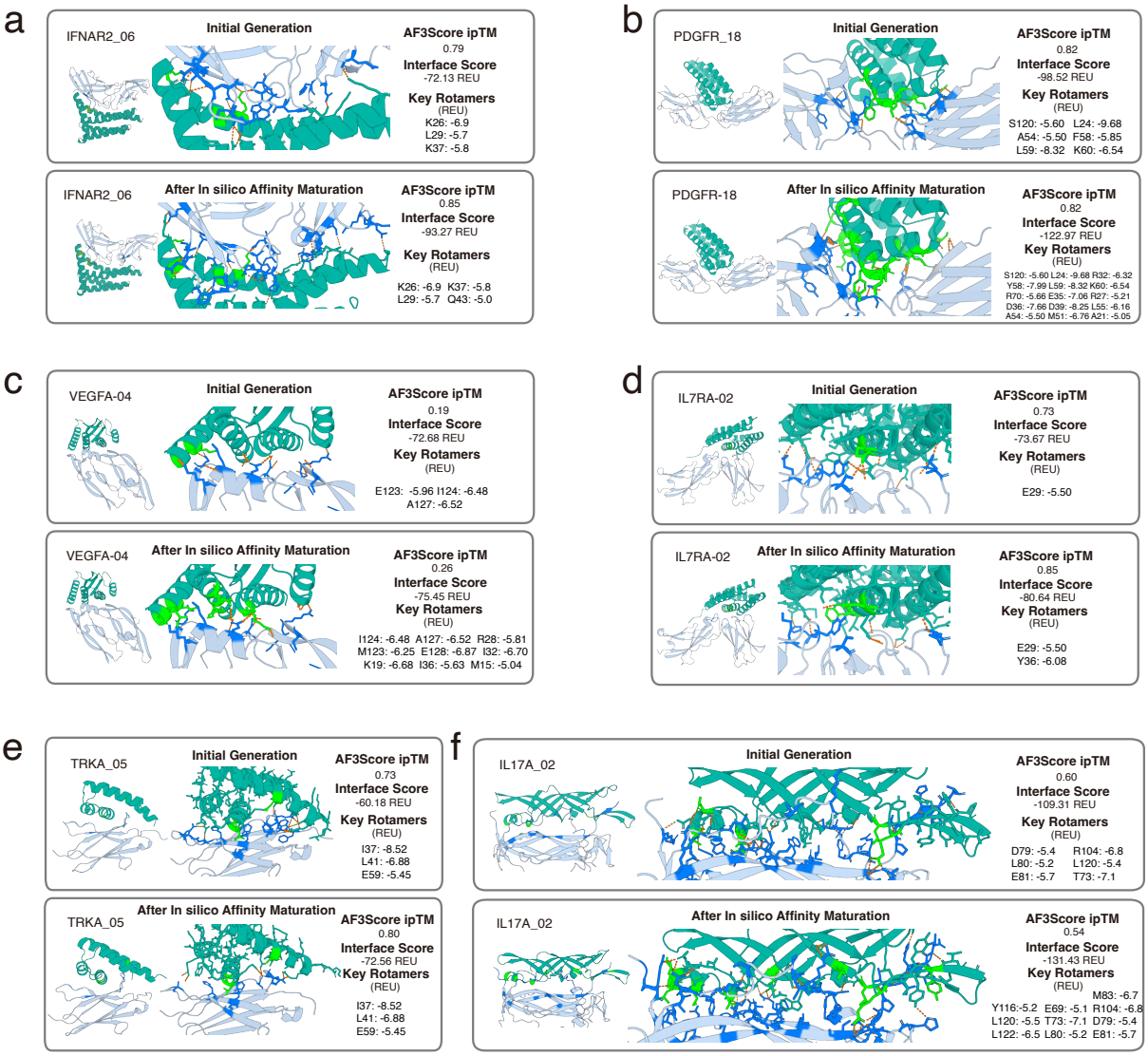

Figure S8: Affinity maturation and structural characterization of designed binders.

(a–f) Optimization of lead candidates for each target. (Note: PD-L1 is omitted here as it is presented in the main figure). Each panel displays a comparative view between the initial generative model output (top) and the variant after affinity maturation (bottom). **Structural details:** Left panels illustrate the global fold and magnified interface interactions. Key residues on the designed binders are highlighted in *green*, with target-binding residues shown in *marine*. Hydrogen bonds are represented by *orange dashed lines*. **Computational metrics:** The corresponding AF3Score confidence scores and Rosetta interface energy scores are provided to the right of each structure. The interface decomposition highlights critical residues achieving total interaction energy < -5 Rosetta Energy Units (REU).

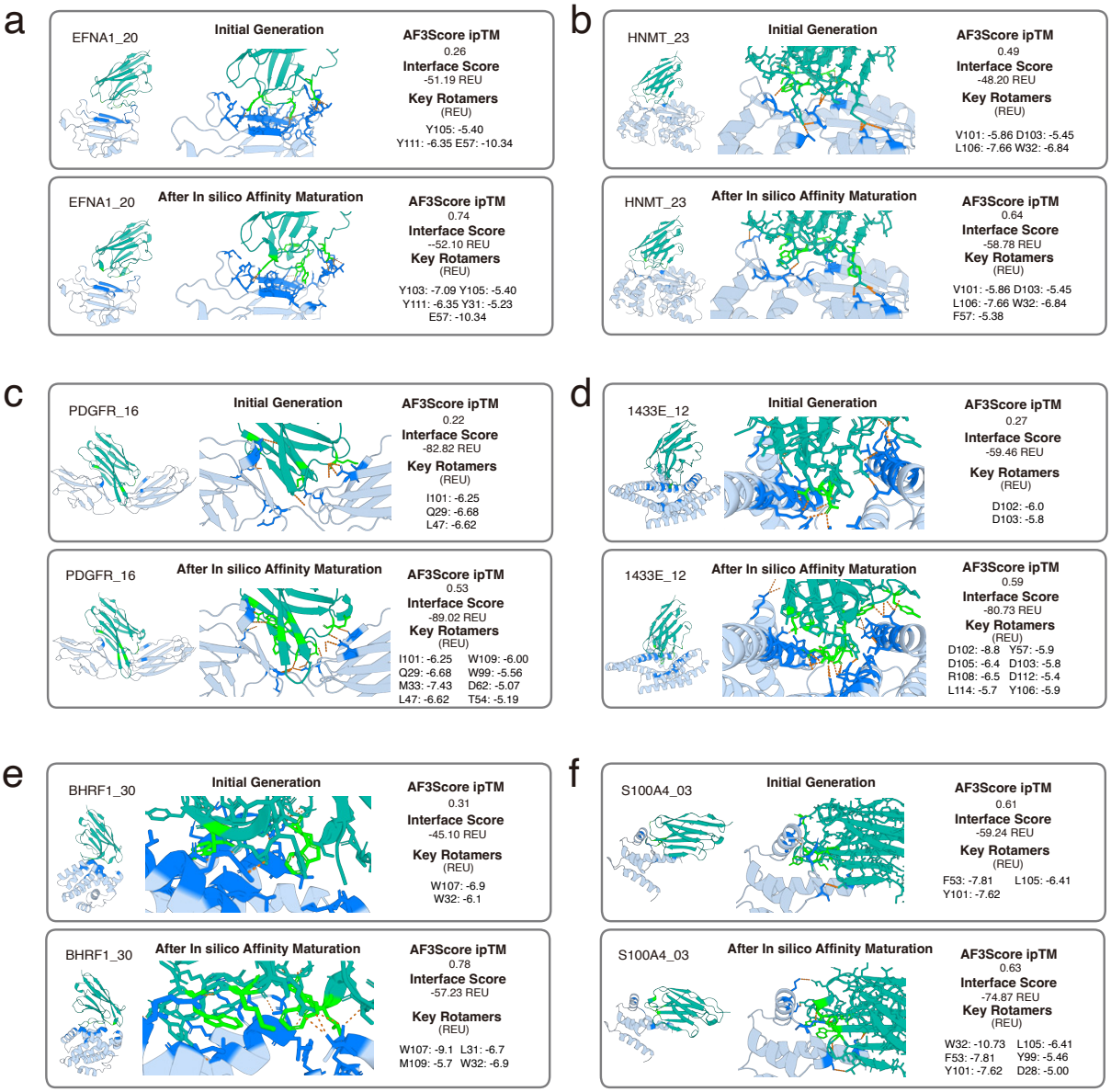

Figure S9: Affinity maturation and structural characterization of designed VHHs.

(a–f) Optimization of lead candidates for each target. (Note: CCL2 is omitted here as it is presented in the main figure). Each panel displays a comparative view between the initial generative model output (top) and the variant after affinity maturation (bottom). **Structural details:** Left panels illustrate the global fold and magnified interface interactions. Key residues on the designed binders are highlighted in *green*, with target-binding residues shown in *marine*. Hydrogen bonds are represented by *orange dashed lines*. **Computational metrics:** The corresponding AF3Score confidence scores and Rosetta interface energy scores are provided to the right of each structure. The interface decomposition highlights critical residues achieving total interaction energy < -5 Rosetta Energy Units (REU).

Appendix E Supplementary Tables

Table S4: Binder design task specifications for *in silico* benchmarking and experimental testing.

Design target	PDB ID	Input	Hotspot residues	Length range
PDGFR	3mjg	X124–312	X136, X138, X186, X246, X259, X264	90–150
IL7Rα	7opb	B36–231	B50, B76, B81, B97, B103, B155, B158, B162, B183, B187, B211, B212	90–150
IFNAR2	3se4*	C34–232	C46, C48, C76, C80, C98, C100, C133, C138, C186, C189, C190	90–150
PDL1	8znl	B20–133	B50, B64, B118, B126	60–130
IL17A	4hsa	A17–131, B19–127	A20, A85, A96, A99, A105, A127, B25, B26, B27	120–160
TRKA	1www	X282–382	X294, X296, X333	60–150
VEGFA	1bj1	V14–107, W14–107	W81, W83, W91	90–150

* For IFNAR2 (PDB: 3se4), missing residues at the protein interface were repaired using homology modeling via SWISS-MODEL.

Table S5: VHH design problem specifications for *in silico* benchmarking and experimental testing.

Design target	PDB ID	Input	Hotspot residues	CDR length range
CCL2	4dn4	M9-69	M28, M39, M55, M61	8,8,9-21
PDGFR	3mjg	X124-312	X136, X138, X270	8,8,9-21
1433E	2br9	A3-232	A175, A198, A218, A229	8,8,9-21
BHRF1	2wh6	A2-158	A64, A71, A80, A87, A106	8,8,9-21
IL13	1ijz	A1-113	A11, A14, A15, A101, A107, A108	8,8,9-21
EFNA1	3hei	B18-149	B46, B90, B114	8,8,9-21

Table S6: Design summary for protein and unique scaffolds information.

Target	Format	Unique Scaffolds	Hits to Wet Lab
IL17A	Binder	30	30
IL7Rα	Binder	22	30
IFNAR2	Binder	26	30
PDGFR	Binder	23	30
PDL1	Binder	26	30

Target	Format	Unique Scaffolds	Hits to Wet Lab
TRKA	Binder	27	30
VEGFA	Binder	28	30
1433E	VHH	30	30
BHRF1	VHH	30	30
CLL2	VHH	30	30
EFNA1	VHH	16	30
HNMT	VHH	30	30
IL13	VHH	20	30
PDGFR	VHH	30	30
S100A	VHH	30	30

Table S7: Sequences and binding affinities of all binders per target.

Design	K_D (M)	Sequence
IL17A_01	2.49×10^{-8}	MSGMTYLVMNPGDVDSGNVNPYLIAKYWDEIEALAKEVVANGG APVTKTLTETEKITVTFTTWEAAEPLYPTGRLPPNSTFLSTET VTVTVKTETTLTAELLWYDPELNIAMVRVTIKVKVTLLDDPSD PYVQALLQLPQEGTGEITVLVSGSGSHHWGSTHHHHHH
IL17A_02	7.47×10^{-10}	MSGSTMHIKSSDLVGAWVSGLSTTVSVTRPDGTTVTLTVSGEA RIVSAEDATLTFDPADPTKAEGTFKATVEVENTSIDNVDLEVM EQVGGSLTANVTLKLSLDPERSYTGTDSSGNTYYSGLLLVEPV ESEPAVINGSGSHHWGSTHHHHHH
IL17A_05	1.39×10^{-7}	MSGIVVSPSSISAAPGSSISITVTLTGVPSGSVVYVEVSLYES DFTDLYQLLDSATLNTATSTSVTFTINLSSLKSFSTELTLVDG SKVTRTRKIVARYSLMTPSVDPATGTPIYVARPGNVDGSDSTT LSEGSGSHHWGSTHHHHHH
IL17A_08	1.66×10^{-7}	MSGGTSILVAHVKGEDAKVELLTPVVEDTLPPPGTKNLLSSKI YDEKGNEVEEYLKSKGKFMIVILLDTYEVTLIFRTKEEDADEI LKKYPTLIFEYVAYRGEKKLVEDGMDPETNMPDITEKYQWWVE RVTAKGKLKKVSPEELPALKAKLLGFGLWEGSGSHHWGSTHHH HHH
IL17A_10	2.72×10^{-8}	MSGAAPAVTISETTTKLSTTYTANSDGTITLTVTITTPDGTTK TITFTFRPANPLASTIVSATLSDITVTLINVTITAPADNAVTV KYYKENSTKPILETETIAPGQSGTVIFPRIEGTLTLTTRGELG GEVIDEETKTIPVATYPASLELTSNGATYSVNVGSGSHHWGST HHHHHH
IL17A_11	1.32×10^{-7}	MSGTRSLNLLTVTLTISHDVDISKGEEAEITITVTVTSADGSK ITSTLVLSSVMNRLSSGSPDIHTTVSIDEKNGTITVELVFPAE PGEYKVDATVNIKTRNFDGETSSKTEKVEAKLSLETIELEPGE SKQLSEDLYVVNPLGSGSHHWGSTHHHHHH

Continued on next page...

Table S7 (Continued)

Design	K_D (M)	Sequence
IL17A_12	8.30×10^{-8}	MSGGIDFSFLTEEDVGKWVEVESSLKASVDDYEVEIEGTFAVK VSRSYTVTSPDGSSSSTAIVVSDYSLLSGKITVKIPKEVYDAA KKWGEDHVTDVLNDLVRSMLGFIIPSDTKWEFVSTSEDGMATY EAEVKLPRPPGSGSHHWGSTHHHHHH
IL17A_14	6.38×10^{-8}	MSGGVSEDIPEEEALALATEALTKAYNGKTVTRTFANETSDIP VDAPFKERMAVEWYLEGDDDRVVIVPVEATFEGERTLTSVDGE PLDPAEMKAIAAKAKAAGKKISLGEIANEYTKSTTIFGLPEIH SYITVEEKVKLVKVEILPEFKGKVLVKTLGSGSHHWGSTHHHH HH
IL17A_17	7.45×10^{-9}	MSGSVTVTIEFEETIYPSNYFTGIETDDLIIELTLLSYKVKYK GSAVVENGVAVIRPEDMEPLKVLEAKVKLTVFDHFAPGKSTTI SLKDENGNELVSLEVKGGEIKSKEFTFKIETDKLLDVTEEIKK YIYLDGKPLGSGSHHWGSTHHHHHH
IL17A_19	2.93×10^{-8}	MSGSNSKIEVDKEEKIEGDKLIIELDIELEGLANESVQKLVEE IKKELGEDTNIEIYVEGKPLKWPKELPLDIMAPVNARVSIKIK IVAFLGSGSHHWGSTHHHHHH
IL17A_20	1.42×10^{-8}	MSGKKTYMFAIAKVTFTFFDDASIFSDATATVTVYKDGKNITG DPNLTVSMSYDYTLSLSKTVTVLVRYVEEVKDENTKYTVNVTV TATFTPLPDPEFRAALTSNVLPATTTKTSTVEAKKIYVTIPEG YSLSISYDPYHDTVSVEISPGSGSHHWGSTHHHHHH
IL17A_21	3.82×10^{-7}	MSGMDKALIVLLKGKLKEPLEIMKKNNLSILEMEELIVKRIKE EGLSSLNMEIVDVYRLEDGKLTKLEEEKITMEEVDKMKGVIAI DLRYTTTPKPETLNEDGIPDWTSKPYGDREITDIELYAAVVTT PEGEPLKEYAKELAIYLVRKYAEESGSGSHHWGSTHHHHHH
IL17A_22	4.90×10^{-6}	MSGGSTSYVLNDPVVSIKGVPEEEVEKIEVDEEKTITLKPNMN ISDLVEELLKLIKEMEKKLLEKVQANLESLKVGEVVELKTLIK LTPAGGKPVTISANSFMGPDLASRLANDLINVFLNDFGAKKSA DGFSITLPAKPLYLLLTVSISISSRGSGSHHWGSTHHHHHH
IL17A_24	6.20×10^{-7}	MSGMVTVSVTVDLTEKGTLVSRTETTGATTTSLDTSLDNRDRA SDPVVTSISIVDVETGSSEGIEIESITIMELPEPQADTNWRYL VTLSVKLPEGSSFSKTLNITLTTSYNKTTVTTSNRPGVNDDFV TMSEVNTQTSTVTETWSATVNVTFKPPGSGSHHWGSTHHHHHH
IL17A_27	1.09×10^{-7}	MSGATETIVLTEDDITVTANEKSLTVTPDTTSLTFTATLTIKA LPHDLGEITVTFSLAYFQSQGLIVSGAPVTVTVKAGETVTVTR TLTVPLSKLKNIVQRLKWGWEGEEQLVIAAELTSENLDGGKAP RVYSDPITIKVVLPEGSGSHHWGSTHHHHHH
IL17A_28	8.48×10^{-8}	MSGMKTTYITVPLGETTTITVTLTADQHPSMGPTVTVTVKIAV NTFYYSTPAGFDQTLQSQTVARGSTTTITISLNNKELAGDRML DGFAEITVLVYYETHVPIAPPFTVNGKTYYPMESVLSGEKVII GVREGSGSHHWGSTHHHHHH
IL17A_29	8.41×10^{-7}	MSGMTVTLPTLPKLTLINSRGDDPNSVSLNIRENGKFKLYSVN FGESKTVTTTLLDANGNYVPVTLTLTLSEPKTVKPRTLLAEFE EAGLREWEVVKESTLTISVTVLATGASASTSTPVTVIEYSTEV GSGSHHWGSTHHHHHH

Continued on next page...

Table S7 (Continued)

Design	K_D (M)	Sequence
IL7RA_02	3.16×10^{-10}	MSGALKPPTPAEQLKDIAAAIKEAAAKGELIEMTQLLSFTLLV ASKIFGLDPELAAEMLRLLYLAAISENPEPIVKKAIELLNKLA EEAAKVDPETAAILKEAAERLAENPENVEPVLAELGIALAEHL AKHPKVKEMGSGSHHWGSTHHHHHH
IL7RA_04	1.73×10^{-8}	MSGKIKISEELMASISVMIGIIAQELREAGKEVDPELAKKLEK LAEEMEKLMEEIGKLMQDPNAKEEEIKEKVKKLVKVLEEAAKL AKELGKPELAEAIKELIKIIKEVVEDPSKQEEALKRVEEIINK IQDEIIKKRGSGSHHWGSTHHHHHH
IL7RA_06	4.35×10^{-8}	MSGKEKELEEIDKLVEEVIELMEKVAKALGISEERKEEIEKEI KEKGAEEVFVELAESGPLEEALYAAALALKETKNLPIEERLKK IARIMAAISSYLEYIIENKGEEIPNLELLKELLELTNELLDKI QELEKKGSGSHHWGSTHHHHHH
IL7RA_07	4.41×10^{-8}	MSGMSEEIKEKIDKLKAEGNEDEIIKLTYSILSLLVGLFEDVG AEAVVKGLYDDLFFGDNKEEAEEVIKEFLGLVENAAYGIKLIF PEEAETMEEIVKLAKEAVEYLKEGKVEEAVKKLNEIYELLLEP LKKLGELLEKKLSGSGSHHWGSTHHHHHH
IL7RA_08	8.85×10^{-8}	MSGDNITKEEFDEEIIKKLKELAEGKLEFENVDEAYAFLALVA RIIAKKTGKEEEIGKILSRAYIGMKYAEDESTLEKALEIAKEF AEEVEKMRKEGIFNAEYIVLAFAAYFIAKFLEKKGVKEAAEIR ERIKEAVKEGAEKVIKIIKEGSGSHHWGSTHHHHHH
IL7RA_12	8.65×10^{-8}	MSGEELLKELAEEIKRLLEDTEKLEEKLKAQGKPEEGKEAARR LLISFSLRMINRYLQKKPELKEIAKLIGKAILLLDEGKLEEAI KELEKAVELLKKLEGLEKRFGEIVELIAKILKAELEGNEKEAE KLYKKLKELLEKLAEELEKGSGSHHWGSTHHHHHH
IL7RA_14	6.98×10^{-8}	MSGDWRAEQLARLAELEAELAKLMKEADSKEVMEVLEKAHALL SLAQSLLEEDEDVSLSLFIYSILVLSKWPELKKEIYEEVAKKS PELLKKLEEIEKLIEEQKKNPENLEIVKELKKLLKELRADEEA VRALLEVLLEHLERLLAEARKLLGSGSHHWGSTHHHHHH
IL7RA_15	6.05×10^{-8}	MSGDITEEELKKAEIEVAAILIAITIVVLIFAGMYTKELVEKL LSTPVEEVKKLLEELEDLIEEALEKIYSRKDEKIGPIKEEILA KLKEAIAIAKALKPKSGELATLVAERLKAAAEVVKKMPDDATI TEALSKAIDAIRGHGSGSHHWGSTHHHHHH
IL7RA_17	1.16×10^{-7}	MSGDELFKEVNKEMKELLEKGKPELAEIIEEAMFLLDVSKKLA KKAKIVLETKDEELKKDLLEALKEFVERLKKFVEKVKKNIEEL SEATAKLIALMAKELKKTAKEIEKVDPELAKEIKKLAEELEAI LKSNPKHKKVVEELEGSGSHHWGSTHHHHHH
IL7RA_27	1.77×10^{-8}	MSGSGPTEEEYLEELLKEYEELKKKFEENPESMTLDDIVTLSA IARFLLSKGKKEEAMEVLAYAVKMAVAQGKYRTALALAAEIAK VAGDEELAKKIEEVFEKIETLDKETAKKLAAKALKEAAKALKK KGFEKTAKILKEAAKELEKGSGSHHWGSTHHHHHH
IL7RA_28	1.15×10^{-7}	MSGDLIEEAKKIEDETLKKIVEIMLTIDPSLAELPEEEKKLIA RAFVYLLYRHEEKLKYLDDKEKLLEILEELLKDAKNGAKTSLD EKVKKALDKLAEILEKLIKLAKEGDTSYFKKIVNTIEEGEKQI QELLKSASGSGSHHWGSTHHHHHH

Continued on next page...

Table S7 (Continued)

Design	K_D (M)	Sequence
IL7RA_29	1.12×10^{-7}	MSGSGPTLEEYLEELKKEYEALKKKFAEDPASMTDDDIVTLSA IARALLSEGKKEEAMLVLADAAAMAAAQGKYRTLLQLVAALAE AAGDKELAEEIKKAFEEAETLSPEEAAKLAAKMVEKAAKALKE KGYEEAAKRLKEIAKRLKAGSGSHHWGSTHHHHHH
IL7RA_30	9.74×10^{-8}	MSGLEEVAEEVKKLIEEIIKLLEELLSKLEIPEEDLAELEEML KKKSPEEVFVETAEGGPIGVTILAAIEALKSVLKLPVEEFLEK AARFMAALSNYFEERKEEIVKKSGNEELVKKIIEKAEKALDLI QSIKLAGSGSHHWGSTHHHHHH
IFNAR2_06	1.38×10^{-12}	MSGSEEKKKRENLRKAVNEVHRAVAKPLKESLNELISPLKTRE EVQQAIKEIHEIRKYLLENAEKYPLFKEAMKKAEEAKKKLEEF KENPFDEEAREEMLKKLKEAVKLAEKFEDLLERTAVLLIIAEK LKEVVEELSKKAREGSGSHHWGSTHHHHHH
IFNAR2_07	3.52×10^{-7}	MSGSAEIDANAARLEALLRSDPELAKAVNNLIHRKLGEKIKEI FEYLSKGEPEKAAELVMEMVDELIEELADPSLSEREAVVILLV LAIIYLRFGVAESAALLLDAVEAHRADPDAAIDRAAIVAALRA RRAEDRERILKNIEEVLKKLGSGSHHWGSTHHHHHH
IFNAR2_09	1.37×10^{-9}	MSGSEEEEKKRKLLRNLKYRIAKEFKPIVDKIVEILKESLHAG TFKEALSDGSVFVPYKDELIAIIDKAIASLKAMRDELESIDPE LAKKLGALIDKLQALRDAIKADPANFNYLEAFSALFREIQELL EEISKEIRGSGSHHWGSTHHHHHH
IFNAR2_12	1.13×10^{-8}	MSGGNHATLERYVGEVLKAAIDAARYARETGDLDAALARLVER AAEELAKLFRALGYEDTAAELGRRLAELLAELLRVVHDPSATQ EEADAIAAEALALAREATADAPEDDREALLRLLAQLLESLKNL WEVLDKVDAYLSGSGSHHWGSTHHHHHH
IFNAR2_14	7.10×10^{-7}	MSGMLEINAELSYLAAKAGRPYREEGAEVGMLKYKGDPSWKEK HAKVAAKLAAGRVEAAAKVVEKYFAEEWPEILKKLKEVAELTK KAVELAEKGEKKEAQALLKEAAKKLKEILKELPEEWKTLKEIV KLSIELLKTAAEGGSGSHHWGSTHHHHHH
IFNAR2_15	2.52×10^{-7}	MSGMAIRLERLKQLLETNKEAFLKRLKRMKEDAEKMEKIARTL LKLLKEYAEEHPEKKEELEKVLKKAEEIEKKIEELVKELKKLL EEAIKEVKEGNIEEAKKLLEKIVEIEDEILKLLREMRAMVEAL VGEDALSKRIIERNKAGITGSGSHHWGSTHHHHHH
IFNAR2_23	8.34×10^{-9}	MSGSVREAIRAIRRAVEAILAAVQLAIAEKAGLIDAAEAAAKL AKAFAIIKASLEKIKPFMDKETYEKINKLVAKMEKAIAAGKLD EAIKAAIEILELLKKLAEKFKKIPEVKEEAERAIKEIEEAIKE LKYLSENWEEIMKKIKEKIDSLGSGSHHWGSTHHHHHH
IFNAR2_25	7.95×10^{-7}	MSGSELEKRRRVTLAANIGALLAMLEQIEELLKEDPSLKNNPA VQKLFKDTTEKLEKLLKELSKLYPELKPLLAELAEQIKKALED PENREEYMAKAKELAAKILEKLKEIDPEAAAAFEKAYETYNNK EAVKKAIEILSGSGSHHWGSTHHHHHH
IFNAR2_26	3.48×10^{-9}	MSGMTPVQKAARAAVLKLLKKIKDAMNKISNLPALKGMDNKER SEVLRLLNVKEAIAAITEIPDEELDALGELLLAAGFPAELVER LRELVARLKALADNPYLKSWTQDASKEELKKLLKEKEKAKEAE EAFQELLRLLGEVLAAFERKGSGSHHWGSTHHHHHH

Continued on next page...

Table S7 (Continued)

Design	K_D (M)	Sequence
IFNAR2_27	1.22×10^{-10}	MSGGPYANTERKLAKIRKVILDAIYKAIKTGNVEEEMAKLAEK VAALLEELLAPYLAPEEAKALAKEIAKEIADLILKYFKGEITK EQLAAELDAIAARILAAFASAAAGEQALIARLLAIMRSEIVNA KEVFEKVLKRLSGSGSHHWGSTHHHHHH
IFNAR2_28	2.12×10^{-8}	MSGSAIKRERRKAITEEAAKVMKEVKAYIDALLKEAGKSKSEV LLEMIEKLKTEDFKAKLLEAAEIAKEAVKEGVAAIKAAIAADP KDIATVKKLAKEVLKKAAEVGKELAAKETDVATKVAIITTVTT TAIKLVAEAVAAGSGSHHWGSTHHHHHH
IFNAR2_29	3.53×10^{-7}	MSGSELGRRVRQIARLVVALASAMLLGDLDRAEEILRRLGKLV PGAREAFEAAVARTRALRAAGLPAAEILRAAAAAIREALEVAE REIVERLRAAGFPEEAIRLLRELFEAVREALRALADEGDAERA RELLRRAIELAEELDRLLRGSGSHHWGSTHHHHHH
IFNAR2_30	3.86×10^{-9}	MSGMELLKEAMARIAAALEDPELAALIREMAEHPGVVKMLFSR ARKLLEERGFLTPEDLLEILDLIGEVLQKVAEREGRKLPELEL VERLRATLRALPEEERARLVELLVEEIKKIVEKLEGKKRGSGS HHWGSTHHHHHH
PDGFR_01	1.14×10^{-8}	MSGMEEARKRAAELISRKTALLMLAISVAGLLTGVSRQELWDA ARAPLSPEELRAWAEALGKLSDEFIEKLLELLTSKDLRKQAAL ILELIRELAELLGDLREAALFLIRLLDEVSTLTARFLQEGESL EEAVRKGIEELREELLAQVGSGSHHWGSTHHHHHH
PDGFR_03	2.17×10^{-6}	MSGGRFADIDKVIKGLMGLFGIDYEEFKKNLEEGKLKEAAEQI KKLAKKMVELSEDLSKLRLMLLTAMALTVLLQKLVEEAKKSKD LEEKEYVLKTVEEIIKMIEEIIEKLEKHVKENPEDEESKEAAE FLRDILEWIKKMLEELKKTLGSGSHHWGSTHHHHHH
PDGFR_05	1.60×10^{-8}	MSGGGNRMSPFVKEVMKWIYEKFMEILDKKLKGEDIDEDVEEF VEEIIELLRETRGKEVEVSFGIALGLVLAIERYKKKHPGSEKV ITEIMRKIGEALARRVAAEGFEEEGREIAELIEKGGEIAATGD FGEAMKLFRKAFLLLAQVLARSGSGSHHWGSTHHHHHH
PDGFR_06	4.85×10^{-9}	MSGMPLIERIDEELERAKKDPEGVAEEEERKAVGAFYTLKLSA KNDKKFVSPELIRIELIEITFIAKELYEKTGDFEKSVEEAKKI AKEKLEKKLEKIKEGKLKEVLDELLELAKKYVEELNEELAELL KKVYKYLKEKFLSGSGSHHWGSTHHHHHH
PDGFR_08	1.13×10^{-10}	MSGRFSTVAGVVRTKDGYSFMIQFPVHLIDEEIGEKIAEEVKK VLGKYDEKTAEYIAKLIIEAGKEKDYEKKLKLMSKALMMLKVF LGSDMPSAKAFEAAYEILEAAVKIFLERGLPEEEVAGLRKSAE EAKKLKEEVEKLGKGSGSHHWGSTHHHHHH
PDGFR_09	6.35×10^{-11}	MSGMFEEIKKLVKEIFEKIQSNTAAQLAFRSVLLRLREDLDDD ATEWLIRLFGMLAALIKYLKISEELAEKLRELVKMLEEVEKKV KEKLSDEEKKKKYEELQKRIQEELRELVERVEQPNISLNTEVI PEFEKLVLEYIEGYKEIISGSGSHHWGSTHHHHHH
PDGFR_11	5.13×10^{-8}	MSGSNLTLAKIALARAAKLLRKGLEEGKLEPYLERAAALLFLA YKYSGNNLIAGIFALLLRALASPEDLRGQEAMLKKLEKDGAPK ELVEALRELVEEISKTSDEEKRRELVERLIELLERAVKGEVDL EEITEEIKEMIEFLKGSGSHHWGSTHHHHHH

Continued on next page...

Table S7 (Continued)

Design	K_D (M)	Sequence
PDGFR_13	3.74×10^{-8}	MSGTVAAGRVLNVATAAAFAVALSLGEISEEEAEELISETNHI ELLKKVFKILTKALEKIGEEERKEIISLIFDLVEEARTLPKDE LIKKLKEREEELKKKLEELKKKGADEKEIHKEEIKYNIYKAAL IAVQNNDTQKTLREILKYYKEGSGSHHWGSTHHHHHH
PDGFR_14	2.53×10^{-7}	MSGSMAKKNLVKMAMAASFVSGKPIALIPGKEFEISIELIMEK LKEVTDLDEAEEIIEMFFLIIAIAIKGRSEEERKKLIELAAKK LAETLNELVEKLKDPEGVARAVVEALERLSKMMKKEDVEYLRK LIIENLSEELAKLLEKGGSGSHHWGSTHHHHHH
PDGFR_15	$< 1.00 \times 10^{-12}$	MSGRFSTMAGVVRLKDGTAVMLSFNVELLASEVGAEIAEIVKE ILEPVNPKVGEYLKELILKMQKEKDYEEQVKLVSKFLMMLKVL LGSDMDTEEALEILIEIMRRIIEAALAAGYPEELTAGMRKTAE EAEKLLEERRARGEGSGSHHWGSTHHHHHH
PDGFR_16	2.86×10^{-9}	MSGSMKKEIDKLMAQLTGVVLGFLRKLGMSRKLRSLVLDGAQK LSEEVKEFIKEQLKLKDKVEAVRKLIKLAEELSKEPGKEKEVI FILALAFLLAYLAGDKELAREAVERLAEELKKSMPDKEEGERI AEELIARVDELLSGSGSHHWGSTHHHHHH
PDGFR_17	6.48×10^{-9}	MSGSKLQKIKQLEQLEVKQMQRLLERMKKLWEETGDKDELLRE IDRLFARHAATAYAIGKIDKELSKLELEHAKWLADEIIKLAND PNVSIEEVFKVLEKIIEFEEEFAKDISKAKSIEEVIEIFKEYV EKIKEFLGSGSHHWGSTHHHHHH
PDGFR_18	$< 1.00 \times 10^{-12}$	MSGMVEKTLEKAKEAKELILKNTAAQLAMRSVLLRLEEDLDDD AIEVLIRLLKMTAALLRYLKLDEKLAELLREIARGLEELKKEV EKKLSDEEIKKKVEELSKEIQKKLKEILEKAKQPGVSLEETVA PEVMDLVIKAIETYAELLSGSGSHHWGSTHHHHHH
PDGFR_19	6.17×10^{-11}	MSGSEIKELKLLLTKLVAAIRYASRHPEDFLDILRLAKEIFER VLEGIKKHPELIPFLSSALQQILAIIKKWMEDPRNQSAELLEA VAEFLEEIIKKLEEVLEYLKSSITPENEEELQKKIEILEATIK RLKELKEEILEKARKLKELEGSGSHHWGSTHHHHHH
PDGFR_20	1.97×10^{-7}	MSGMKKEIEETKKYIEEVIKKVEDDPVLVQILERLLKVLELYE EGKIEEALKELSRVGLMLVALFEANYEDIVEAVYKLLKKKGID SKELAEKEAEKFGKEIKKTALVSYPDFIAKQVKEMVEFLEELY NLLKLKKGSGSHHWGSTHHHHHH
PDGFR_27	5.96×10^{-8}	MSGMLSTLGKIAIVRAYKLIKKGLEEGKIEESLERAAALLFLA SKFEGNNKILLVLTTLIISIASPEDIRGAEAVLEKAKSEGLSE ELYEAVKEFIELMSKIKDEEKHKLAVERLAELLELAGKGELTE EKLTEHIKEMIEELKGSGSHHWGSTHHHHHH
PDGFR_29	1.24×10^{-5}	MSGMDKELAKELLKLLEELEEKLRKEYRNLAGGLGKAMLIFLD IAPWLREKGYEKVAKRTLDILADITEYLRKAGVRTEKEFLEVL KEKVDELIEEAKEALKKGDFEYVFAVILALSILSVGSSKEVQE YLEEKKNELVELLKKEIGSGSHHWGSTHHHHHH
PDGFR_30	1.24×10^{-9}	MSGRQVKVAVALKVKDKALRKMFEKLLEVINKLEDLEKANKGA LYLGATQHIIANETNYELTEENVEDVGEIIAKMIAALMDVSGI PEDDLVEAIKIMYEELVKEGREEMAKKLLETIAKELEKRGYPE LAKKVREILGSGSHHWGSTHHHHHH

Continued on next page...

Table S7 (Continued)

Design	K_D (M)	Sequence
PDL1_07	5.26×10^{-7}	MSGMDEEDLLRLIEKAKKLIEKLENEEIEDLKEKLRMLSLAAM YILLALKQPSAEKYLEELRELLERVKKLVEELKEKEGVEDKAT ELLLEDAERLLKEGSGSHHWGSTHHHHHH
PDL1_10	2.02×10^{-7}	MSGMWEELEKTLSEDEEVKEEALKKVREYVEKILEEAKKKGKL TPQQEFELLKVVAMLTYVDPEFVEEIIEKVEEIDDERAKKLVE KMKRHLEVAKKRPLRGSGSHHWGSTHHHHHH
PDL1_11	4.17×10^{-8}	MSGSEKEEKTLYLLKVAALFVRQYSKEAAELIEEALELFKQGK YEEALEKVEEARKEIEALGPEHKGLADLLDTVAKEIRELIGSG SHHWGSTHHHHHH
PDL1_13	5.57×10^{-8}	MSGSMMELMEELFKEIGVLFEVMKVRPELEEELRKVMELIRQA LRLLADGEDLAKAEEKLREAWELLEKHKEELLKAIEEVIEKNK DKPKLVKELEEFKKKLEGSGSHHWGSTHHHHHH
PDL1_15	1.09×10^{-6}	MSGMVKELIEAFEKGDEETVLKLLKEAVKLLKEGKLSKSDLIK ITIIATNFLDEPVTDEFIEELEKLDDEWAQRLAETLRRNKEGS GSHHWGSTHHHHHH
PDL1_17	5.03×10^{-7}	MSGSEEELERLRDKILLLLRALILALKDFPELAELLEELREAI EEGDLERTEELLEEIEELVEERREELSKAVLDALESLLRDVRR YIELEKKGSGSHHWGSTHHHHHH
PDL1_18	9.20×10^{-7}	MSGKEKEIEELKDKILLLLRALALALRDDPELVELIEKIAELL EKGDLEKAKELFEEFLELVEKRREELSKAVLDAIESLGKLFEE LLELKKEGSGSHHWGSTHHHHHH
PDL1_24	5.19×10^{-8}	MSGSMSLEEKFKKIMEKMKEAGFIPDKSFSSLEEVAESEDITV LTKVTMFLTNDEEVAKKFLEILEKQYKKLEEEVKKNPEDEELK RKAEHLKKLIEHLRKNLGSGSHHWGSTHHHHHH
PDL1_25	8.30×10^{-10}	MSGSSDLKAAERFLQNVLSFLLPEEAAKKLYEFILELVEKEPD LSREELKERIRELAAELGVELSDKELDSIVDIVELLRKLSGSG SHHWGSTHHHHHH
PDL1_26	5.14×10^{-12}	MSGSSDLEAAKRFLYNVLKFLLPEEVAEKLYEFILELVENEPD LSDEELKKKIRELAKKLGAELTDKQLDSIVDIVNLLRKLSGSG SHHWGSTHHHHHH
PDL1_27	9.11×10^{-8}	MSGDIFEDALAMLRAAALALRMVDEELQEAAEMIEEAVRLAKE GPDDPEALRKALEMVKEAREKVKELRKKSKNKKGLQSLIDMLD KAIELLEEYLKSGSGSHHWGSTHHHHHH
TRKA_05	7.41×10^{-8}	MSGMTEEQLRGLEEIGREVAEVGSLREIMARRPELAGLTIALM LKYGSWEVTVEQVEEAKEEVRRAGEERLARGSGSHHWGSTHHH HHH
TRKA_20	8.74×10^{-8}	MSGSITVSTASSVSVKEGSSLTLTATVTSDFDLSKHPVTVMLE RQFPGEEWELLGFISRRDGETTTAIDGRFQKAFNGGVSLSLTQ VSPHTLQVTLAIGNVKKEKDTAVYRFSVGVLDDEGWSRHNATG ADTKVTVTDGSGSHHWGSTHHHHHH

Continued on next page...

Table S7 (Continued)

Design	K_D (M)	Sequence
VEGFA_01	1.11×10^{-9}	MSGMKFKITIKLGNVPASEETKATLERILKKVAEEFGVKASIS FDFEKGTGEFVFEIEGPLEEAQEAILTLLRAVGMFLADISLGL SFELTIESIEFETDDSGFESPVDLSSLRGKPVLEAARFLFDKV EELEKGSGSHHWGSTHHHHHH
VEGFA_03	3.33×10^{-10}	MSGKKEDEETALFKRLLMVLVKDEKTTTETRALAIAMDIVLDS NKDLKVTKIEAEGLSLEEVEELIRNDIPVIGKFTVTIKKGDEE GKITINIKEEDGKIVVEIEGDPNDKLSSEIVEEIKKLAEMILE AEKAGSGSHHWGSTHHHHHH
VEGFA_04	$< 1.00 \times 10^{-12}$	MSGSEKERIRALFHRLLMLLVKDERTTDEARALAIAMEIYFTS TKDLEIVDINVNGMSQEEVEEKISKGEVILGKIEITFELDGKK HTIYIEIYEEDGKIKAEISADPNDKVSQELVKKIKELAEMILA AEKAGSGSHHWGSTHHHHHH
VEGFA_07	3.00×10^{-9}	MSGSMAELIELSEEVKMVVYTYELPETNRLVLHILLEVPEELV EEIIEKIKELLKKKGLPELEEVEAGEVMAKGREGKNVYAVVPG EGKAIIEIMLVFEGPREESLKKAEEVLEEIIELLKKILGSGSH HWGSTHHHHHH
VEGFA_11	3.14×10^{-9}	MSGMEEAVRLAVAALRELAKVLSRHLSPEARREIWEIVKRTAE EMARLAGIEIDGRDIARAEAMILAALDGSKDIPEELYEPAKRL GEAVAAVREALDDPAADVAAAIEELTEVMEEVLREGGAPEEAI EVLREGVERIIEIVRREGLAGSGSHHWGSTHHHHHH
VEGFA_12	1.21×10^{-8}	MSGMFDELLKAYEGVKPVDLTEEQTPTLQEVVEELEARGIERP EGFSFDSARGVRQAFLHLGHRALQNPEEHLEEVLTIIEVLLER IKELVDLLKDPENSHLDKEVLKHTLAVLLDILMELVFLNFEHL PKDFQEKLLKVVKEASEVLKGSGSHHWGSTHHHHHH
VEGFA_24	1.12×10^{-8}	MSGMHAPDPSMSVKDVLLLLKHFLEEVLDLLYALTQLEDPEKE ADKLVELVRKLGDAYGIHPEIVELIQEVIEKHKDDAKKALEEI EKFLKLVEGLLSLAPILEEKGVSVDELVKLLVELLKKIEEEGI DPEELIKELKEELEGSGSHHWGSTHHHHHH
VEGFA_25	7.88×10^{-9}	MSGMGQSALRVTMNIEVGDIKAGSNLDIIKLPDGTSLLIFEGP GLFDIRELSEEELEQPLRSIVVPLFQKSAENFAKIVIERLGSE DVEAKISVSAQVFDENGKPKIPELSASGTTKVKDLAKEVAELT TKLVDELEKKFGKTLKEILGSGSHHWGSTHHHHHH
VEGFA_26	1.85×10^{-9}	MSGMNLDVASLLVQLSGFDIEKVKEVAEKFVEYLKKNVPDMVI RINVYSSEDSLWIEIHGALPLTEALYKMFKIIAENKDKPLEEI KKKATEEATEIIRRLLEEAGEPELGEKVVSHVEEITELLVELL EKGVESIDSVLNRPGRRPGSGSHHWGSTHHHHHH
VEGFA_28	1.78×10^{-8}	MSGSFSFEYTLEADSEEEREALAVALIGSLYEMKLENPDIISS LTVRLLDSEEEALEESESAIPLVEKILKEKKVTKGSVIHVHLV FLPEKDGKYLLKVHVDVILATGMSKEEQEEVKKKIEELFEEVI KRAKEKVESFKDVLGSGSHHWGSTHHHHHH
VEGFA_30	2.24×10^{-8}	MSGMEALRKLKALLINSSVGADDSTIIAALLLIEIVDASELRL KSKDPNLPEEEKKKLLEDVKWRIENLAKFVKELLEKYAPDVKL EDVVKKVEELAEKVAEKIKELKVKAEELVENLEEVAEELKKLG LDELAKALEEAAEKLKEVSKLGSGSHHWGSTHHHHHH

Sequences listed include vector-derived residues resulting from subcloning into the pIVEX vector. The N-terminus contains an MSG prefix, and the C-terminus includes the extension GSGSHHWGSTHHHHHH, comprising a SNAC cleavage tag and a 6×His affinity tag.

Table S8: Sequences and binding affinities of all VHHs per target.

Design	K_D (M)	Sequence
CLL2_01	1.46×10^{-6}	EVQLVESGGGLVQPGGSLRLSCAASGGTFSSYYMGWFRQAPGKGREL VAAISSSGIYTYYPDSVEGRFTISRDNAKRMVYLQMNSLRAEDTAVY YCAAAEKAIDVFFSASGAKWWGQGTQVTVSSGGGGSHHHHHH
CLL2_02	5.04×10^{-7}	QVQLQESGGGLVQPGGSLRLSCAASGYTFSSYFMAWFRQAPGKERER VAKIYPGSGSTYLADSVKGRFTISQNNAKSTVYLQMNSLKPEDTAMY YCARIDRTKSYDYWGQGTQVTVSGGGGSHHHHHH
CLL2_04	1.59×10^{-6}	QVQLQESGGGLVQPGGSLRLSCAASGFTTSYYAMAWFRQAPGKERER VAKISSSGRYTYLADSVKGRFTISQNNAKSTVYLQMNSLKPEDTAMY YCAASDISTSGFTTSSFSYWGQGTQVTVSGGGGSHHHHHH
CLL2_07	6.57×10^{-7}	QVQLQESGGGLVQPGGSLRLSCAASGFTTSYYFMAWFRQAPGKERER VAKINPATGSTYLADSVKGRFTISQNNAKSTVYLQMNSLKPEDTAMY YCARQNSLTTYDSWGQGTQVTVSGGGGSHHHHHH
CLL2_08	1.77×10^{-6}	EVQLVESGGGLVQPGNSLRLSCAASGFTFSSYRMSWVRQAPGKGLEW VSSISTSGGSKLYADSVKGRFTISRDNAKTTLYLQMNSLRPEDTAVY YCSRRLYTYGSLSSSDVSSQGTLVTVSSGGGGSHHHHHH
CLL2_12	2.06×10^{-7}	EVQLVESGGGLVQPGNSLRLSCAASGFTFSTYRMSWVRQAPGKGLEW VSSISSGGTYKLYADSVKGRFTISRDNAKTTLYLQMNSLRPEDTAVY YCSAVLSSSSNPTSLVSSQGTLVTVSSGGGGSHHHHHH
CLL2_14	1.91×10^{-7}	EVQLVESGGGLVQPGGSLRLSCAASGFTFSSYAMGWFRQAPGKGREL VAAISSGSRNTYYPDSVEGRFTISRDNAKRMVYLQMNSLRAEDTAVY YCARLKTYYSIPFSLTTSAFDSWGQGTQVTVSSGGGGSHHHHHH
CLL2_15	5.80×10^{-8}	QVQLQESGGGLVQPGGSLRLSCAASGSFSIVDRMAWFRQAPGKERER VAKISLYSGNTYLADSVKGRFTISQNNAKSTVYLQMNSLKPEDTAMY YCARTLGYDGSDADYWGQGTQVTVSGGGGSHHHHHH
CLL2_18	3.04×10^{-7}	QVQLQESGGGLVQPGGSLRLSCAASGTLSSVDRMAWFRQAPGKERER VAKMNLYNGNTYLADSVKGRFTISQNNAKSTVYLQMNSLKPEDTAMY YCVRSGGSGSSYWGQGTQVTVSGGGGSHHHHHH
CLL2_21	2.50×10^{-10}	EVQLVESGGGLVQPGNSLRLSCAASGFTFSTYAMSWVRQAPGKGLEW VSSISSSGSYTLYADSVKGRFTISRDNAKTTLYLQMNSLRPEDTAVY YCSRLLYSFSLVKSTLKTSYFGSSSQGTLVTVSSGGGGSHHHHHH
CLL2_22	4.32×10^{-7}	QVQLQESGGGLVQPGGSLRLSCAASGFTTSSAFMAWFRQAPGKERER VAYISSGGGNIYLADSVKGRFTISQNNAKSTVYLQMNSLKPEDTAMY YCASYYNDSSLNRGKRVWGQGTQVTVSGGGGSHHHHHH
CLL2_24	2.82×10^{-6}	EVQLVESGGGLVQPGNSLRLSCAASGFRFSSYAMSWVRQAPGKGLEW VSSISWDGSNKLYADSVKGRFTISRDNAKTTLYLQMNSLRPEDTAVY YCRRTGSYDSTSLSSGLGSSQGTLVTVSSGGGGSHHHHHH
CLL2_27	8.41×10^{-7}	EVQLVESGGGLVQPGGSLRLSCAASGGSFSYYRMGWFRQAPGKGREL VAAISYSGGSTYYPDSVEGRFTISRDNAKRMVYLQMNSLRAEDTAVY YCARLLTTRADSAPDYWGQGTQVTVSSGGGGSHHHHHH

Continued on next page...

Table S8 (Continued)

Design	K_D (M)	Sequence
1433E_04	5.71×10^{-8}	EVQLVESGGGLVQPGGSLRLSCAASGDYGTDYNMAWYRQAPGKGREL VAGISYDGRYKSYADSVKGRFTISRDNAKNTLYLQMNSLRPEDTAVY YCRAARRDAYYVRSDSYVAWGQGTLVTVSSGGGGSHHHHHH
1433E_10	1.13×10^{-7}	EVQLVESGGGLVQPGGSLRLSCAASGALLDMSTMAWYRQAPGKGREL VAGINLYSGTTSYADSVKGRFTISRDNAKNTLYLQMNSLRPEDTAVY YCVSRTEFSDTAYARRHQAYFWGQGTLVTVSSGGGGSHHHHHH
1433E_11	2.85×10^{-8}	QVQLQESGGGLVQPGGSLRLSCAASGATSSVDYMAWFRQAPGKERER VAKMNVWYGNTYLADSVKGRFTISQNNAKSTVYLQMNSLKPEDTAMY YCAAVTTLFSGRAYAYWGQGTQVTVSGGGGSHHHHHH
1433E_12	6.47×10^{-9}	EVQLVESGGGLVQPGGSLRLSCAASGGTLSSYYMGWFRQAPGKGREL VAAISRSGIYTYYPDSVEGRFTISRDNAKRMVYLQMNSLRAEDTAVY YCAAVPYDDIDYWRRAGDYLYWGQGTQVTVSSGGGGSHHHHHH
1433E_24	5.11×10^{-8}	EVQLVESGGGLVQPGGSLRLSCAASGFTFSRAAMGWFRQAPGKGREL VAAISSDGSYHYYPDSVEGRFTISRDNAKRMVYLQMNSLRAEDTAVY YCATVYENYYSGMMYEAWGQGTQVTVSSGGGGSHHHHHH
1433E_27	1.66×10^{-8}	EVQLVESGGGLVQPGGSLRLSCAASGSYRGFDFMAWYRQAPGKGREL VAGINDGSGYTSYADSVKGRFTISRDNAKNTLYLQMNSLRPEDTAVY YCRAATIYFSGRATVTWGQGTLVTVSSGGGGSHHHHHH
PDGFR_01	4.44×10^{-8}	EVQLVESGGGLVQPGGSLRLSCAASGGTFIETFMGWFRQAPGKGREL VAAISSSGSRTYYPDSVEGRFTISRDNAKRMVYLQMNSLRAEDTAVY YCAAYYLDRSSKTLKVSWGQGTQVTVSSGGGGSHHHHHH
PDGFR_03	1.69×10^{-7}	EVQLVESGGGLVQPGGSLRLSCAASGSSSSSYFMAWFRQAPGQEREF VAGINWSGNRTLYADSVRGRFTNSRDNSKNTLYLQMNSLRAEDTAVY YCTTLDMRNRSVSYWGQGTLVTVSSGGGGSHHHHHH
PDGFR_04	3.61×10^{-7}	EVQLVESGGGLVQPGGSLRLSCAASGASLHSGFMGWFRQAPGKGREL VAAINNRNGDTYYPDSVEGRFTISRDNAKRMVYLQMNSLRAEDTAVY YCAVMGYYTSYSSKTTNKAYWGQGTQVTVSSGGGGSHHHHHH
PDGFR_05	2.97×10^{-8}	EVQLVESGGGLVQPGGSLRLSCAASYGNQIITMMAWFRQAPGQEREF VAGIYVASGYTLYADSVRGRFTNSRDNSKNTLYLQMNSLRAEDTAVY YCSSWYYSSSGSLTNTWGQGTLVTVSSGGGGSHHHHHH
PDGFR_06	1.12×10^{-7}	EVQLVESGGGLVQPGGSLRLSCAASGSTSSYTAMAWFRQAPGQEREF VAGIYAGSGTTLYADSVRGRFTNSRDNSKNTLYLQMNSLRAEDTAVY YCASYLISGTLTVTWGQGTLVTVSSGGGGSHHHHHH
PDGFR_07	1.56×10^{-8}	EVQLVESGGGLVQPGGSLRLSCAASGGTFTSYAMAWFRQAPGQEREF VAGINSSGGFTLYADSVRGRFTNSRDNSKNTLYLQMNSLRAEDTAVY YCARHSHSWITKYTSTFSPSYMYWGQGTLVTVSSGGGGSHHHHHH
PDGFR_08	4.11×10^{-8}	EVQLVESGGGLVQPGGSLRLSCAASGTYAFVALMGWFRQAPGKGREL VAAISISSGYTYYPDSVEGRFTISRDNAKRMVYLQMNSLRAEDTAVY YCAAMTLSSGKSVISWGQGTQVTVSSGGGGSHHHHHH
PDGFR_09	9.24×10^{-8}	EVQLVESGGGLVQPGGSLRLSCAASGFSGYAAMMAWFRQAPGQEREF VAGISWNGSYTLYADSVRGRFTNSRDNSKNTLYLQMNSLRAEDTAVY YCAQLDMKSGKSTVYWGQGTLVTVSSGGGGSHHHHHH

Continued on next page...

Table S8 (Continued)

Design	K_D (M)	Sequence
PDGFR_11	8.09×10^{-9}	EVQLVESGGGLVQPGGSLRLSCAASGGTFSNYFMAWFRQAPGQEREF VAGISWSGSRTLYADSVRGRFTNSRDNSKNTLYLQMNSLRAEDTAVY YCASIGIYSGTVKTYWGQGTLVTVSSGGGGSHHHHHH
PDGFR_12	3.10×10^{-8}	EVQLVESGGGLVQPGGSLRLSCAASGGSFSTNFMAWYRQAPGKGREL VAGISFSGSRTSYADSVKGRFTISRDNAKNTLYLQMNSLRPEDTAVY YCSAFEIKRGKLTVYWGQGTLVTVSSGGGGSHHHHHH
PDGFR_13	1.56×10^{-7}	EVQLVESGGGLVQPGGSLRLSCAASGGTFYQYFMAWFRQAPGQEREF VAGISVNGSYTLYADSVRGRFTNSRDNSKNTLYLQMNSLRAEDTAVY YCATLSVRGGSSTWGQGTLVTVSSGGGGSHHHHHH
PDGFR_14	3.96×10^{-8}	EVQLVESGGGLVQPGGSLRLSCAASGDRGGVYPMAWYRQAPGKGREL VAGISSGGSQTSYADSVKGRFTISRDNAKNTLYLQMNSLRPEDTAVY YCARGYWTAATAWVAGMFAYYGYWGQGTLVTVSSGGGGSHHHHHH
PDGFR_15	1.57×10^{-8}	EVQLVESGGGLVQPGGSLRLSCAASGSLTGGYWMAWFRQAPGQEREF VAGLLYHGTRTLYADSVRGRFTNSRDNSKNTLYLQMNSLRAEDTAVY YCAVMDLRNSSTSYWGQGTLVTVSSGGGGSHHHHHH
PDGFR_16	4.09×10^{-9}	EVQLVESGGGLVQPGGSLRLSCAASGTTQSIVMMAWYRQAPGKGREL VAGISNTGRYISYADSVKGRFTISRDNAKNTLYLQMNSLRPEDTAVY YCAVWQISYSGSTTWTVYWGQGTLVTVSSGGGGSHHHHHH
PDGFR_17	1.89×10^{-6}	EVQLVESGGGLVQPGGSLRLSCAASGGTFTSYFMAWYRQAPGKGREL VAGTSWSGIRKSYADSVKGRFTISRDNAKNTLYLQMNSLRPEDTAVY YCTALEIRGTSDGTARADYTYWGQGTLVTVSSGGGGSHHHHHH
PDGFR_18	2.42×10^{-7}	EVQLVESGGGLVQPGGSLRLSCAASGTISSVVIMAWFRQAPGQEREF VAGIYVWSGSTLYADSVRGRFTNSRDNSKNTLYLQMNSLRAEDTAVY YCSTFAISSGTLTVTWGQGTLVTVSSGGGGSHHHHHH
PDGFR_20	6.37×10^{-9}	EVQLVESGGGLVQPGGSLRLSCAASGTTGNIALMAWYRQAPGKGREL VAGISRSGSYTSYADSVKGRFTISRDNAKNTLYLQMNSLRPEDTAVY YCAAFAASYSGSSSWTVVWGQGTLVTVSSGGGGSHHHHHH
PDGFR_21	1.82×10^{-8}	EVQLVESGGGLVQPGGSLRLSCAASGGTFSSYFMAWFRQAPGQEREF VAGISPGGGRTLYADSVRGRFTNSRDNSKNTLYLQMNSLRAEDTAVY YCATIPFSSSYRLSKDTSPYWGQGTLVTVSSGGGGSHHHHHH
PDGFR_22	8.26×10^{-8}	EVQLVESGGGLVQPGGSLRLSCAASGGTFTNHFMAWFRQAPGQEREF VAGISPSGSTTLYADSVRGRFTNSRDNSKNTLYLQMNSLRAEDTAVY YCAAIDLRTGSTVWGQGTLVTVSSGGGGSHHHHHH
PDGFR_23	9.66×10^{-8}	EVQLVESGGGLVQPGGSLRLSCAASGGNFHNYFMAWFRQAPGQEREF VAGISSSGSYTLYADSVRGRFTNSRDNSKNTLYLQMNSLRAEDTAVY YCAAYDYSGNTVWGQGTLVTVSSGGGGSHHHHHH
PDGFR_25	5.90×10^{-8}	EVQLVESGGGLVQPGGSLRLSCAASGGTFSSYGMAWFRQAPGQEREF VAGISGSGSSTLYADSVRGRFTNSRDNSKNTLYLQMNSLRAEDTAVY YCAKDMFSGLRIRVTASSMLAWGQGTLVTVSSGGGGSHHHHHH
PDGFR_26	2.32×10^{-7}	EVQLVESGGGLVQPGGSLRLSCAASGGTFISHFMGWFRQAPGKGREL VAAISWNGSSTYYPDSVEGRFTISRDNAKRMVYLQMNSLRAEDTAVY YCASWYWSSSGTLKVTWGQGTQVTVSSGGGGSHHHHHH

Continued on next page...

Table S8 (Continued)

Design	K_D (M)	Sequence
PDGFR_27	1.53×10^{-7}	EVQLVESGGGLVQPGGSLRLSCAASGSSSGASHMAWYRQAPGKGREL VAGIDRGTGDTSYADSVKGRFTISRDNAKNTLYLQMNSLRPEDTAVY YCASTYYAGKTFILGYITSLFRYWGQGTLVTVSSGGGGSHHHHHH
PDGFR_29	1.52×10^{-7}	EVQLVESGGGLVQPGGSLRLSCAASGGSLAGGFMAWFRQAPGQEREF VAGINLASGSTLYADSVRGRFTNSRDNSKNTLYLQMNSLRAEDTAVY YCARLYWDRSTKKWKYVWGQGTLVTVSSGGGGSHHHHHH
PDGFR_30	8.16×10^{-8}	EVQLVESGGGLVQPGGSLRLSCAASGGNLLDHFMGWFRQAPGKGREL VAAISASGSSTYYPDSVEGRFTISRDNAKRMVYLQMNSLRAEDTAVY YCAAISVYGSSAAWGQGTQVTVSSGGGGSHHHHHH
BHRF1_04	3.64×10^{-7}	EVQLVESGGGLVQPGGSLRLSCAASGGTFSSYGMAWYRQAPGKGREL VAGISSSGSSTSYADSVKGRFTISRDNAKNTLYLQMNSLRPEDTAVY YCAAEDEISYYGLYIYATVAWGQGTLVTVSSGGGGSHHHHHH
BHRF1_05	2.38×10^{-7}	EVQLVESGGGLVQPGGSLRLSCAASGGTFSLYAMGWFRQAPGKGREL VAAISGGGSYTYYPDSVEGRFTISRDNAKRMVYLQMNSLRAEDTAVY YCAREFFGTTIAWGQGTQVTVSSGGGGSHHHHHH
BHRF1_09	2.38×10^{-7}	EVQLVESGGGLVQPGGSLRLSCAASGSSTTAMIMAWYRQAPGKGREL VAGILNGLSITSYADSVKGRFTISRDNAKNTLYLQMNSLRPEDTAVY YCARERFVSTSSGTVRWSTYWGQGTLVTVSSGGGGSHHHHHH
BHRF1_13	5.95×10^{-7}	EVQLVESGGGLVQPGGSLRLSCAASGFTFSLWDMGWFRQAPGKGREL VAAISNGGDYTYYPDSVEGRFTISRDNAKRMVYLQMNSLRAEDTAVY YCAAVLGYDWIRSGLYWGQGTQVTVSSGGGGSHHHHHH
BHRF1_30	1.31×10^{-7}	EVQLVESGGGLVQPGGSLRLSCAASGGTFSLWDMGWFRQAPGKGREL VAAISSSGSSTYYPDSVEGRFTISRDNAKRMVYLQMNSLRAEDTAVY YCARGGRYLDYFWGMSWGQGTQVTVSSGGGGSHHHHHH
EFNA1_02	6.51×10^{-6}	EVQLVESGGGLVQPGGSLRLSCAASGSSGMPDIMGWFRQAPGKGREL VAEMHIFTGDTYYPDSVEGRFTISRDNAKRMVYLQMNSLRAEDTAVY YCAGRDSSSGGTVYWGQGTQVTVSSGGGGSHHHHHH
EFNA1_03	8.76×10^{-6}	EVQLVESGGGLVQPGGSLRLSCAASGETSSVSYMGWFRQAPGKGREE VAAINTVSGYTYYPDSVEGRFTISRDNAKRMVYLQMNSLRAEDTAVY YCAARDARDDGISWGQGTQVTVSSGGGGSHHHHHH
EFNA1_04	3.12×10^{-7}	EVQLVESGGGLVQPGGSLRLSCAASGLSTTGYAMAWFRQAPGQEREF VAGISGDGSYTYYADSVRGRFTNSRDESKNTLYLQMNSLRAEDTAVY YCARSTSSYYYGVEDMDYWGQGTLVTVSSGGGGSHHHHHH
EFNA1_06	7.17×10^{-7}	EVQLVESGGGLVQPGGSLRLSCAASGETSVLSVMAWYRQAPGKGREL VAGISYDGSITSYADSVKGRFTISRDNAKNTLYLQMNSLRPEDTAVY YCAGSTSYSTSWELSSFSYWGQGTLVTVSSGGGGSHHHHHH
EFNA1_07	6.86×10^{-7}	EVQLVESGGGLVQPGGSLRLSCAASGGTFSYYSMGWFRQAPGKGREL VAAISWDGSETYYPDSVEGRFTISRDNAKRMVYLQMNSLRAEDTAVY YCAAETSYYPYPGDTSYAYWGQGTQVTVSSGGGGSHHHHHH
EFNA1_08	8.22×10^{-7}	EVQLVESGGGLVQPGGSLRLSCAASGGEISSYSMAWYRQAPGKGREL VAGISADGRYTSYADSVKGRFTISRDNAKNTLYLQMNSLRPEDTAVY YCATLTANYLNYDFTNTGDFDYWGQGTLVTVSSGGGGSHHHHHH

Continued on next page...

Table S8 (Continued)

Design	K_D (M)	Sequence
EFNA1_09	7.21×10^{-7}	EVQLVESGGGLVQPGGSLRLSCAASGIYDYASYMGWFRQAPGKGREL VAEMSIFTGNTYYPDSVEGRFTISRDNAKRMVYLQMNSLRAEDTAVY YCAALQSGGSYDVYWGQGTQVTVSSGGGGSHHHHHH
EFNA1_10	1.06×10^{-6}	EVQLVESGGGLVQPGGSLRLSCAASGETSVMSVMAWYRQAPGKGREL VAGISYDGSITSYADSVKGRFTISRDNAKNTLYLQMNSLRPEDTAVY YCAASTSYSTSYELSSFDYWGQGTLVTVSSGGGGSHHHHHH
EFNA1_12	7.08×10^{-7}	EVQLVESGGGLVQPGGSLRLSCAASGGTFSTYPMAWFRQAPGQEREF VAGIGAGGDYTLYADSVRGRFTNSRDNSKNTLYLQMNSLRAEDTAVY YCARYKYETDASNAWEFEDFDSWGQGTLVTVSSGGGGSHHHHHH
EFNA1_13	1.33×10^{-6}	EVQLVESGGGLVQPGGSLRLSCAASGGTFSSYAMAWFRQAPGQEREF VAGINYNGNDTLYADSVRGRFTNSRDNSKNTLYLQMNSLRAEDTAVY YCARLSLQWEAYNEEDVDAWGQGTLVTVSSGGGGSHHHHHH
EFNA1_14	8.55×10^{-7}	EVQLVESGGGLVQPGGSLRLSCAASGSSSSYSIMGWFRQAPGKGREL VAEMSTFTGNTYYPDSVEGRFTISRDNAKRMVYLQMNSLRAEDTAVY YCAALDMSGTYDYYWGQGTQVTVSSGGGGSHHHHHH
EFNA1_15	2.96×10^{-6}	EVQLVESGGGLVQPGGSLRLSCAASGGTFSYYSMGWFRQAPGKGREL VAAITYDGSETYYPDSVEGRFTISRDNAKRMVYLQMNSLRAEDTAVY YCASASSYYAYSDDSSYYYWGQGTQVTVSSGGGGSHHHHHH
EFNA1_16	2.76×10^{-7}	EVQLVESGGGLVQPGGSLRLSCAASGGDVSSRTMAWYRQAPGKGREL VAGISADGRYTSYADSVKGRFTISRDNAKNTLYLQMNSLRPEDTAVY YCATADRNYLNYDFTSTSDFSYWGQGTLVTVSSGGGGSHHHHHH
EFNA1_17	4.33×10^{-7}	EVQLVESGGGLVQPGGSLRLSCAASGSTSIITSMAWYRQAPGKGREL VAGISRSGGYTSYADSVKGRFTISRDNAKNTLYLQMNSLRPEDTAVY YCAATTSLIYSYDSEIITDSMQFWGQGTLVTVSSGGGGSHHHHHH
EFNA1_18	8.09×10^{-7}	EVQLVESGGGLVQPGGSLRLSCAASGPADDLSVMAWYRQAPGKGREL VAGIWYDGSNTSYADSVKGRFTISRDNAKNTLYLQMNSLRPEDTAVY YCAGQLSYYTSYETSSFQYWGQGTLVTVSSGGGGSHHHHHH
EFNA1_19	1.29×10^{-6}	EVQLVESGGGLVQPGGSLRLSCAASGFTFSYYAMGWFRQAPGKGREL VAAITYDGSETYYPDSVEGRFTISRDNAKRMVYLQMNSLRAEDTAVY YCAAVSSSYPYLDDTSYAYWGQGTQVTVSSGGGGSHHHHHH
EFNA1_20	5.66×10^{-7}	EVQLVESGGGLVQPGGSLRLSCAASGFTFSSYMMGWFRQAPGKGREL VAAISYDGSSTYYPDSVEGRFTISRDNAKRMVYLQMNSLRAEDTAVY YCARLGVHSSTAEEIAARNVDSWGQGTQVTVSSGGGGSHHHHHH
EFNA1_21	1.01×10^{-6}	EVQLVESGGGLVQPGGSLRLSCAASGDSDYFAIMGWFRQAPGKGREL VAEMHVFTGNTYYPDSVEGRFTISRDNAKRMVYLQMNSLRAEDTAVY YCAALNMAGTYDYYWGQGTQVTVSSGGGGSHHHHHH
EFNA1_22	9.30×10^{-7}	EVQLVESGGGLVQPGGSLRLSCAASGDASSVQTMAWYRQAPGKGFEL VAGMNRDGSSTSYADSVKGRFTISRDNAKNTLYLQMNSLRPEDTAVY YCVASGSTRTSDIALSYADWGQGTLVTVSSGGGGSHHHHHH
EFNA1_24	2.79×10^{-6}	EVQLVESGGGLVQPGGSLRLSCAASGFTFSYYAMGWFRQAPGKGREL VAAITNDGSETYYPDSVEGRFTISRDNAKRMVYLQMNSLRAEDTAVY YCAATSSSYPYLDDTSYRYWGQGTQVTVSSGGGGSHHHHHH

Continued on next page...

Table S8 (Continued)

Design	K_D (M)	Sequence
EFNA1_25	4.47×10^{-6}	EVQLVESGGGLVQPGGSLRLSCAASGDYDSVSIMGWFRQAPGKGREE VAAINMVSGHTYYPDSVEGRFTISRDNAKRMVYLQMNSLRAEDTAVY YCAARDASNGGVVWGQGTQVTVSSGGGGSHHHHHH
S100A4_01	3.67×10^{-7}	QVQLQESGGGLVQPGGSLRLSCAASGYTTSYYWMAWFRQAPGKERER VAKIIPILGYTYLADSVKGRFTISQNNAKSTVYLQMNSLKPEDTAMY YCARSKSWTYDSTSFDYWGQGTQVTVSGGGGSHHHHHH
S100A4_03	2.38×10^{-7}	EVQLVESGGGLVQPGGSLRLSCAASGQDAYIWAMAWYRQAPGKGREL VAGIYFGGGTTSYADSVKGRFTISRDNAKNTLYLQMNSLRPEDTAVY YCATYTYSGSLSRTWGQGTLVTVSSGGGGSHHHHHH
S100A4_07	3.71×10^{-7}	EVQLVESGGGLVQPGGSLRLSCAASGGPDYFFYMAWYRQAPGKGREL VAGINFMGGSISYADSVKGRFTISRDNAKNTLYLQMNSLRPEDTAVY YCRFAQFASLSSNGGSVLTYSWGQGTLVTVSSGGGGSHHHHHH
S100A4_17	7.17×10^{-7}	QVQLQESGGGLVQPGGSLRLSCAASGSSNAWIAMAWFRQAPGKERER VAKIYFFGTNKYLADSVKGRFTISQNNAKSTVYLQMNSLKPEDTAMY YCVSYSPSTSSSGGYTRAWGQGTQVTVSGGGGSHHHHHH
S100A4_20	5.41×10^{-7}	EVQLVESGGGLVQPGGSLRLSCAASGDTSFIIAMAWYRQAPGKGREL VAGLNRLTSSISYADSVKGRFTISRDNAKNTLYLQMNSLRPEDTAVY YCAAARVLGGTTERAWGQGTLVTVSSGGGGSHHHHHH
HNMT_03	7.68×10^{-8}	EVQLVESGGGLVQPGNSLRLSCAASGFSFSDYWMSWVRQAPGKGLEW VSSISWNGSRKLYADSVKGRFTISRDNAKTTLYLQMNSLRPEDTAVY YCYRLGRFVSSLNVEKDTFLGSSQGTLVTVSSGGGGSHHHHHH
HNMT_10	2.66×10^{-9}	EVQLVESGGGLVQPGNSLRLSCAASGFSFSRYAMSWVRQAPGKGLEW VSSISGSGSYKLYADSVKGRFTISRDNAKTTLYLQMNSLRPEDTAVY YCTRLIDSDADMDIVRSSYVSSQGTLVTVSSGGGGSHHHHHH
HNMT_12	2.51×10^{-9}	EVQLVESGGGLVQPGNSLRLSCAASGFSFSRYGMSWVRQAPGKGLEW VSSISSSGGTKLYADSVKGRFTISRDNAKTTLYLQMNSLRPEDTAVY YCSRYWYFDELLFTYYSSQGTLVTVSSGGGGSHHHHHH
HNMT_18	4.37×10^{-8}	EVQLVESGGGLVQPGGSLRLSCAASGYTGSDYYMAWYRQAPGKGREL VAGISWTGITKSYADSVKGRFTISRDNAKNTLYLQMNSLRPEDTAVY YCTSSRFRSYDGRAEPDAYWGQGTLVTVSSGGGGSHHHHHH
HNMT_23	2.50×10^{-9}	EVQLVESGGGLVQPGGSLRLSCAASGGDVSYWSMAWYRQAPGKGREL VAGISGSGRFTSYADSVKGRFTISRDNAKNTLYLQMNSLRPEDTAVY YCAVGGVGDTGLFWGQGTLVTVSSGGGGSHHHHHH
HNMT_25	1.15×10^{-7}	EVQLVESGGGLVQPGGSLRLSCAASGFAFSLYSMGWFRQAPGKGREL VAAIKGWSGNTYYPDSVEGRFTISRDNAKRMVYLQMNSLRAEDTAVY YCASGRWFGPLTTSDFSSWGQGTQVTVSSGGGGSHHHHHH

For expression in CHO cells (pCDNA3.4 vector), an N-terminal signal peptide (MGWSCIILFLVATATGVHS) was fused to the listed sequences but is omitted from the table. The C-terminus includes the shown extension GGGGSHHHHHH (flexible linker and 6×His tag).

References

[1] Longxing Cao et al. “Design of protein-binding proteins from the target structure alone”. In: *Nature* 605.7910 (2022), pp. 551–560.

[2] Georges Köhler and Cesar Milstein. “Continuous cultures of fused cells secreting antibody of predefined specificity”. In: *Nature* 256.5517 (1975), pp. 495–497.

[3] George P Smith. “Filamentous fusion phage: novel expression vectors that display cloned antigens on the virion surface”. In: *Science* 228.4705 (1985), pp. 1315–1317.

[4] Greg Winter et al. “Making antibodies by phage display technology”. In: *Annual review of immunology* 12.1 (1994), pp. 433–455.

[5] Frances H Arnold. “Directed evolution: bringing new chemistry to life”. In: *Angewandte Chemie (International Ed. in English)* 57.16 (2017), p. 4143.

[6] Frances H Arnold. “Design by directed evolution”. In: *Accounts of chemical research* 31.3 (1998), pp. 125–131.

[7] Ivan Anishchenko et al. “De novo protein design by deep network hallucination”. In: *Nature* 600.7889 (2021), pp. 547–552.

[8] Jue Wang et al. “Scaffolding protein functional sites using deep learning”. In: *Science* 377.6604 (2022), pp. 387–394.

[9] Milong Ren et al. “Accurate and robust protein sequence design with CarbonDesign”. In: *Nature Machine Intelligence* 6.5 (2024), pp. 536–547.

[10] Joseph L Watson et al. “De novo design of protein structure and function with RFdiffusion”. In: *Nature* (2023), pp. 1–3.

[11] Nathaniel R Bennett et al. “Atomically accurate de novo design of antibodies with RFdiffusion”. In: *Nature* (2025), pp. 1–11.

[12] Martin Pacesa et al. “One-shot design of functional protein binders with BindCraft”. In: *Nature* 646.8084 (2025), pp. 483–492.

[13] John B Ingraham et al. “Illuminating protein space with a programmable generative model”. In: *Nature* 623.7989 (2023), pp. 1070–1078.

[14] Pablo Gainza et al. “De novo design of protein interactions with learned surface fingerprints”. In: *Nature* 617.7959 (2023), pp. 176–184.

[15] Luis S Mille-Fragoso et al. “Efficient generation of epitope-targeted de novo antibodies with Germinal”. In: *bioRxiv* (2025).

[16] Yaron Lipman et al. “Flow matching for generative modeling”. In: *International Conference on Learning Representations* (2023).

[17] Ricky T. Q. Chen and Yaron Lipman. “Flow Matching on General Geometries”. In: *International Conference on Learning Representations* (2024).

[18] Jason Yim et al. “Fast protein backbone generation with SE(3) flow matching”. In: *arXiv preprint arXiv:2310.05297* (2023).

[19] Avishek Joey Bose et al. “Se (3)-stochastic flow matching for protein backbone generation”. In: *arXiv preprint arXiv:2310.02391* (2023).

[20] Yu Liu et al. “Af3score: A score-only adaptation of alphafold3 for biomolecular structure evaluation”. In: *Journal of Chemical Information and Modeling* 65.15 (2025), pp. 8207–8214.

[21] John Jumper et al. “Highly accurate protein structure prediction with AlphaFold”. In: *Nature* 596.7873 (2021), pp. 583–589.

[22] Josh Abramson et al. “Accurate structure prediction of biomolecular interactions with AlphaFold 3”. In: *Nature* 630.8016 (2024), pp. 493–500.

[23] Yeqing Lin et al. “Out of many, one: Designing and scaffolding proteins at the scale of the structural universe with genie 2”. In: *arXiv preprint arXiv:2405.15489* (2024).

[24] Tomas Geffner et al. “Proteina: Scaling flow-based protein structure generative models”. In: *arXiv preprint arXiv:2503.00710* (2025).

[25] Zhuoqi Zheng et al. “MotifBench: A standardized protein design benchmark for motif-scaffolding problems”. In: *arXiv preprint arXiv:2502.12479* (2025).

[26] Tianyu Lu et al. “Conditional protein structure generation with protpardelle-1c”. In: *bioRxiv* (2025).

[27] Hannes Stark et al. “Boltzgen: Toward universal binder design”. In: *bioRxiv* (2025), pp. 2025–11.

[28] Nathaniel R Bennett et al. “Improving de novo protein binder design with deep learning”. In: *Nature Communications* 14.1 (2023), p. 2625.

[29] Justas Dauparas et al. “Robust deep learning–based protein sequence design using ProteinMPNN”. In: *Science* 378.6615 (2022), pp. 49–56.

[30] Frédéric A Dreyer et al. “Inverse folding for antibody sequence design using deep learning”. In: *arXiv preprint arXiv:2310.19513* (2023).

[31] Rebecca F Alford et al. “The Rosetta all-atom energy function for macromolecular modeling and design”. In: *Journal of chemical theory and computation* 13.6 (2017), pp. 3031–3048.

[32] Matthias Glögl et al. “Target-conditioned diffusion generates potent TNFR superfamily antagonists and agonists”. In: *Science* 386.6726 (2024), pp. 1154–1161.

[33] Jin Sub Lee and Philip M Kim. “FlowPacker: protein side-chain packing with torsional flow matching”. In: *Bioinformatics* 41.3 (2025), btaf010.

[34] Ian Sillitoe et al. “CATH: increased structural coverage of functional space”. In: *Nucleic acids research* 49.D1 (2021), pp. D266–D273.

[35] Helen M Berman et al. “The protein data bank”. In: *Nucleic acids research* 28.1 (2000), pp. 235–242.

[36] Martin Steinegger and Johannes Söding. “MMseqs2 enables sensitive protein sequence searching for the analysis of massive data sets”. In: *Nature biotechnology* 35.11 (2017), pp. 1026–1028.

[37] James Dunbar et al. “SAbDab: the structural antibody database”. In: *Nucleic acids research* 42.D1 (2014), pp. D1140–D1146.